Title
Dynamics of Microtubules Composed of Mutated Beta-Tubulins: A Structure-Function
Study using Saccharomyces cerevisiae as a Model System

Permalink
https://escholarship.org/uc/item/49p6397h

Author
Tsuchiya, Etsuko

Publication Date
2002-06-01

Peer reviewed

INFORMATION TO USERS

This manuscript has been reproduced from the microfilm master. UMI films the text directly from the original or copy submitted. Thus, some thesis and dissertation copies are in typewriter face, while others may be from any type of computer printer.

The quality of this reproduction is dependent upon the quality of the copy submitted. Broken or indistinct print, colored or poor quality illustrations and photographs, print bleedthrough, substandard margins, and improper alignment can adversely affect reproduction.

In the unlikely event that the author did not send UMI a complete manuscript and there are missing pages, these will be noted. Also, if unauthorized copyright material had to be removed, a note will indicate the deletion.

Oversize materials (e.g., maps, drawings, charts) are reproduced by sectioning the original, beginning at the upper left-hand corner and continuing from left to right in equal sections with small overlaps.

Photographs included in the original manuscript have been reproduced xerographically in this copy. Higher quality 6" x 9" black and white photographic prints are available for any photographs or illustrations appearing in this copy for an additional charge. Contact UMI directly to order.

UNIVERSITY OF CALIFORNIA

Santa Barbara

Dynamics of Microtubules Composed of Mutated Beta-Tubulins: A Structure-

Function Study Using *Saccharomyces cerevisiae* as a Model System

A dissertation submitted in partial satisfaction of the requirements for the degree

Doctor of Philosophy

in Biochemistry and Molecular Biology

by

Etsuko Tsuchiya

Committee in charge:

Professor Leslie Wilson, chair

Professor Louise Clarke

Professor Stuart C. Feinstein

Professor John Lew

June 2002

UMI Number: 3056034

Copyright 2002 by

Tsuchiya, Etsuko

All rights reserved.

UMI®

The dissertation of Etsuko Tsuchiya is approved.

_____
Louise Clarke
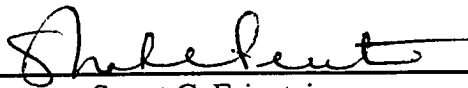
_____
Stuart C. Feinstein

_____
John Lew

_____
Leslie Wilson, Committee Chair

June 2002

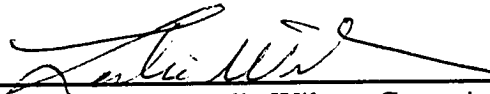Dynamics of Microtubules Composed of Mutated Beta-Tubulins: A Structure-

Function Study Using *Saccharomyces cerevisiae* as a Model System

Copyright © 2002

by

Etsuko Tsuchiya

iii

ACKNOWLEDGEMENTS

This dissertation couldn't have been written, nor the research accomplished, without the advice, support and assistance of many people. First, I'd like to express my sincere thanks and appreciation to my advisor, Dr. Leslie Wilson, for his wisdom and guidance throughout my Ph.D. I have been extremely fortunate to have been taken under his wing. The many members of the Wilson lab, past and present, have been invaluable and generous in sharing their knowledge and experience with me. I especially want to acknowledge those members who have overlapped with me the longest: Jennifer DeLuca, Cori Newton, Kathy Mitchelson, Doug Thrower and Vivian Ngan. I will sorely miss Mr. Herb Miller, the lab's tubulin wizard, whose warmth and friendship kept me buoyed. Thanks Grandpa Herb! To my committee members, Drs. Louise Clarke, Stu Feinstein, and John Lew, my sincere thanks for their advice and guidance. Drs. Kevin Farrell and Richard Himes were invaluable with their advice during the early and latter sections of my Ph.D. Mr. Bob Fletcher has been amazing in keeping the old fermentor running, and I thank him and the BioShop gang for helping me out so often over the years. The labs of Drs. John Carbon, Louise Clarke, John Lew and Joel Rothman have been extremely generous with their help and friendship over the years. Thank you to all our friends, for all the fun times. You have truly made Santa Barbara an unforgettable time and place. And finally, my love and gratitude to my family, especially Brent and Kentaro: they have been my unwavering cheering section. BANZAI, BANZAI, BANZAI!!

VITA OF ETSUKO TSUCHIYA

June 2002

EDUCATION

Bachelor of Science, Queen's University, Kingston, Ontario, Canada, June, 1986
Master of Science, Carleton University, Ottawa, Ontario, Canada, January, 1990
Doctor of Philosophy, University of California, Santa Barbara, California, USA, June 2002 (expected)

PROFESSIONAL EMPLOYMENT

1991-1992: Biologist, Federal Department of Fisheries and Oceans, Habitat Management Branch, Ottawa, Ontario, Canada
1992-1994: Research Assistant, Biology Department, University of California, Santa Barbara
1994-1997: Teaching Assistant, Department of Molecular, Cellular, and Developmental Biology

PUBLICATIONS

Tsuchiya, E. & Wilson, L. (2002). Altered microtubule dynamics and drug sensitivity in *Saccharomyces cerevisiae* mutated in the putative colchicine-binding site of β-tubulin. *In preparation.*

Tsuchiya, E. & Wilson, L. (2002). Modulation of benomyl sensitivity by mutation of β-tubulin at Arginine 318. *In preparation.*

Dumontet, C., Jaffrézou, J.P., **Tsuchiya, E.**, Duran, G.E., Chen, G., Derry, W.B., Wilson, L., Jordan, M.A. & Sikic, B.I. (1999). Resistance to microtubule-targeted cytotoxins in a K562 leukemia cell variant associated with altered tubulin expression and polymerization. *Electronic Journal of Oncology*, **2**: 33-44.

Jaffrézou, J.P., Dumontet, C., Derry, W.B., Duran, G.E., Chen, G., **Tsuchiya, E.**, Wilson, L., Jordan, M.A. & Sikic, B.I. (1995). Novel mechanism of resistance to paclitaxel (Taxol$^{\circledR}$) in human K562 leukemia cells by combined selection with PSC 833. *Oncology Research*, **7**: 517-527.

v

FIELDS OF STUDY

Major Field: Biology

M.Sc. advisors: Professors H. Gray Merriam & George Carmody. Thesis title: Genetic differentiation of mitochondrial DNA at the landscape scale in patchy populations of *Peromyscus leucopus*.

vi

ABSTRACT

Dynamics of Microtubules Composed of Mutated Beta-Tubulins: A Structure-

Function Study Using *Saccharomyces cerevisiae* as a Model System

by

Etsuko Tsuchiya

The effects of structural changes in yeast β-tubulin on the dynamic properties of

microtubules (MTs) were measured in *Saccharomyces cerevisiae* using real time

digital microscopy. A galactose inducible GFP-TUB3 plasmid construct was

transformed into yeast strains that were mutated at the putative colchicine binding site

in the sole β-tubulin gene (TUB2). The dynamic properties of cytoplasmic MTs

(cMTs) of two mutated strains and their respective wild-type strains were examined

in vivo. CLC9 is a haploid strain in which TUB2 was mutated in a conserved residue

(R318W), and is highly resistant to benomyl. In CLC8, a diploid benomyl sensitive

strain, TUB2 is mutated in the sequence between amino acids 310-324 so that this

region is identical to the porcine tubulin sequence. Several differences in specific

dynamic parameters have been uncovered. For CLC9, all parameters were similar to

wild-type except that the catastrophe frequency was higher and the mean attenuation

duration lower. For CLC8, the shortening rate, catastrophe frequency, and the

percent unrescued catastrophes, were higher than wild-type, while the mean

attenuation duration was lower. Together, the cMTs in CLC8 are less stable than

those in wild-type cells, which is reflected by the strain's longer doubling time. In

the presence of increasing concentrations of benomyl, the three yeast strains sensitive to the drug exhibit greatly reduced MT dynamics while the super resistant strain showed little change. From 2 µg/ml to 3 µg/ml benomyl, MTs in the CLC8 strain transitioned from a highly dynamic state, to a completely attenuated state, whereas at 5 µg/ml MTs completly depolymerized. In contrast, MTs in the CLC9 strain at 10 µg/ml benomyl were as dynamic as MTs in untreated cells. These data support *in vitro* data demonstrating the stabilization of MT dynamics by low concentrations of antimitotic drugs but expand this fundamental property to a system in which the relationship between tubulin structure and dynamic function can be efficiently analyzed *in vivo*. This system will also be useful to elucidate how cellular factors modulate *in vivo* dynamics directly, and for identification of regions in the tubulin protein critical for modulating MT dynamics.

TABLE OF CONTENTS

LIST OF FIGURES

LIST OF TABLES

xvi

DEFINITIONS

BEN	benomyl; 1-butylaminocarbonyl-2-carbamomethoxybenzimidazole
CEN	centromere
CLC	colchicine
cMT	cytoplasmic microtubule
DAPI	4', 6-diamidino-2-phenylindole dihydrochloride
DMSO	dimethyl sulfoxide
DO	drop out plates; minimal media plates missing one amino acid, used to identify the genotypes of yeast strains
DT	doubling time
FPLC	fast pressure liquid chromatography
FRAP	fluorescent redistribution after photobleaching
FSM	fluorescent speckle microscopy
GAL1	galactokinase gene; galactose metabolism
GFP	green fluorescent protein
kMT	kinetochore microtubules
MAP	microtubule binding protein
MBC	methyl benzimidazol –2-yl carbamate
MT	microtubule
SD	minimal media; nitrogenous base without amino acids
TC complex	tubulin-colchicine complex
URA3	orotidine-5'-phosphate decarboxylase gene; uracil auxotrophy

VBL	vinblastine
WSC	cell wall integrity and stress response component genes
WT	wild type
YPD	yeast peptone dextrose media
YPD + G	yeast peptone dextrose plus galactose media; used to induce production of GFP-tubulin
YPD + S	yeast peptone dextrose plus sorbitol media; used to grow and maintain yeast strains with the cell wall defect

Genotypes of *Saccharomyces cerevisiae* Strains Used in this Study

Strain	Genotype	Reference
ADY101:pADwt	*HIS4/his4, leu2/leu2, LYS4/ly24, trp1/trp1, tub2-590/TUB2-URA3, ura3/ura3*	Davis et al., (1993)
CLC1	*HIS4/his4, leu2/leu2, LYS4/ly24, trp1/trp1, tub2-590/CLC1-URA3, ura3/ura3*	Sage (1994)
CLC2	*HIS4/his4, leu2/leu2, LYS4/ly24, trp1/trp1, tub2-590/CLC2-URA3, ura3/ura3*	Sage (1994)
CLC3	*HIS4/his4, leu2/leu2, LYS4/ly24, trp1/trp1, tub2-590/CLC3-URA3, ura3/ura3*	Sage (1994)
CLC5	*HIS4/his4, leu2/leu2, LYS4/ly24, trp1/trp1, tub2-590/CLC5-URA3, ura3/ura3*	Sage (1994)
CLC7	*HIS4/his4, leu2/leu2, LYS4/ly24, trp1/trp1, tub2-590/CLC7-URA3, ura3/ura3*	Sage (1994)
CLC8	*HIS4/his4, leu2/leu2, LYS4/ly24, trp1/trp1, tub2-590/CLC8-URA3, ura3/ura3*	Sage (1994)
CLC9	*Mata his4, leu2, LYS4, trp1, CLC9-URA3*	Sage (1994)
ADY103	*HIS4/his4, leu2/leu2, LYS4/ly24, trp1/trp1,TUB2/TUB2, ura3/ura3*	Davis et al., (1993)
FY41	*Mata his4, leu2, trp1, ura3*	Sage, (1994)
ADY101:pADwt-A6B	*Mata his4, leu2, LYS4, trp1,TUB2-URA3*	this study
ADY101:pADwt-1Ia	*Mata HIS4, leu2, lys4, trp1,tub2-590, ura3*	this study
CLC2-1D	*Mata his4, leu2, LYS4, trp1,CLC2-URA3*	this study
CLC7-1'A	*Mata HIS4, leu2, LYS4, trp1,CLC7-URA3*	this study

xx

Chapter I: Introduction

1

Chapter I: Introduction/Significance

Microtubules: Functions and Gross Structure

Microtubules are essential organelles in higher eukaryotic cells. These tubular

cytoskeletal components play a variety of roles throughout the cell cycle, from

cellular morphology, motility and vesicular transport during interphase, and

chromosome congression and chromatid segregation in mitosis (Dustin, 1984).

During cell cycle progression, a great deal of microtubule (MT) rearrangement

occurs, from the net-like structure in interphase to the highly organized mitotic

spindle in mitosis. The ability to reorganize their structure is an intrinsic property of

MTs and is critically dependent on their dynamic characteristics. In most MTs, 13

linear protofilaments associate laterally to form a hollow tube of approximately 25

nm in diameter (Dustin, 1984). Each protofilament is a polymer assembled from α-

and β-tubulin heterodimers, which associate in a head to tail manner; this

arrangement of heterodimers imparts an inherent polarity in the overall structure of

MTs.

α- and β-Tubulin, are acidic proteins with a relative molecular mass of 50 kDa each,

and are composed of approximately 450 amino acids. They are highly conserved

throughout evolution, and display a high degree of identity to one another at the

amino acid level (Dustin, 1984). Each subunit of the heterodimer has the capability

to bind guanosine triphosphate (GTP); one molecule of GTP binds to the non-

2

exchangeable site on the α-subunit, while a second molecule of GTP binds to the β-subunit and is freely exchangeable with unbound GTP in solution. As heterodimers polymerize to form a MT, the GTP at the exchangeable site is hydrolyzed to GDP and inorganic phosphate. The rate of GTP hydrolysis is one of the modulators of MT dynamics. There are many other modulators of MT dynamics, such as the MT associated proteins (MAPs) (e.g. MAP2 and tau), motors, and antimitotic drugs such as colchicine and taxol, to name a few.

Three-dimensional structure of the tubulin dimer and the MT

Until the ground breaking paper by Nogales et al., (1998), the 3-dimensional (3D) structure of tubulin had not been solved and existing structural information on tubulin had been derived primarily from limited proteolysis, antibody binding, chemical, and UV cross-linking experiments using mammalian protein. Nogales et al., (1998) solved the structure of tubulin, at a resolution of 3.7 Å, by high resolution electron crystallography of zinc sheets (see Figures 1.1A and 1.1B). Tubulin polymerized in the presence of Zn^{2+} ion assembles into 2-dimensional sheets, where the protofilaments form in an antiparallel arrangement. Nogales and coworkers prepared the zinc sheets in the presence of taxol for stability. The α-tubulin subunit of the 3D structure was missing the last 10 amino acids, while the β-tubulin subunit was missing the last 18 amino acids. Because of the high number of acidic amino acid

3

residues in the C-terminal ends, it was expected that the ends of the proteins would be

highly disordered, and thus not resolvable.

Figure 1.1A: Ribbon diagram of the structure of α and β-tubulin. From Nogales et al., (1998). Stereo view from the outside of the MT. The arrow indicates the polarity and the axis of the MT. Sequence information of the labeled strands and helices appear in Figure 1.1B. GTP is docked in the N-site, GDP in the E-site, and taxol in its binding site.

4
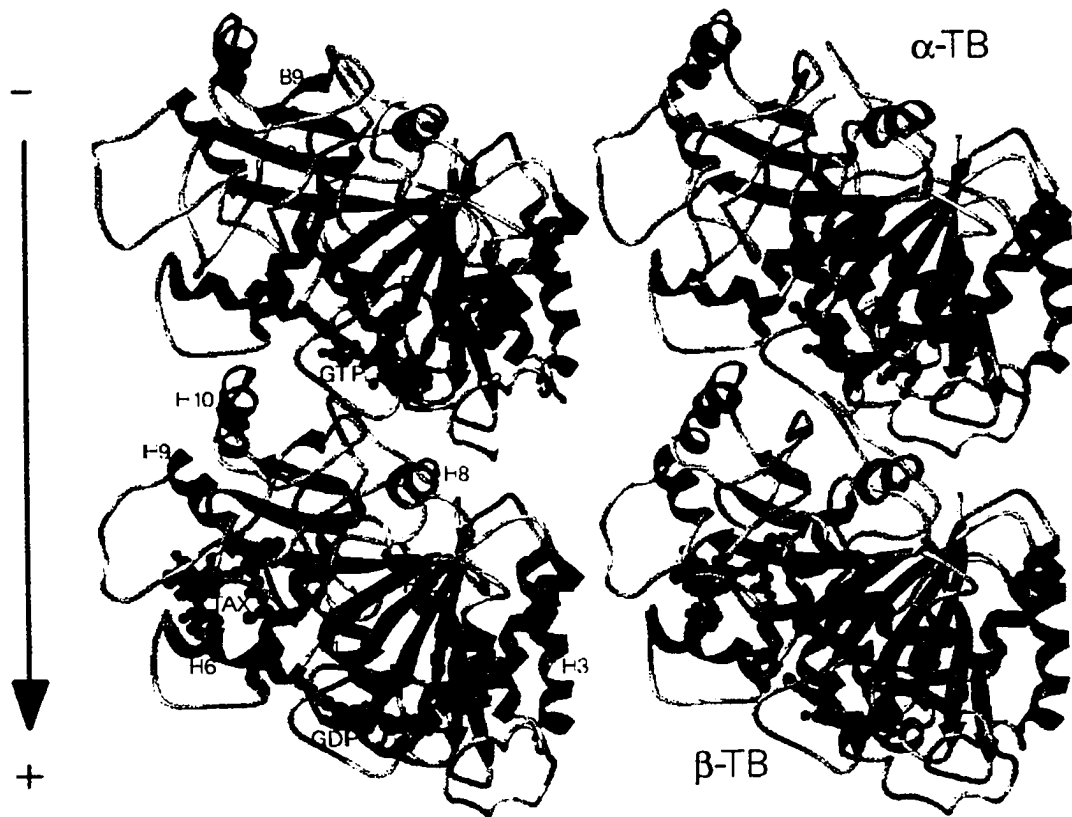
Figure 1.1B: Protein sequence and structural motifs of α and β-tubulins. From Nogales et al., (1998). The sequence for α-tubulin is on the top of each row, while the sequence for β-tubulin is on the bottom of each row. Strands are indicated by blue arrows, helices by red barrels.

N-terminal domain

```
          10        20        30        40        50        60        70        80        90        100
α-TB  MRECISIHVGQAGVQIGNACWELYCLEHGIQPDGQMPSDKTIGGGDDSFNTFFSETGAGKHVPRAVFVDLEPTVIDEVRTGTYRQLFHPEQLITGKEDAA
β-TB  MREIVHIQAGQCGNQIGAKFWEVISDEHGIDPTGSYVGDSDLQL..BRINVYYNEAAGNKYVPRAILVDLEPGTMDSVRSGPFGQIFRPDNFVFGQSGAG
                          B1              H1                                      B2                      B3
```

```
          110       120       130       140       150       160       170       180       190       200
α-TB  NNYARGHYTIGKEIIDLVLDRIRKLADQCTGLQGFSVFHSFGGGTGSGFTSLLMERLSVDYGKKSKLEFSIYPAPQVSTAVVEPYNSILTTHTTLEHSDC
β-TB  NMWAKGHYTEGAELVDSVLDVVRKESESCDCLQGFQLTHSLGGGTGSGMGTLLISKIREEYPDRIMNTFSVVPSPKVSDTVVEPYNATLSVHQLVENTDE
                      H3              B4              H4                  B5                      H5
```

Intermediate domain

```
          210       220       230       240       250       260       270       280       290       300
α-TB  AFMVDNEAIYDICRRNLDIERPTYTNLNRLIGQIVSSITASLRFDGALNVDLTEFQTNLVPYPRAHFPLATYAPVISAEKAYHEQLSVAEITNACFEPAN
β-TB  TYCIDNEALYDICFRTLKLTTPTYGDLNHLVSATMSGVTTCLRFPGQLNADLRKLAVNMVPFPRGHFFMPGFAPLTSRGSQQYRALTVPELTQQMFDAKN
            B6              H6                      H7                  H8                      B7      H9
```

C-terminal domain

```
          310       320       330       340       350       360       370       380       390       400
α-TB  QMVKCDPRHGKYMACCLLYRGDVVPKDVNAAIATIKTKRSIQFVDWCPTGFKVGINYEPPTVVPGGDLAKVQRAVCMLSNTTAIAEAWARLDHKFDLMYA
β-TB  MMAACDPRHGRYLTVAAVFRGRMSMKEVDEQMLNVQNKNSSYFVEWIPNNVKTAVCDIPP........RGLKMSATFIGNSTAIQELFKRISEQFTAMFR
            B8          H10                 B9                                    B10            H11
```

```
          410       420       430       440       450
α-TB  KRAFVHWYVGEGMEEGEFSEAREDMAALEKDYEEVGVDSV.E.GEGEEEGEEY..
β-TB  RKAFLHWYTGEGMDEMEFTEAESNMNDLVSEYQQYQDATADEQGEFEEEGEEDEA
                              H12
```

5

The high resolution crystal structure of the dimer was docked into a low resolution (20 Å) 3D map of the MT (Nogales et al., 1999). The structure of a complete protofilament from the Zn^{++} sheet was rotated and translated to fit into the MT map. Since there is an inherent polarity to the protofilament, there was only one orientation that the protofilament could fit into the map. The outside surface of the MT is characterized by helices H11, H12, and a well defined loop between H10 and S9 in the C-termini of the monomers, while the inside surface of the MT is characterized by the long loops formed by H1-S2, H2-S3, and S9-S10. By molecular modeling, the C-terminal ends of the monomers, which were not resolved in the crystal structure, were postulated to be located on the outer side of the MT surface where MT associated proteins such as MAP2 bind to the C-termini of α and β-tubulin. The structural model of tubulin elucidated many aspects of tubulin and MT function; it became readily apparent how GTP hydrolysis is accomplished, why there are exchangeable and non-exchangeable GTP sites, and which residues are important in lateral interactions between protofilaments (Downing and Nogales, 1998, 1999, Nogales et al., 1998, 1999).

Dynamics and their importance in the cellular function of MTs

MTs display two dynamic properties termed dynamic instability (Mitchison and Kirschner, 1984) and treadmilling (Margolis and Wilson, 1978). Dynamic instability describes the slow growth and rapid shortening of individual MTs due to the gain and

6

loss of tubulin heterodimers at the ends of the MT. Treadmilling occurs at polymer mass steady state, when the differences in the association and disassociation rate constants at opposite ends of the MT result in the net flux or treadmilling of tubulin subunits through the MT lattice, from the 'plus' to the 'minus end'. Under conditions where dynamic instability is suppressed, treadmilling in MTs assembled from highly purified bovine brain tubulin is rapid (0.2 μm/min) (Panda et al., 1999). *In vitro*, MTs can self-nucleate at a critical tubulin subunit concentration, which is lowered in the presence of axoneme fragment 'seeds' or MT stabilizers such as glycerol or DMSO (Dustin, 1984). *In vivo*, MTs are nucleated from spindle pole bodies or MT organizing centers, with the 'plus end' of the MTs extending out (review by Doxsey, 2001). The dynamic behavior displayed by MTs *in vitro* and *in vivo* is most likely a combination of both dynamic instability and treadmilling (Farrell et al., 1987).

The dynamic behavior of individual MTs can be quantified by several kinetic parameters such as the rates of MT growth and shortening, as well as the catastrophe and rescue frequencies (Walker et al., 1988). Catastrophes are defined as transitions from growth or attenuation (where the MT appears to neither grow nor shorten) to rapid shortening. Rescues are transitions from rapid MT shortening to either growth or attenuation. Other parameters that characterize a MT's behavior are the duration of growth, shortening and attenuation, the overall proportions of time a particular MT spends in those three phases, and the rate of total detectable dimer exchange, or dynamicity (Toso et al., 1993).

7

Endogenous Modulators of MT dynamics

Endogenous regulators of MT dynamics alter the behavior of MTs though the cell cycle. The dynamics of MTs in mitotic cells and mitotic extracts are different from cells and extracts in interphase (Saxton et al., 1984; Belmont et al., 1990). MT associated proteins (MAPs) such as tau bind to the MT lattice to kinetically stabilize MTs, promote assembly of tubulin into MTs, and effectively dampen MT dynamics. XMAP215 and XKCM1 are examples of proteins that regulate MT dynamics in *Xenopus* cells. XMAP215 is a MT stabilizer that increases polymerization at the plus end while XKCM1 is a kinesin motor protein that increases the frequency of catastrophes.

Drugs as modulators of MT dynamics

Pharmacologically relevant drug binding sites are named for the prototype inhibitors (for example, the colchicine, vinblastine and taxol binding sites) (Hamel, 1996). Tubulin has binding sites for a number of antimitotic drugs (Downing, 2000; Hamel, 1996; Jordan and Wilson, 1998; Wilson et al., 1999). Antimitotic drugs can be divided into two classes: those that induce tubulin polymerization (e.g., taxol) and those that induce MT deploymerization (e.g. colchicine, nocodazole, benomyl). The antimitotic compound taxol acts like a neuronal stabilizing MAP and stabilizes MT dynamics at substoichiomentric concentrations (Derry et al., 1995). Many other

8

antimitotic drugs bind to tubulin or MTs and alter their dynamic properties, much like

the endogenous cellular regulators. Typically, high drug concentrations depolymerize

MTs causing cells to become blocked in mitosis. The dynamic behavior of mitotic

MTs is suppressed by drug concentrations that do not alter MT polymer mass (Wilson

and Jordan, 1995). Low drug concentrations that do not alter polymer mass can also

block cells at the G2/M interface. Therefore, antimitotic drugs are useful tools for

examining the role of regulators of MT dynamics, as well as uncovering which

dynamic parameters contribute most to MT function *in vivo*. Conversely,

understanding how MTs function in the cell can aid in development of new

antimitotic drugs.

Higher Eukaryotes as Model Systems

MTs have been studied in a host of different organisms, cytologically, biochemically,

and genetically. Cells of higher eukaryotes are ideal model systems for examining

MTs cytologically. The gross effects of various manipulations on MTs throughout

the cell cycle, and especially during mitosis, can easily be examined by electron- and

immunofluorescence microscopy (Dustin, 1984; Byers, 1981; Byers and Goetsch,

1974, 1975). Most of the biochemical and dynamic properties of MTs have been

determined by using *in vitro* systems (reviewed in Valiron et al., 2001). The

dynamics of MTs can be examined in real time by video-enhanced differential

interference contrast microscopy (VEDIC). VEDIC enables the direct measurement

of length changes of individual MTs at high resolution.

9

For most *in vitro* dynamics studies, tubulin has been isolated from mammalian neuronal tissue, which is an extremely rich source of the protein (Luduena, 1979). Mammalian tubulin is a complex mixture of multiple isotypes of α- and β-tubulin, which is also modified post-translationally in various ways (reviewed in Sullivan, 1988). MTs composed of isotypically mixed α-tubulins but isotypically pure β-tubulin have different dynamic properties from other purified α/β combinations, as well as from the unfractionated mixture (Banerjee and Luduena, 1992; Panda et al., 1994; Derry et al., 1997). It has also been shown that different antimitotic drugs have a range of effects on tubulin isotypes: β-tubulin isotypes have different binding affinities for the antimitotic drug colchicine (Banerjee and Luduena, 1992), assembly properties are different in the presence of the antimitotic drug vinblastine (Khan and Luduena, 1994), and the dynamic properties of MTs assembled from isotypically pure β-tubulin isotypes are differentially modulated by taxol (Derry et al., 1997).

More recently, technology has advanced and methods have been developed to visualize and investigate the dynamic properties of MTs *in vivo* in higher eukaryotes. Cassimeris et al., (1988) studied the *in vivo* dynamics of individual MTs at the leading edge of newt lung cells using VEDIC microscopy, and observed that the behavior of many of the MTs was dynamic instability; MTs which were polymerizing or depolymerizing, did not exhibit phases of attenuated behavior. Other MTs in the population appeared stable and did not display discernable changes in length

10

(Cassimeris et al., 1988). Shelden and Wadsworth (1993) microinjected rhodamine-labeled tubulin into PtK_1 epithelial cells and CHO fibroblasts, and determined that MT dynamic instability behavior is regulated in a cell-type specific manner. MTs in these cell types exhibited phases of attenuation, as well as phases of growth and shortening. Gonçalves et al. (2001) microinjected rhodamine labeled bovine brain tubulin into taxol-resistant and taxol sensitive human lung cancer cells, measured the dynamics of interphase MTs near the periphery of these cells, and determined that resistance to taxol was due to altered MT dynamics. As powerful as this type of *in vivo* examination of MT dynamics in higher eukaryotic cells may be, it is limited to MTs near the periphery of these cells, in cell types which are very flat. Also, while higher eukaryotic cells are a good source for purified protein and for visualization of MTs *in vivo*, the microheterogenity of tubulin can mask subtle effects. The separation of isotypes can be accomplished for *in vitro* purposes but it is not a trivial procedure (see Luduena, 1998). At this time, it is not possible to determine how each isotype contributes to the dynamic characteristics of MTs in the cell, *in vivo*.

Yeast as a model system for tubulin structure-function studies

The problems of multiple isotypes and genetics can be overcome in using a lower eukaryote as a model system. The yeast *Saccharomyces cerevisiae* is a much simpler organism than the higher eukaryotics often used in the study of tubulin and MTs, yet totally amenable to molecular biology, biochemistry and genetics (reviewed by Winsor and Schiebel, 1997). The number of cytoskeletal genes is few in comparison

11

to higher eukaryotes, and yet many of the functions of MTs are conserved. Greater than 70 % of the amino acid residues of β-tubulin in yeast are identical to that of higher eukaryotes (Neff et al., 1983; Barnes et al., 1992; Reijo et al., 1994).

Tubulin from lower eukaryotes and higher eukaryotes are capable of coassembly into MTs *in vitro* (Kilmartin, 1981). Chimeric constructs composed of 75 % of the chicken β-tubulin-2 gene (forming the N-terminal portion of the protein) and 25 % of *S. cerevisiae* β-tubulin gene (forming the C-terminal portion of the protein), when expressed in mouse 3T3 cells, produced functional protein that associated with the endogenous α-tubulin, and coassembled with endogenous tubulin heterodimers into functional MTs (Bond et al., 1986; Fridovich-Keil et al., 1987). However, chimeric constructs that contained additional 5' yeast β-tubulin sequence, when expressed were less stable than the chimeric constructs containing 25 % yeast tubulin and failed to assemble into MTs (Fridovich-Keil et al., 1987). The data from these chimeric proteins showed that although tubulin is highly conserved, higher eukaryotic tubulin may have evolved so that proteins that recognize and interact with it cannot do the same with yeast tubulin.

Many studies have uncovered information on the function of MTs by genetic methods. Since the entire genome has been completely sequenced, and since *S. cerevisiae* is amenable to manipulation by genetic and molecular biological techniques, it is much easier to determine clearly the function of MTs and interacting

12

players in yeast. With respect to MT function, the significance of many genes and proteins throughout the cell cycle has been determined by examination of phenotypes of mutants, and those phenotypes resulting from addition of antimitotic drugs. However, these studies stop short because they rely on gross defects in MT function; the effect of mutations and drugs at the molecular level has not been examined. Nevertheless, yeast is probably the best system to carry out mutational structure-function studies on tubulin.

Until recently, two of the drawbacks of using yeast as a model system for the study of MTs had been the inability to visualize individual MTs *in vivo*, and the difficulty of obtaining sufficient quantities of pure yeast tubulin to perform *in vitro* biochemical studies. It has become possible to visualize yeast MTs *in vivo* by the expression of green fluorescent protein (GFP)-linked tubulin constructs in living cells (Straight et al., 1997, 1998; Carminati and Stearns., 1997). Thus, as in higher eukaryotes, the dynamic properties of MTs, both *in vitro* and *in vivo* can now be examined, but in a much cleaner, simpler system in which specific alterations to the protein can be made. *S. cerevisiae* has only one β-tubulin gene, TUB2 (Neff et al., 1983), and two α-tubulin genes, TUB1 and TUB3 (Schatz et al., 1986a, b). Because of the lack of multiple isotypes of β-tubulin, the effect that any mutation in TUB2 has on the overall structure and function of the heterodimer can be examined. With this system, the dynamic instability properties of the MT polymer and the effects on the drug binding capacity of tubulin and/or MTs composed of the mutated β-tubulin can be readily assessed.

13

Dynamics of *S. cerevisiae* cytoplasmic microtubules

Microtubules in yeast are responsible for several processes in the life cycle of the organism. There are two distinct populations of MTs in yeast cells: the nuclear MTs (nMTs) which form the spindle and are enclosed within the nuclear membrane, and the cytoplasmic MTs (cMTs) which exist outside the nucleus, eminating from the spindle pole bodies than are embedded in the nuclear membrane (Byers and Goetsch, 1975; Pillus and Solomon, 1986). Besides the segregation of chromosomes by the kinetochore MTs during mitosis, the cMTs also have very important roles in mitosis, ensuring that the spindle is correctly positioned so that proper segregation of chromosomes occurs between mother and daughter cells (Botstein et al., 1997). Unlike higher eukaryotic cells, the plane of cell division is predetermined by the position of the bud (emerging daughter cell), not the position of the spindle or metaphase plate. During vegetative growth, cMTs are important players in the migration of the nucleus to the bud neck, spindle orientation, movement of spindle through the bud neck (Botstein et al., 1997). Because the nuclear envelope does not break down during the cell cycle, the MTs that make up the spindle are in a very different environment from the cMTs (McIntosh and O'Toole, 1999). cMTs also are important in karyogamy (Botstein et al., 1997). In mating cells, the cMTs search for the site where the mating projection (shmoo tip) will form. Maddox et al., (1999)

14

showed that a stable attachment is made to the cell cortex by cMTs, and a bundle of cMTs forms between the shmoo tip and the spindle pole body. Shortening and growth of the cMT bundle causes the nucleus to oscillate, eventually reaching the tip of the schmoo projection. Fusion of nuclei from cells of opposite mating type occurs after the internuclear MTs shorten and bring the nuclei close together (Maddox et al., 1999).

Carminati and Stearns (1997) showed that GFP-tubulin fusion protein, expressed from a galactose-inducible plasmid construct, incorporated into the MT lattice and did not affect normal MT function. The cMTs, as well as the spindle, could be readily visualized by fluorescence microscopy. cMT dynamics were found to be differentially modulated during the cell cycle. Also, by examination of cMTs in dynein-mutant cells, it was determined that distinct interactions with the cell cortex were associated with spindle orientation and movement. Maddox et al. (2000) determined by fluorescent redistribution after photobleaching (FRAP) and fluorescent speckle microscopy (FSM) that the MTs in the yeast spindle did not treadmill, and that yeast cMTs exhibited only dynamic instability (dynamics occuring only at the plus end of the cMTs).

Davis et al., (1993, 1994), Sage et al., (1995a, b) and Gupta (2001) have taken advantage of the utility of yeast as a genetic, cytological and biochemical model organism for the analysis of the importance of different segments of the β-tubulin

15

sequence with respect to MT function. The β-tubulin sequence was altered, and the effects of the mutations were examined at both the phenotypic and molecular levels. The mutated segments were the putative GTP binding and colchicine (CLC) binding sites, and the 6 highly conserved cysteine residues.

By comparing amino acid sequences of several members of the GTPase superfamily, sequences in β-tubulin thought to be involved in GTP-binding were identified (Sternlicht et al., 1987). Specific mutations in TUB2 were created by site-directed mutagenesis, and a model for the GTP-binding site on β-tubulin was tested (Davis et al., 1993, 1994; Sage, 1994; Sage et al., 1995a, b). The significance of these changes in the protein sequence to the structure/function of tubulin was analyzed by observing the *in vivo* effects on cell growth at a gross level, as well as the more subtle *in vitro* effects on nucleotide binding, GTP-hydrolysis rate, polymer mass and MT dynamics. From this body of work, Davis et al., (1993) and Sage, (1994) were able to rule out two regions and substantiate one region of the β-tubulin sequence that had been proposed to interact with GTP. The KGHYTEG sequence (amino acids 103 to 109) was identified by Sternlicht et al., (1987) to be homologous to the phosphate binding motif GXXXXGK, but in the reverse orientation in β-tubulin. Mutations in this region were found to affect MT-dependent GTPase activity (Davis et al., 1994). Mutations to the DAKN (amino acids 295 to 298) and DNEA (amino acids 203 to 206) sequences, equivalent to the NKXD and DXXG/A motifs, did not affect the GTPase activity. Davis et al., (1993, 1994), Sage (1994), and Sage et al., (1995a, b)

16

also confirmed that the GTPase activity of tubulin modulated MT dynamics. Additionally, their data suggested that the cell monitors MT dynamics, and changes in dynamics at mitosis can be detected by cell cycle control mechanisms.

The anitimitotic drug colchicine was the first drug found to bind to tubulin (Borisy and Taylor, 1967a, b; Wilson and Friedkin, 1967). Binding poorly or not at all to the MT, CLC exerts its effects through forming a complex with soluble tubulin. The tubulin-colchicine (TC) complex is formed in a 2-step manner (reviewed in Hastie, 1991). The first step of the binding process is rapid and reversible, while the second step is a slower, poorly reversible conformational change. The MT lattice is stabilized and MT dynamics are suppressed when very few molecules of the TC complex are incorporated into the polymer; tubulin exchange at the ends of the MT is inhibited by substoichiometric concentrations of TC complex (Skoufias and Wilson, 1992; Panda et al., 1995). MT stabilization occurs at concentrations far below what is necessary to cause MT depolymerization. Low concentrations of CLC decreased the rates of growth and shortening in MTs formed *in vitro* from purified bovine brain tubulin (Panda et al., 1995). CLC also decreased the frequency that MTs transitioned from growth to shortening, and increased the frequency of transitions from shortening to growth or attenuation. The percentage of time MTs were in an attenuated state increased. The overall stabilization of MTs by low concentrations of CLC is reflected by the decrease in the total rate of dimer exchange (Panda et al., 1995).

17

According to Downing and Nogales (1998, 1999), the colchicine binding site is located at the interface between the α and β subunits, in the center of the dimer. When positioned within the MT lattice, the binding site is on the lumen side of the MT, similar to the taxol binding site. The taxol binding site was resolved because the drug was bound to the Zn^{++} sheet during the crystallography. However, their determination of the CLC binding site is based on the cross-linking studies of Bai et al., (1996) and Uppuluri et al., (1993). CLC binds to the tubulin dimer and causes a conformational change, much like the conformational change that occurs after hydrolysis of GTP to GDP at the E-site of the dimer (Downing and Nogales, 1998, 1999). When this dimer in a 'kinked' conformation assembles into the MT lattice, it may distort the lattice, impeding the ability of additional dimers to polymerize into the lattice efficiently (Skoufias and Wilson, 1992; Wilson et al., 1999).

The putative CLC binding site, as proposed by Burns (1992), was defined by correlating CLC binding association constants with the primary amino acid sequences of β-tubulins from a number of different organisms. The sequences used in the analysis were restricted to purified β-tubulin isoforms used in CLC binding studies. It was suggested that the residues around amino acid 316 were important determinants of the relative affinities of β-tubulin for CLC. The mutagenesis of TUB2 at the putative CLC binding site, conducted by Sage (1994) was designed and accomplished prior to the solving of the 3D structure of tubulin. However, the putative CLC-binding site, as proposed by Burns, resides in a pocket at the surface of

18

the dimer, and positioning of aa316 in the 3D structure places it in the same vicinity

as the CLC site proposed by Downing and Nogales (1998, 1999) (see Figure 1.1A

and B, and Figure 1.2).

Figure 1.2: Positioning of colchicine in β-tubulin subunit. From Downing and Nogales, 1998. β-tubulin subunit on the bottom, α-subunit on top. See Figure 1.1B for sequence information.

19

Colchicine binds vertebrate brain tubulin with a mean binding constant of 1.8×10^6 M^{-1} (Burns, 1992). In polymerization inhibition studies with purified bovine brain tubulin, CLC inhibited polymerization by 50 % at a concentration of 12.9×10^{-6} M while benomyl inhibited polymerization at a concentration of 58.3×10^{-6} M (Friedman and Platzer, 1978). CLC bound to mycelial extracts from *Aspergillis nidulans* (presumably to tubulin) with a binding constant of 2.5×10^5 L/mol [$K_d = 4$ μM] (Davidse and Flach, 1977). Methyl benzimidazol –2-yl carbamate (MBC), which is thought to be the active breakdown product of benomyl, bound to mycelial extracts from wild-type *A. nidulans* at 4.5×10^5 L/mol [$K_d = 2.2$ μM] (Davidse and Flach, 1977). The binding of MBC to tubulin is competitively inhibited by nocodazole, another member of the benzimidazole family, and also colchicine, although only to a slight extent (Davidse and Flach, 1977) (inhibition constant for CLC is 0.4×10^{-3} M). Benomyl and the benzimidazole family of compounds binds various tubulins with varying affinities. As the binding constants demonstrate, colchicine binds mammalian tubulin much better than fungal tubulin, while benomyl binds fungal tubulin better than mammalian tubulin. The differences in binding affinities may be due to the slight but important differences in the tubulin sequences between higher and lower eukaryotes. CLC fails to inhibit mycelial growth of *A. nidulans* on agar (Davidse and Flach, 1977); it may be that CLC has difficulty passing through the cell wall and cell membranes, which also could contribute to its lack of efficacy in inhibiting growth of lower eukaryotic cells.

20

Preliminary studies on the effect of benomyl, nocodazole and colchicine on the *in vitro* polymerization of yeast tubulin purified from the heterozygous diploid control strain ADY101:pADwt (TUB2/tub2-590) and CLC8 (CLC8/tub2-590), which was mutated to resemble mammalian tubulin at the putative CLC binding site (Burns, 1992), confirmed the results of the assay for drug sensitivity at the cellular level. The mutant strain's tubulin was 5 and 16 times more sensitive to CLC-site drugs than the WT tubulin (benomyl: 200 μM for WT and 12.5 μM for CLC8; nocodazole: 2.5 μg/ml for WT and 0.5 μg/ml for CLC8) (Sage, 1994; K.W. Farrell, personal communication). The antimitotic drugs were less effective on the whole cell, indicating perhaps that the drugs were unable to pass through the yeast cell wall as readily as cell membranes. MT polymerization assays also showed drug sensitivity differences not readily revealed by cell growth assays; cells were sensitive to colchicine at a concentration of 10 mM, while MT polymerization assays showed sensitivity at 0.5 mM (Sage, 1994; K.W. Farrell, personal communication). What effects these mutations have on the actual dynamic properties of MTs remained to be determined.

The original aim of this project was to examine the dynamic properties of yeast tubulin, both *in vitro* and *in vivo*. Despite much time and effort spent in modifying the protein purification methods of Barnes et al., (1992) and Davis et al., (1993), it became apparent that it would not be possible to purify sufficient amounts of yeast tubulin to homogeneity by these methods to examine MT dynamics *in vitro* with

21

confidence (see Appendix A). Around the same time, it became possible to image yeast MTs *in vivo* using GFP-linked tubulin constructs. It was decided that because of the problems associated with the *in vitro* methodology, the project would focus on the dynamic properties of yeast MTs *in vivo*. While the *in vivo* approach placed minor limitations of the types of mutations that could be examined (e.g., tubulin mutations that are haploid lethal must be examined in a wild-type background), the methodology proved to be excellent for the assessment of how alterations in the β-tubulin sequence of the putatuve CLC binding site affected the dynamic properties of yeast MTs.

22

Chapter II: Phenotypic characterization of wild-type

and mutant (CLC) yeast strains

23

Chapter II: Phenotypic characterization of wild-type and mutant (CLC) yeast strains

Introduction

In order to examine the role of the putative colchicine binding site in regulating MT function, several mutants were generated in the β-tubulin gene (Table 2.1; Fig. 2.1, Sage, 1994). The CLC mutants previously generated in the Wilson lab (Sage, 1994) were thoroughly characterized at the phenotypic level. This was necessary to determine whether any of the mutant strains had any gross discernible defects in MT function. The mutants were created in a diploid background where one copy of the β-tubulin gene was pseudo wild-type, with the carboxyl-terminal 12 amino acids deleted (tub2-590), while the other copy was either the full length wild type or the mutated β-tubulin gene (TUB2 or CLC, respectively). The mutations were created in a pseudo wild-type background for two reasons: first to support any β-tubulin mutation that could render the mutant strain recessive lethal, and second, to be able to check with antibody staining that both pseudo wild-type and mutant β-tubulin coassembled into the MTs.

The strains were constructed in this manner to allow tracking of both gene products in mutant strains, which were not viable in the haploid form. Expression of the protein products of both copies of the β-tubulin gene was followed *in vivo*, by antibodies

24

generated to the last 12 amino acids ('anti-tail') or the 11 amino acids immediately preceding the last 12 amino acids ('anti-stump') of β-tubulin (Davis et al., 1994; Sage, 1994). It was shown by immunofluorescence of the cells that both β-tubulin isotypes coassembled into the MTs (Sage, 1994).

The truncated (pseudo wild-type) tubulin is fully functional, and the deleted C-terminal 12 amino acids did not affect mitotic or meiotic processes (Katz and Solomon, 1988); the only phenotype the truncation confers was the slight increase in sensitivity to the antimitotic drug benomyl in strains heterozygous for the truncation (Katz and Solomon, 1988, Sage et al., 1995a). The full length wild-type and mutated β-tubulin genes had the URA3 metabolic marker gene cloned into the downstream sequences flanking TUB2/CLC. When the constructed mutations were integrated into the genome, these strains were stable and the wild-type copy of TUB2 was replaced with the mutant copy of the β-tubulin gene.

Phenotypes, which reflect MT function, were characterized both in the wild-type and the mutant strains. These analyses were carried out to determine which of the mutant strains would be most appropriate for characterization of MT dynamics *in vivo*. The majority of the phenotypic characterizations used here assessed the function of vegetative cells, that is, cells that were dividing mitotically. Doubling time (DT) is a measure of the strain's ability to grow vegetatively. Mitotic growth requires functional MTs for spindle positioning and segregation of the chromosomes.

25

Characterization of bud growth in an unsynchronized population of cells can reveal

problems that are detected by the cell cycle check point, some of which may involve

MT driven processes. Nuclear migration is a MT-dependent process that can be

examined simultaneously with bud growth; problems arising from compromised cMT

function can be distinguished from defects in kinetochore and spindle MT function.

Stresses such as high and low temperatures and antimitotic drugs can uncover subtle

alterations in tubulin function during vegetative growth. Compromised MT function

during meiosis were assessed first by checking the ability of the diploid strains to

sporulate, and second, by examination of the segregation of metabolic markers in the

four haploid spores of the tetrad.

Table 2.1: β–tubulin genotype and amino acid sequences of the original CLC mutant yeast strains

strain	β–tubulin genotype	amino acid sequence	marker genotype
ADY101:pADwt	TUB2/tub2-590	310-YLTVAAFFRGKVSVK-324	URA+
CLC1	CLC1/tub2-590	......V........	URA+
CLC2	CLC2/tub2-590	..........R....	URA+
CLC3	CLC3/tub2-590	........T.RM.ML	URA+
CLC5	CLC5/tub2-590	..........RM.L.	URA+
CLC7	CLC7/tub2-590	..........RM.M.	URA+
CLC8	CLC8/tub2-590	......V...RM.M.	URA+
CLC9* bovine brain	CLC9	........W...... 310-YLTVAAVFRGRMSMK-324	URA+

* haploid strain

26

When possible, the haploid forms were examined indepth since they carry only the mutated form of β-tubulin. For mutants for which the meiotic products were not viable, the diploid forms were used (i.e., one copy of the pseudo wild-type and one copy of the mutant β-tubulin gene) and compared to the appropriate diploid control, ADY101:pADwt (TUB2/tub2-590).

Figure 2.1: 3-D structure of the tubulin dimer. α-tubulin on the left, β-tubulin on the right. The amino acid stretch 310-324 is highlighted in pink. The position of specific amino acid changes is highlighted in green. See Table 2.1 for specific mutants.

27
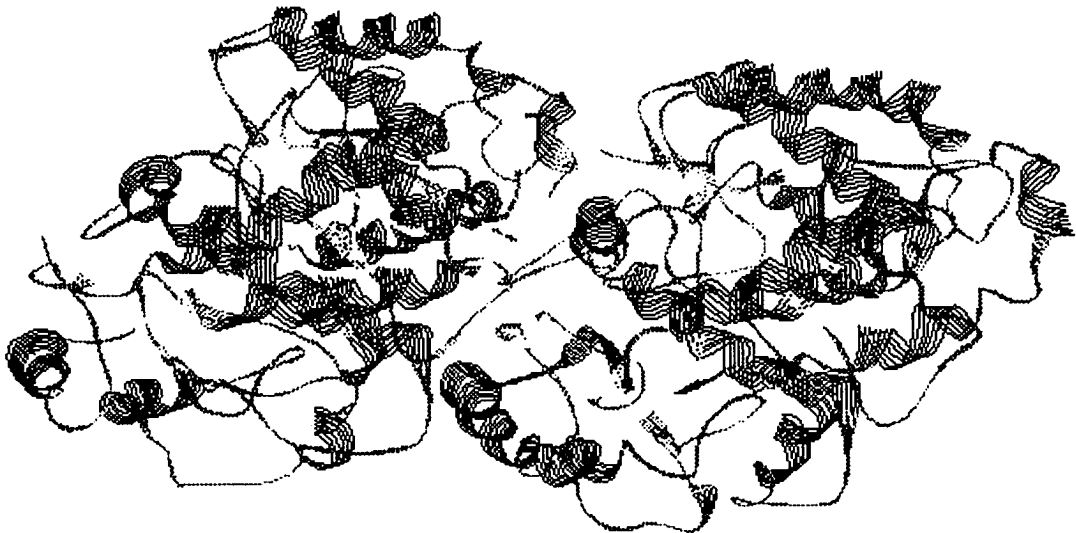
Materials and Methods

1) Cell doubling times: Starter cultures (10 ml) of all yeast strains were grown with agitation, overnight (16 h) in YPD (10 % yeast extract, 20 % gelysate peptone, 2 % dextrose, plus 20 % bactoagar for plates) at 30 °C. At t = 0, 50 ml of fresh YPD in 250 ml Erlenmeyer flasks was inoculated to an A_{600} of approximately 0.1 with the appropriate amount of the original overnight yeast culture. After inoculation, a 1 ml sample was taken from each Erlenmeyer flask, in a sterile manner, and the absorbance at A_{600} determined; absorbance is an indirect measure of cell density. The cultures were returned to the 30 °C incubator and allowed to grow on a shaker. One ml samples were taken for absorbance measurements at approximately 2 hr intervals. Vegetative growth was measured over 5 doubling times by recording the increase in absorbance at A_{600}, or by direct cell counting using a hemocytometer. To obtain the DT, the natural log of the absorbancy values or cell counts, was plotted against time, and the slope of the linear portion of the plot was used in the equation:

$$DT = 0.693/slope$$

DT is a good initial indicator of MT function, as vegetative growth requires functional tubulin in cMTs, and in the MTs forming the mitotic spindle.

2) Bud morphology: Emergence and size of the daughter bud in *S. cerevisiae* is an indicator of position in the cell cycle: unbudded cells are in G1, small budded cells are in S phase, and large budded cells are in G2/M (Pringle and Hartwell, 1981). Cells were fixed and stained by the method of Pringle et al., (1991) then scored by

28

light microscopy. At least 300 cells were scored. By determining the number of cells in an unsynchronized population at each stage of budding (unbudded, small budded, and large budded, where the bud is >75% of the diameter of the mother cell) and comparing those to wild-type proportions, strains with functional defects detected by the cell cycle checkpoints can be identified. For example, an increase in the proportion of cells in the unbudded and small budded stages is an indicator of growth and DNA synthesis problems, while an increase in the proportion at the large budded stage is a hallmark of mitotic defects.

3) Nuclear migration: Concurrent with bud morphology assessment, nuclear migration during mitosis can also be followed by staining the nuclei with the DNA intercalator 4', 6-diamidino-2-phenylindole dihydrochloride (DAPI). Using fluorescence microscopy, the position and state of the nucleus can be assessed in large budded cells, the morphological state when mitosis occurs. Shifts in the proportions of cells that have single nuclei, a single nucleus at the neck between mother and daughter cells, and divided nuclei, can indicate defects in mitotic segregation. Also, the position of divided nuclei with respect to the mother and daughter cells can indicate whether there are defects in spindle positioning, which is controlled in part by the cMTs and dynein (Palmer et al., 1992; Sullivan and Huffaker, 1992; Carminati and Stearns, 1997).

29

4) Temperature sensitivity: All strains were tested for the ability to grow at low (16-18 °C) and high temperatures (37 °C). Cultures grown overnight in YPD media at 30 °C were 'spotted' in 2 µl aliquots on YPD plates as undiluted and diluted (1:10 and 1:50) samples. Growth was assessed after 3 days at the specified temperatures. Changing the growing conditions in this manner may reveal changes in MT function not readily detectable at 30 °C. Many conditional mutants are found to be caused by point mutations in the gene of interest. Since the CLC mutants are altered in only 1 to 5 codons in the β-tubulin sequence (Table 2.1), it is possible that they may also be conditional mutants.

5) Tetrad formation: Meiosis, which involves the ability to sporulate, segregate chromosomes correctly and form tetrads, requires proper meiotic spindle function. In yeast, the two meiotic divisions take place within a single nuclear mass (Moens and Rappaport, 1971). Meiosis involves a first division with one spindle in meiosis I which separates the homologous chromosomes, followed by the dissolution of the spindle and a second division with 2 new spindles that separate the sister chromatids (meiosis II), thereby generating the four spores in a tetrad.

ADY101:pADwt (control strain) and all diploid CLC strains (CLC1, 2, 3, 5, 7, 8) were grown at 30 °C on presporulation plates, then transferred to supplemented sporulation plates and reincubated at 30 °C. Sporulation was determined by microscopy, starting 6 to 10 days from the transfer date. When tetrads were visible, a

30

sample of the sporulated strain was transferred onto dissection plates. Tetrads were dissected using a Singer MSM System Series 200 micromanipulator. After dissection, the dissection plates were incubated at 30 °C. When colonies were visible and had grown to at least 1 mm in diameter, a small sample was suspended in sterile water. The genotype of each spore in a tetrad was determined by 'spotting' 2 µl samples onto a variety of minimal media 'drop-out' (DO) plates. All tetrads were examined for 2+/2- segregation of the URA marker. Spores that carried the URA+ marker (that is, prototrophic for uracil) were challenged with alpha (α)-factor. α-factor is a mating hormone that stimulates the production of schmoo processes in haploids that are of the a mating type. For those that were of a mating type, the β-tubulin gene was then sequenced to confirm that the mutations in β-tubulin were intact. (Haploids of a mating type were maintained for synthetic lethality tests with various checkpoint mutant strains.) Impaired sporulation was a characteristic found in other β-tubulin mutants (Davis et al., 1994; Sage et al., 1995a,b; Sage, 1994). Table 2.2 indicates the haploid viability of diploid CLC strains.

6) **Drug sensitivity:** Antimitotic drugs such as benomyl, nocodazole, colchicine, and curacin A (Figure 2.2) are known to affect the stability of MTs, and the ability of tubulin to polymerize into MTs. They are commonly used tools for the investigation of tubulin function and associated phenotypes. Benomyl, its breakdown product carbendazim, and nocodazole, are all members of the benzimidazole family of compounds. The benzimidazoles are known to compete with colchicine for binding

31

to tubulin (reviewed in Lacey, 1988). Curacin A has also been shown to compete with colchicine (Blokhin et al., 1995). Since the CLC mutants were created by altering the putative binding site of colchicine, it is informative to determine whether there is a change in sensitivity to drugs which are known to compete for the same binding site. Since sensitivity to certain drugs can be temperature dependent, the strains were 'spotted' in 2 μl volumes onto YPD or supplemented SD plates containing a range of drug concentrations (0.5 to 70 μg/ml benomyl, 0.5 to 5 μg/ml nocodazole (1.7 μM-17 μM), 1 to 10 mM colchicine, 1 to 10 μM curacin A), incubated for 3 days at 25 °C and 30 °C, then scored for growth (Botstein et al., 1997). Sensitivity to a drug was defined as the minimum drug concentration required to alter the growth of cells, relative to untreated cells. The extent of growth of each 'spot' on each plate containing drug was compared to the growth of the equivalent 'spot' on the control plate which did not contain any drug. Stock concentrations of all drugs were dissolved in DMSO, and stored at –20 °C. Benomyl, which was a kind gift from R.Ostrum, DuPont, is 95 % pure; the concentration of this drug is commonly reported in terms of μg/ml rather than molar units. Changes in the ability of the cells to grow in the presence of antimitotic drugs indicate whether the mutations have indeed affected the ability of the tubulins to bind drug *in vivo*.

Figure 2.2: Chemical structures of the antimitotic compounds colchicine, carbendazim, benomyl, curacin A and nocodazole.
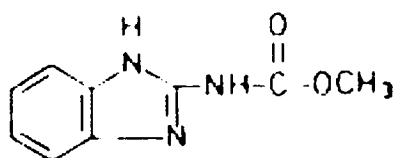
carbendazim (MBC)
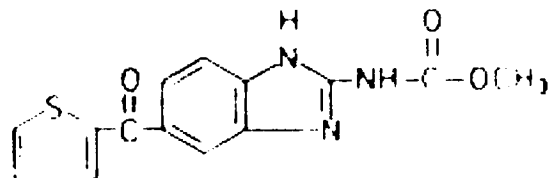
nocodazole (NOC)
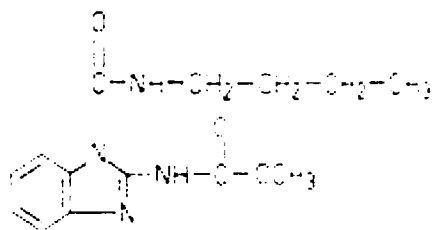
benomyl (BEN)
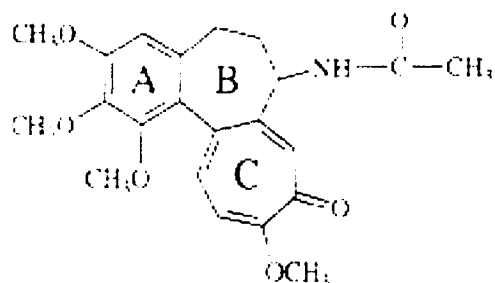
colchicine (CLC)

curacin A

33
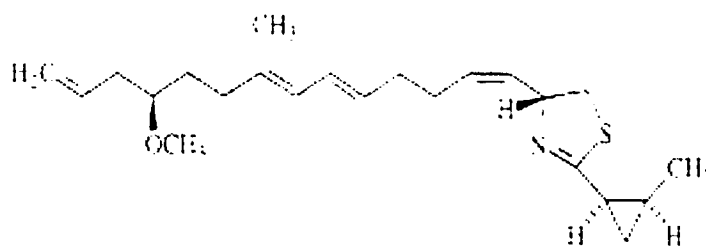
Results

The phenotypes of the *S. cerevisiae* strains mutated in the putative colchicine binding

site were thoroughly characterized to determine whether any of the strains showed

phenotypes indicative of altered MT function. Several of the seven diploid CLC

strains showed striking phenotypes. The most revealing of the six phenotypic tests

were tetrad formation, the doubling time, and the drug sensitivity assays (see Tables

2.2-2.4, Figure 2.3A, 2.3B).

The doubling times for the strains, determined by monitoring vegetative growth at 30

°C on YPD, were in accordance with doubling times determined by Sage (1994)

(Table 2.2). There were some slight differences which could be due to the differences

in the media used; Sage, 1994, used supplemented (SD) minimal media at 30 °C. The

doubling time for the CLC8 strain, was longer than that of the wild-type strain on

YPD media, but it was not as long as determined previously on supplemented SD

media (247 min, Sage, 1994). The doubling times ranged from 105 to 110 min for

the wild-type strains, and 94 to 141 min for the various mutant strains.

All seven diploid strains and the haploid strain CLC9 grew well at cooler (16 - 18 °C)

as well as at 37 °C, indicating that the β-tubulin mutations did not exert a dominant

phenotype at these temperatures (Table 2.4). Tubulin in the wild-type and mutated

strains were functional at those temperatures and could form MTs that supported

34

vegetative growth. While other studies (Huffaker et al., 1988, Reijo et al., 1994; Li et al., 1996) have found that some point mutants are conditional mutants, none of the CLC mutants were found to be temperature sensitive.

Four of the seven diploid strains, when sporulated, did not segregate the metabolic markers in a 2+/2- fashion among the spores in the tetrad (Table 2.2). The tetrad dissection results were unusual, with some markers on occasion segregating 3+/1-, for example. The results were inconsistent and seemed random, as no clear pattern of segregation was observed. There was no lethality observed with the segregation of the URA marker, which was linked to either the wild-type (TUB2) or mutated (CLC) β-tubulin gene; presence of the mutated β-tubulin alone was not lethal. However, the irregularity of marker segregation upon sporulation of CLC1, 3, and 5, suggests that perhaps these strains were aneuploid.

One strain, CLC8, did not sporulate at all, indicating perhaps a meiotic defect. Since this strain is able to grow vegetatively, the meiotic spindles may be more sensitive to the effects of the mutated β-tubulin. Sage (1994) showed by antibody staining that both the mutated and pseudo wild-type β-tubulins coassembled into the cellular MTs equally well in this strain. Because the strain did not sporulate, it is not known whether a haploid strain having CLC8 as the sole copy of β-tubulin would be viable, although from these results it is presumed that it would not.

35

Figure 2.3A: Benomyl sensitivity of wild-type and mutated yeast strains (diploids). On each plate, left to right: ADY101:pADwt, CLC1, CLC2, CLC3, CLC5, CLC7, CLC8. Row 1, left to right: plate 1, control no drug, plate2, 2μg/ml benomyl, plate 3, 5μg/ml benomyl; Row 2, left to right: plate 4, 10μg/ml benomyl, plate 5, 20μg/ml benomyl, plate 6, 30μg/ml benomyl; Row 3, left to right: plate 7, 50μg/ml benomyl, plate 8, 70μg/ml benomyl.

36
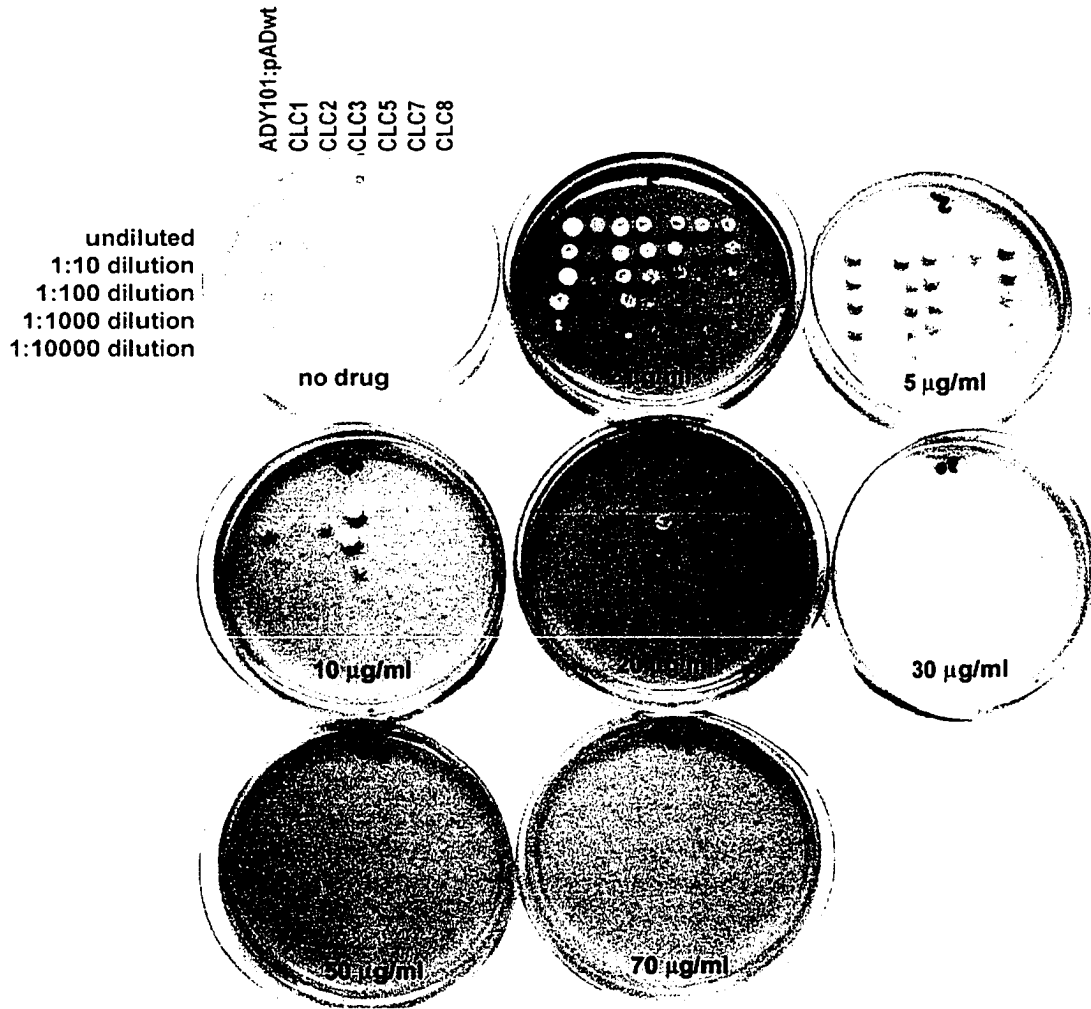
Figure 2.3B: Benomyl sensitivity of wild-type and mutated yeast strains (haploids). On each plate, left to right: ADY101:pADwt-A6B (full length), ADY101:pADwt-1Ia (truncated), CLC2-1D, CLC7-1'A, CLC9. Row 1, left to right: plate 1, no drug, plate 2, 2μg/ml benomyl, plate 3, 5μg/ml benomyl; Row 2, left to right: plate 4, 10μg/ml benomyl, plate 5, 20μg/ml benomyl, plate 6, 30μg/ml benomyl; Row 3, left to right: plate 7, 40μg/ml benomyl, plate 8, 50μg/ml benomyl, plate 9, 60μg/ml benomyl; Row 4: plate 10, 70μg/ml benomyl.
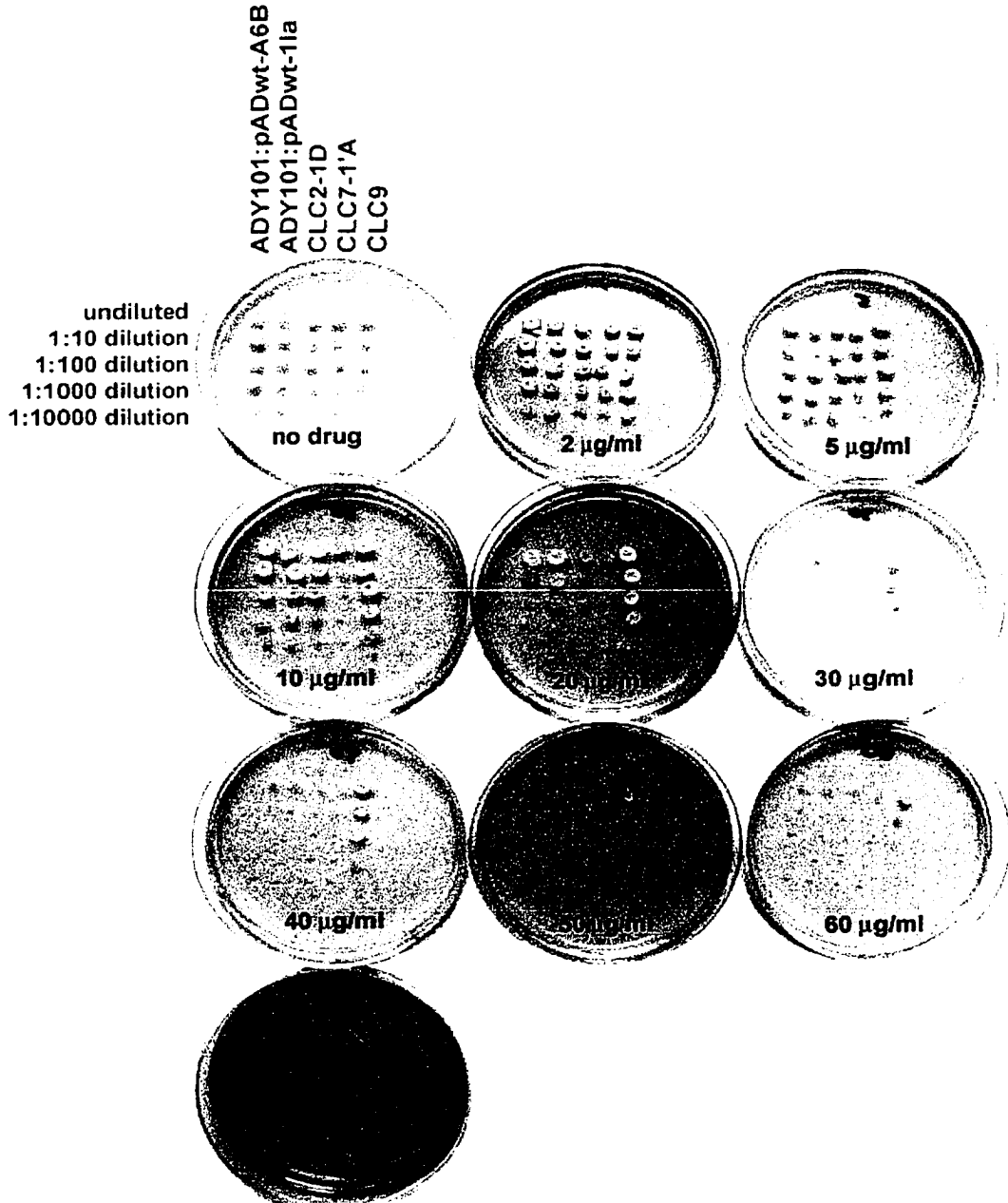
Table 2.2: Tetrad formation and doubling times of CLC yeast strains

strain	ploidy	tubulin genotype	sporulation/ haploid viability	n	doubling time ± SD (min)
ADY101:pADwt	diploid	TUB2/ tub2-590	yes	8	110 ± 11
CLC1	diploid	CLC1/ tub2-590	no - irregular tetrad dissection results	7	121 ± 15
CLC2	diploid	CLC2/ tub2-590	yes	6	96 ± 8
CLC3	diploid	CLC3/ tub2-590	no - irregular tetrad dissection results	8	115 ± 14
CLC5	diploid	CLC5/ tub2-590	no - irregular tetrad dissection results	6	118 ± 15
CLC7	diploid	CLC7/ tub2-590	yes	5	95 ± 12
CLC8	diploid	CLC8/ tub2-590	no tetrad formation	6	141 ± 12
FY41*	haploid	TUB2		2	107 ± 5
ADY101-6B	haploid	TUB2		3	105 ± 3
CLC2-1D	haploid	CLC2		3	130 ± 13
CLC7-1'A	haploid	CLC7		4	94 ± 5
CLC9	haploid	CLC9		3	105 ± 11

* FY41 is the parental strain of CLC9

38

Table 2.3: Bud morphology and nuclear migration in wild-type and CLC yeast strains

strain	Bud Morphology (% of total cells)			Nuclear Migration (% of total cells) [% of large bud]		
	no bud	small bud	large bud	mother only	neck	both cells
ADY101:pADwt	65.9	19.8	14.4	6.5 [45.3]	1.2 [8.0]	6.7 [46.7]
CLC1	51.8	31.2	17.0	6.3 [40.9]	3.9 [23.2]	6.6 [38.7]
CLC2	61.3	25.0	13.8	4.8 [35.5]	2.9 [21.2]	6.0 [43.3]
CLC3	64.9	21.9	13.2	6.1 [46.0]	1.2 [9.0]	5.9 [45.0]
CLC5	73.4	19.9	6.6	2.2 [32.2]	1.6 [23.6]	2.9 [44.3]
CLC7	58.7	25.1	16.3	6.8 [41.5]	4.4 [26.8]	5.1 [31.3]
CLC8	74.1	14.0	11.9	6.3 [53.4]	0.7 [6.0]	4.8 [40.7]
FY41	54.8	20.3	24.3	9.6 [39.7]	2.1 [8.6]	12.5 [51.7]
ADY101-A6B	67.3	15.7	17.0	7.2 [42.3]	2.6 [15.1]	7.3 [42.6]
CLC2-1D	62.3	18.9	21.0	8.2 [39.1]	1.7 [8.1]	11.1 [52.9]
CLC7-1'A	59.4	15.4	25.1	12.4 [49.5]	3.9 [15.6]	8.8 [34.9]
CLC9	51.1	23.5	25.4	11.7 [46.1]	2.7 [10.5]	11.3 [44.6]

39

Table 2.4: Drug and temperature sensitivities of haploid and diploid yeast strains

strain (diploid/haploid)	benomyl‡ (µg/ml)		colchicine (10 mM)	nocodazole (µM)	curacin A (10 µM)	temperature sensitivity	
	25 °C	30 °C	25 °C	25 °C	25 °C	16 - 18 °C	37 °C
ADY101:pADwt (d)	15	20	NE*	≥ 15	NE*	NE	NE
CLC1 (d)	8	4	NE	≥ 15	NE	NE	NE
CLC2 (d)	15	16	NE	≥ 15	NE	NE	NE
CLC3 (d)	30	30	NE	≥ 15	NE	NE	NE
CLC5 (d)	8	8	NE	13.3	NE	NE	NE
CLC7 (d)	8	8	NE	≥ 15	NE	NE	NE
CLC8 (d)	6	2	NE	≥ 15	NE	NE	NE
FY41 (h)	30	30	NE	≥ 15	NE	ND†	ND
ADY101-6B (h)	20	30	NE	≥ 15	NE	ND	ND
CLC2-1D (h)	20	30	NE	≥ 15	NE	ND	ND
CLC7-1'A (h)	15	16	NE	≥ 15	NE	ND	ND
CLC9 (h)	>70	>70	NE	≥ 15	NE	NE	NE

‡ concentration at which growth is inhibited

* No apparent effect on growth (NE)

† Not determined (ND)

40

Bud morphology and nuclear migration in the diploid and haploid strains did not reveal any obvious shifts in the cell cycle, although there was a wide range in the proportions at each stage of the cell cycle as designated by the size of the bud (Table 2.3). None of the strains showed a shift in the proportion of the population in the large budded stage (G2/M), which is a hallmark of mitotic defects. Nuclear migration appeared to be unaffected in all mutant strains, indicating that spindle positioning (a function of cMTs) and anaphase (nuclear MT function) occurred normally. Since none of the strains appeared to be temperature sensitive, it was not necessary to perform the bud morphology and nuclear migration experiments at temperatures other than 30 °C.

The drug sensitivity tests were the most valuable in terms of revealing alterations in MT function among the yeast strains examined (Figures 2.3A and B, Table 2.4). The benomyl sensitivities of the wild-type strains were very similar to those reported by Reijo et al., (1994). While wild-type strains were affected by benomyl concentrations ranging from 15 to 30 μg/ml (depending on the temperature and ploidy), many of the diploid CLC strains were sensitized to the drug. The strains CLC1, CLC5, CLC7 and CLC8 were sensitive to less than 10 μg/ml benomyl. The mutant haploid strains (CLC2-1D, CLC7-1'A, CLC9), derived from the original diploid strains, did not follow this trend. The haploid strains were less sensitive to benomyl than their diploid counterparts, a characteristic found in other strains (Reijo et al., 1994). CLC7-1'A was sensitive at a benomyl concentration that was half of the wild-type

41

strain's sensitivity. CLC9 was the only mutant strain (either haploid or diploid) that was super resistant to benomyl. It was able to grow at a concentration at the limit of solubility of the drug (> 70 μg/ml), which was 2 fold higher than the concentration at which the wild-type failed to grow.

None of the yeast strains showed increased sensitivity to the drugs nocodazole, colchicine, or curacin A. While the tubulin itself may be sensitized to the various drugs, the whole cell assay does not reveal any changes in drug sensitivity. Cells and tubulin of higher eukaryotes show higher sensitivity to these drugs than the cells and tubulin of yeast. It could be that these antimitotic drugs cannot pass through the yeast cell walls very well, or that the tubulin from yeast has a much lower affinity for these drugs than tubulin from higher eukaryotes. Sage (1994) and Farrell (personal communication) have indicated that purified tubulin from CLC8, in polymer assays, is more sensitive to various drugs than tubulin from wild-type cells. Benomyl inhibited *in vitro* polymerization of MTs from WT cells at 200 μM (61 μg/ml), while polymerization of tubulin from CLC8 cells was inhibited at 12.5 μM (3.7 μg/ml) (Sage, 1994).

Discussion

The budding yeast, *Saccharomyces cerevisiae*, is an excellent model organism with which to study the cytoskeletal protein tubulin. With only 3 genes encoding the α-

42

and β-tubulin genes, *S. cerevisiae* represents a relatively simple cell model for studying tubulin; phenotypes associated with alterations in either tubulin subunit can be directly related to changes in the tubulin sequence. The vast number of molecular and genetic techniques and tools available in yeast makes it possible to create mutants easily. With a short generation time, and easily identified phases of the cell cycle, mutations in tubulin that affect general MT-requiring processes such as vegetative growth and meiotic division, as well as more subtle tubulin-specific phenotypes such as antimitotic drug sensitivity, can be quickly screened. In this study, mutants with a series of alterations in the putative colchicine binding site of β-tubulin (Table 2.1) were characterized at the phenotypic level.

Based on the results of the phenotypic characterization, the two mutant strains that were most dramatically affected by mutations in β-tubulin were the haploid inviable, benomyl supersensitive strain CLC8, and the haploid viable, benomyl super resistant strain CLC9. The CLC8 strain is sensitive to 2-6 μg/ml benomyl while the CLC9 strain is resistant to greater than 70 μg/ml benomyl. CLC8 cells grow slower than the CLC9 cells (141 min and 105 min, respectively). The time in which wild-type strains double ranges from 105 min to 110 min. Besides the opposing drug sensitivities, and differences in doubling time, CLC8 and CLC9 strains are also interesting in that CLC9 cells have a single amino acid change in the stretch between 310 and 324, while CLC8 cells have 4 amino acid changes, making it identical to the mammalian protein sequence in that region (see Table 2.1). These two strains display opposing

43

phenotypes that will be useful in understanding the mechanism of action of benomyl as well as basic functional properties of tubulin.

The phenotypes of CLC8 cells indicate that the MTs in this strain are compromised. The β-tubulin in the CLC8 strain completely resembles mammalian β-tubulin in the putative CLC-binding region between amino acid 310 and 324, with changes to amino acids, 316, 320, 321, and 323. The strain is not viable in the haploid form, where the mutated β-tubulin (CLC8) is the only copy of β-tubulin in the cell. This in itself indicates that changing the sequence to that of mammalian tubulin in this region of the protein seriously compromises MT function. When the mutated β-tubulin gene (CLC8) is expressed with the truncated, pseudo wild-type tubulin (tub2-590), the strain is viable. However, even with a pseudo wild-type tubulin background, the CLC8 strain has phenotypes that reveal compromised MT function.

One indicator of compromised MT function is a lengthening in the doubling time for the strain. cMTs which can find the daughter bud and make stable attachments with cortical patches to properly align the spindle, as well as kinetochore MTs that can segregate chromosomes correctly, are necessary for vegetative growth to occur. The doubling time is 28 % longer for the CLC8 strain than for the wild-type strain, indicating that MTs in CLC8 cells are not functioning correctly. Because the proportions of the population in each phase of the cell cycle are not greatly different in CLC8 cells from that of wild-type cells, it is likely that the changes in the amino

44

acid sequence in β-tubulin in the CLC8 strain is altering the stability of the MTs. This should affect MTs throughout the life cycle of the cell, and not just at a particular phase. Also in support of this supposition is that the strain is also unable to form tetrads, indicating that the MTs are unable to carry out the two meiotic divisions. Finally, the MTs of CLC8 cells are super sensitive to the effects of benomyl; CLC8 cells fail to grow at 2-6 µg/ml benomyl, which is less than half the benomyl concentration that is required to stop vegetative growth of the wild-type strain (15-20 µg/ml). It is striking that these MT associated problems are evident even though in the CLC8 strain, half of the β-tubulin is the truncated, pseudo wild-type form (tub2-590).

In contrast to CLC8 cells, the β-tubulin mutation in CLC9 cells is a single amino acid change at position 318. This strain is viable when the mutated tubulin is the sole form of β-tubulin in the cell, unlike the CLC8 strain. While MT-requiring phenotypes such as the doubling time, nuclear migration, and bud formation are all similar to that of the wild-type strain, the CLC9 strain is over 200% more resistant to benomyl than the wild-type strain, and is able to grow in the presence of 70 µg/ml drug. Because all of the CLC strains were mutated in the putative CLC binding site in β-tubulin, the increased resistance of this strain to benomyl is extremely interesting, suggesting that the drug binding site has been affected. Given that the drug sensitivity seems to be the only phenotypic characteristic that has changed in

45

this strain, it appears that the change from arginine to tryptophan at amino acid position 318 drastically alters the ability of β-tubulin to bind benomyl.

A diploid form of the CLC9 strain was created by Huffaker et al., (1988), in which both copies of the β-tubulin gene was mutated (mutant tub2-402). This mutant was obtained in a screen for cells which failed to grow at 14 °C; its growth was completely blocked at 11 °C. At 26 °C, it behaved like the WT strain. However, when tested at 11 °C on supplemented SD media, the tub2-402 mutant displayed several interesting phenotypes. At this low temperature, the strain was cold-sensitive and cells blocked at the large budded stage (62 % compared to 20 % for WT). Nuclei were primarily undivided in the mother cell (81 % versus 22 % for WT cells), indicating that nuclear migration was compromised. Immunofluorescence microscopy examination of the arrested cells using antibodies against α-tubulin revealed that in 60-70 % of the arrested cells, what appeared to be cMTs were present, but mitotic spindles were absent. Nuclear fusion following karyogamy was unimpaired at 26 °C, but was reduced to 60 % of that in WT cells at 11 °C. Thus, when the CLC9 form of β-tubulin is challenged by very low temperatures, the MTs appear to behave in an aberrant manner. Cold temperature usually causes depolymerization of MTs; some of the MTs in the tub2-402 strain may be hypersensitive to cold-induced depolymerization. However, MTs of the tub2-402 mutant strain essentially behave like wild-type MTs at room temperature.

46

CLC8 and CLC9 are two strains of *S. cerevisiae*, mutated in the putative CLC binding site. They have been engineered differently from one another in the β-tubulin gene, and have very different phenotypic characteristics. While CLC8 has been engineered to resemble mammalian tubulin in the stretch of amino acids 310-324, CLC9 has a single amino acid change. Other studies that have examined mutations in the tubulin genes (TUB1, TUB3 and TUB2), have limited their examination of the consequences of mutations to tubulin to whole cell phenotypes (Huffaker et al., 1988; Li et al., 1996; Matsuzaki et al., 1988; Reijo et al., 1994, Richards et al., 2000; Stearns and Botstein, 1988; Thomas et al., 1985). While these studies have characterized their mutants by assessing many MT requiring functions, such as vegetative growth at various temperatures, and benomyl sensitivity, they have not examined what effect the mutations to tubulin have on the function of the MTs directly. None of these studies have looked at the effects of the mutations on the dynamic properties of MTs.

The examination of phenotypic characteristics in this chapter serves as the basis from which strains were chosen for the direct examination of MT dynamics *in vivo* (Chapters 3 & 4). How changes in tubulin sequence affect MT function will be assessed directly by determining the changes in MT dynamic parameters in the mutated strains, compared with the wild-type control strains. Also, since the mutations were directed toward a specific region of β-tubulin, namely the putative CLC binding site, the effects of these mutations on the dynamic instability properties of the MTs in the mutant cells were examined in the presence of benomyl.

Chapter III: *In vivo* Dynamics of Cytoplasmic Microtubules in the

Wild-type Diploid Yeast Strain ADY101:pADwt and the

Chimeric Diploid Yeast Strain CLC8

48

Chapter III: *In vivo* Dynamics of Cytoplasmic Microtubules in the Wild-type Diploid Yeast Strain ADY101:pADwt and the Chimeric Diploid Yeast Strain CLC8

Introduction

The kinetic parameters that characterize MT dynamic instability are different between those that occur with MTs *in vivo* and those that are observed *in vitro*. It has been well documented in higher eukaryotes that the MTs *in vivo* are much more dynamic that MTs assembled from purified tubulin *in vitro* (Cassimeris et al., 1988; Shelden and Wadsworth, 1993; reviews by McNally, 1996 and Desai and Mitchison, 1997). Not only are the dynamics different, but the behavior of MTs assembled *in vitro* are also different from that of MTs *in vivo*.

In *Saccharomyces cerevisiae*, the dynamic characteristics of MTs examined by *in vitro* methods are also different from those of MTs examined *in vivo*. *In vitro* characterization of MTs formed from purified yeast tubulin is valuable in that it reveals the dynamic properties that are intrinsic to the MTs. MTs polymerized *in vitro* from tubulin purified from wild-type cells, grow slowly for extended periods of time before they rapidly, and completely depolymerize to the axoneme seed (Davis et al., 1993, 1994; Sage et al., 1995a, b; Gupta, 2001). Rescues (transitions from rapid shortening to growth or attenuation) are rarely, if ever, observed. Sage et al., (1995a,

b), Davis et al., (1993, 1994), and Gupta (2001) have shown that the *in vitro* growth rates of yeast MTs are relatively slow (0.177 to 0.579 μm/min). Shortening rates, on the other hand, are extremely fast, ranging from 103 to 114 μm/min (Sage et al., 1995a, b; Gupta, 2001). MTs, *in vitro*, do not exhibit periods of attenuation (Sage et al., 1995a, b; Gupta, 2001). The dynamicity of yeast MTs *in vitro*, however, tends to be slightly lower (17 to 26 dimers/sec) than what has been documented for yeast MTs *in vivo* (21 to 37 dimers/sec) (Davis et al., 1993, 1994; Gupta, 2001; Tirnauer et al., 1999; Kosco et al., 2001).

Protein purity and insufficient protein quantity are two significant problems in measuring the dynamic instability parameters of yeast tubulin MTs *in vitro*. It was not possible with the methods and modifications used in this study (see Appendix Z), to obtain tubulin of sufficient purity to examine yeast MT dynamics *in vitro* with confidence. Because rescue events were rarely observed *in vitro*, but frequently observed in living yeast cells (Carminati and Stearns, 1997, Tirnauer et al., 1999, Maddox et al., 1999), an *in vivo* approach to studying MT dynamics might be more representative of true dynamics in a cellular context than *in vitro* analysis using purified yeast tubulin and assembling MTs on axoneme seeds.

Green fluorescent protein fusion constructs have been employed to examine various aspects of yeast MTs *in vivo*. For example, a dynein-GFP construct was used to examine the role of cMT dynamics in spindle orientation and nuclear migration

50

(Shaw et al., 1997, 1998) as well as during mating and the first zygotic division (Maddox et al., 1999). Carminati and Stearns (1997) fused GFP to the minor α-tubulin gene, TUB3, under the GAL1/GAL10 galactose inducible promoter, and tested the ability of an N-terminal GFP fusion and a C-terminal fusion to complement an α-tubulin mutation. Only the N-terminal (GFP-TUB3) fusion was able to complement benomyl supersensitivity, so it was used to examine the role of dynein and cMT dynamics in mitotic spindle positioning as well as interactions of cMTs with the cell cortex. The dynamics of cytoplasmic and kinetochore microtubules was recently examined by fusion of GFP to TUB1. This construct did not complement a tub1 deletion strain, however, expression of this N-terminal chimera, controlled by the native TUB1 promoter, produced fluorescent speckles in the MT lattice (Maddox et al., 2000).

The studies described above involved use of GFP constructs to examine the interaction of MTs with other molecules important in various MT-driven cellular functions, and revealed how those molecules were involved in cellular processes. Other important aspects of MT function have been revealed by studies using GFP-tubulin. Maddox et al. (2000) showed that growing and shortening dynamics of cMTs occurred only at the plus ends of the MTs, and that the MTs displayed only dynamic instability. They also showed that the yeast spindle MTs assemble and disassemble at the plus ends, and therefore do not exhibit treadmilling.

51

The use of GFP constructs has facilitated a real-time analysis of the dynamic properties of MTs as theMTs function to control events in a living cell. Therefore, GFP-constructs are extremely useful tools to study numerous aspects of MT function *in vivo*. They are also very useful in the structure-function analysis of tubulin itself. Scanning to alanine mutational studies have examined the gross phenotypic effects of a series of systematically created mutations to the individual tubulin monomers. The studies of Richards et al., (2000) and Reijo et al., (1994) which involved the systematic mutation of α-tubulin and β-tubulin, have implicated alterations in MT function, based on the various observed phenotypes. Richards et al., (2000) also positioned their mutations on the 3D structure of tubulin, and grouped the mutants based on the observed phenotypes. These mutational studies, however, have not examined how their mutations affect the function of the MTs directly.

Strains of *Saccharomyces cerevisiae*, in which mutations have been made to the sole β-tubulin gene, TUB2, were examined in detail in this study (Chapter 2). Two strains, CLC8 and CLC9 showed interesting phenotypes that indicated possible alterations in MT function. These strains had been modified in the putative colchicine binding region (Burns, 1992), in very different ways. The dynamic properties of the mutant and wild-type MTs were examined *in vivo* to assess how alterations in the protein structure of β-tubulin affected function of the MT.

52

Materials and Methods

A: Construction of strains expressing GFP-α-tubulin.

Wild-type strains (ADY101:pADwt, ADY101:pADwt-A6B and ADY101:pADwt-1Ia) and CLC mutant strains (CLC8 and CLC9) were transformed with a CEN based plasmid containing the minor α-tubulin gene (TUB3) linked to GFP. Expression of GFP-tubulin from this plasmid is controlled by a galactose (GAL1/GAL10) inducible promoter. The original GFP-TUB3 plasmid (pTS417) was a kind gift of J. Carminati and T. Stearns of Stanford University (see Carminati and Stearns, 1997 for details on the construction of the pTS417 plasmid).

Since all mutant yeast strains used in this study are URA$^+$, the URA3 gene on the pTS417 plasmid, which is a metabolic marker, was replaced with the LEU2 gene. The pTS417 plasmid was digested with SalI and SmaI to excise the URA3 marker, and the linearized vector was treated with alkaline phosphatase and then isolated from an agarose gel after electrophoresis. LEU2 was isolated from the YEp13 plasmid as a 2.23kb XhoI-ScaI fragment and ligated to the purified, linearized pTS417 vector missing the URA3 marker. The ligation product was transfected into the XL1-B strain of *E. coli* by the CaCl$_2$ method (Sambrook et al.,1989) and incubated at 37 °C. Candidate plasmids recovered from the transformants were tested by restriction mapping to confirm the presence of the LEU2 insert (see Appendix B).

53

The modified GFP-TUB3 plasmid, pTS417-ETA2, was then transformed into the original yeast strains (ADY101:pADwt, ADY101:pADwt-A6B, ADY:pADwt-1Ia, CLC8, CLC9) by the lithium acetate method (Becker and Guarente, 1991), and transformants were selected on SD plates in the absence of leucine. LEU[+] colonies were grown on YPD media and then transferred to YPD+G media to induce the production of GFP-linked α-tubulin, which is under the control of the galactose promoter. After 12 hr on YPD+G media, cells were examined for GFP-positive spindles and MTs by fluorescence microscopy in the fluorescein channel using a Nikon Eclipse E800 microscope. Clones expressing GFP-α-tubulin were maintained on YPD medium and transferred to YPD+G medium 12 hr prior to observation of *in vivo* MT dynamics.

B: Phenotypic characterization of GFP-α-tubulin-expressing strains.

To ensure that induction of GFP-α-tubulin did not alter the wild-type characteristics of the yeast strains with respect to tubulin function, the benomyl sensitivity and cell DTs were examined in the GFP-plasmid-containing strains, both under uninduced and induced conditions.

54

B1: Benomyl sensitivities of original, uninduced and induced yeast strains containing the GFP-plasmid.

YPD and YPD+G media plates were prepared with the addition of the appropriate amount of a stock solution of 10 mg/ml benomyl in DMSO (the final benomyl concentration ranged from 0 to 70 µg/ml), which was added to the hot sterile media just prior to pouring the plates. All strains were inoculated into 10 ml YPD, and incubated on a shaker apparatus at 30 °C for 16 hr. Next, 2 µl samples of the cultures were spotted onto YPD or YPD+G plates containing benomyl. The yeast cultures were also diluted by factors of 10, 100, 1000, and 10,000 in sterile water, then spotted in 2 µl volumes onto the plates. The plates were then incubated at 25 °C for 3 days, and any growth was noted and compared to control conditions each day. Sensitivity was defined as the minimum drug concentration at which growth differences in individual 'spots' could be detected compared to the equivalent 'spot' on the untreated control plate.

B2: Cell doubling times of uninduced and induced GFP-plasmid-containing yeast strains.

Yeast strains were inoculated into 10 ml of YPD, and incubated on a shaker at 30 °C. After approximately 16 hr, the optical density (OD) was determined at a wavelength

55

of 600 nm with a Gilford Response spectrophotometer. The culture was diluted in 50 ml of YPD or YPD+G media to give a starting OD of approximately 0.1. Flasks containing media with 2 μg/ml, 10 μg/ml and 50 μg/ml benomyl were also inoculated at the same time. All flasks were placed on a shaker at 30 °C, and the OD of 1 ml samples was determined at intervals of approximately 2 hr. At least 5 samples (that is, time points over approximately 5 DTs) were taken to determine the DT for each strain at each drug concentration. The natural log of the OD values was plotted against time, and the slope of the linear portion of the plot was used in the equation:

$$DT = 0.693/slope$$

DT for each strain, in the absence and presence of benomyl, were calculated from the increase in OD over time.

C: Measurement of *in vivo* MT dynamics of yeast strains expressing GFP-α-tubulin.

Strains containing the GFP-α-tubulin plasmid, pTS417ETA2, were streaked onto YPD+G plates 6 to 12 hr prior to measuring MT dynamics. For controls in the absence of drug, cells were transferred from the induction plates to agar pads made on microscope slides. For the agar pads (Figure 3.1), 0.2 mg of bactoagar was placed in 5 ml of M9 buffer (3 g KH$_2$PO$_4$, 11.3 g Na$_2$HPO$_4$-7H$_2$0, 5 g NaCl, 1 ml 1 M MgSO$_4$, in 1 L H$_2$0), and heated at 65 °C until dissolved. M9 buffer was used rather than YPD, YPD+G, or SD media because it was the only medium that did not

56

autofluoresce under the fluorescein channel on the microscope. To make the pads, labeling tape was first placed onto two slides to make the form. The slides with labeling tape were laid side by side on a flat surface, with a clean slide placed in between. A small volume of the hot M9-agar buffer mix was placed on the clean slide. A second clean slide was place on top of the M9-agar spot at right angles to the first clean slide. The slides were pressed together gently to sandwich and flatten the agar pad (see Figure 3.1 for diagram). When the M9-agar solidified (approximately 30 s), the top slide was twisted carefully to release it from the agar pad. Using the broad end of a sterile toothpick, a tiny amount of yeast cells was carefully transferred from the induction plate and spread onto the M9-agar pad. A clean coverslip was placed over the yeast cells on the M9-agar pad, and pressed gently to remove any air bubbles.

For measurement of MT dynamics in the presence of benomyl, cells were either inoculated onto YPD+G plates with the addition of benomyl for 6-12 hr, or onto YPD+G plates without benomyl. The cells were then transferred to agar pads that contained benomyl at the desired concentration. Benomyl was added to M9 buffer prior to heating, and when the bactoagar dissolved, the M9-agar-benomyl solution was mixed well with a Pasteur pipette prior to spotting onto microscope slides. Cells were incubated on the drug-treated pads for at least 20 min at room temperature prior to observation under the microscope.

Figure 3.1: Diagram of M9-agar pad production set-up. View from above.
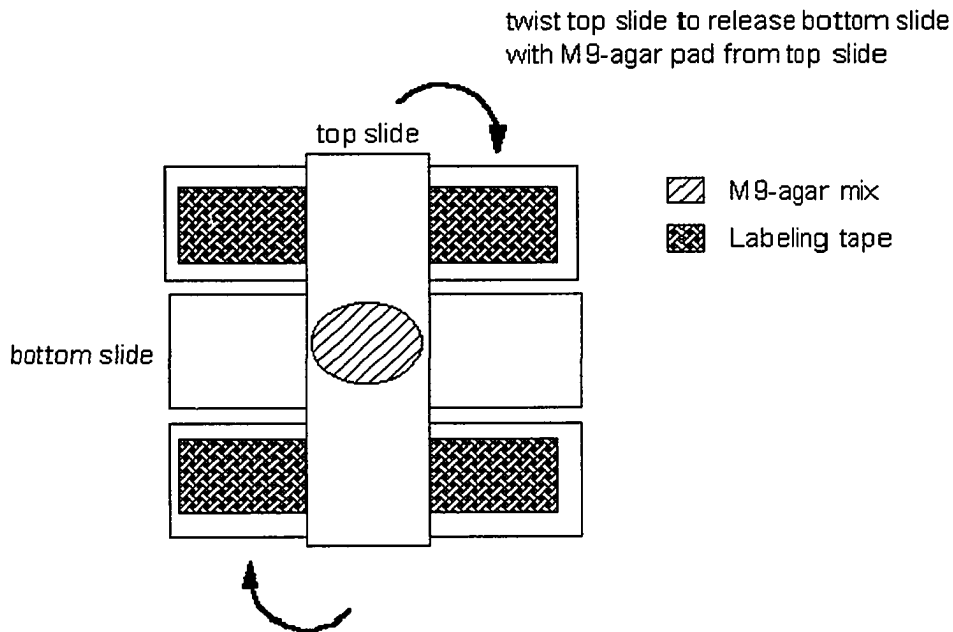
Yeast cells were observed and recorded at room temperature, using a Nikon Eclipse

E800 microscope, a 100X /1.40 PlanApo oil objective, a Hamamatsu C4742-98

cooled charged-coupled device (CCD) camera, and images were recorded in real time

using the MetaMorph™ Imaging system (versions 4.0 and 4.5; Universal Imaging

Corporation, Media, PA, USA). Exposure times ranged from 200-800 ms, depending

on the age of the mercury arc lamp; as the usage time of the mercury arc lamp

accumulated, the brightness decreased, necessitating extended exposure times. The

58

extent to which it was necessary to open the F-aperture also varied with the age of mercury arc lamp.

A series of 8 or 9 images separated by 0.5 μm in the Z-plane was recorded as a stack. Stacks of images were taken approximately every 10 sec for a period of 4 to 8 min. At the end of the series of images, a bright field image stack was recorded to visualize whole cells in order to determine the presence and size of the bud, which is a reflection of the cells' stage in the cell cycle. Images were binned 2 x 2, and only the center quadrant of the chip was used to limit the size of the image, so a maximal number of images in the time lapse series could be recorded.

All image processing was carried out using the MetaMorph™ software program. Stacks of images were first processed by eliminating any images in the stack that were greatly out of focus. The remaining images were compressed into a single 2D image using either the Stack Arithmetic Maximum or Stack Arithmetic Best Focus command in the MetaMorph™ software program. Images were sometimes color inverted to increase contrast and therefore make the MTs more distinct. Each compressed image was placed sequentially into a new stack to make a movie. The movie stack was then calibrated to the 2 x 2 binning and 100 X objective used in image capture. Using the Measure command, each MT was traced and measured from the plus end of the MT to the spindle pole body. The average of 3 measurements was plotted as a function of time to create life history plots for each

59

MT. Only MTs whose lengths were positioned roughly parallel to the microscope stage, and whose entire length remained within the Z-sections of the stack, were chosen to be measured. Often, there were multiple cells within the same recording, and sometimes multiple cMTs within the same cell, that could be measured.

MT dynamic instability parameters were calculated from each life history plot. Rates of growing and shortening were determined from the slopes in the life history plot, phase durations and transition frequencies were determined from the duration of growth or shortening events. Events that had rates of less than $\pm$ 0.2 μm/min and length changes of less than 0.2 μm were classified as attenuation events. Statistical comparisons were made using the Vassar Stats website for Statistical Computation (**www.department.Vassar.edu/~lowry/VassarStats.htm**).

Results

Two of the strains created by mutation of the sole β-tubulin gene in *S. cerevisiae*, in the putative CLC binding site, showed interesting cellular phenotypes with respect to MT function (see Chapter 2). One of the strains, CLC8, which resembles mammalian β-tubulin in the amino acid sequence between 310 and 324, has a longer generation time than the wild-type strain, is supersensitive to the antimitotic drug benomyl, and is haploid inviable (refer to Chapter 2). It is assumed that the alteration in the β-

60

tubulin sequence affected the structure of the tubulin dimer, and consequently, affected MT function in this mutant yeast strain.

To determine how the mutations in the β-tubulin gene affected MT function in CLC8 cells in comparison to wild-type yeast cells, a plasmid which when expressed, resulted in the production of GFP-linked-α-tubulin, was transfected into both the mutant and wild-type strains. This enabled real-time visualization of MTs in live yeast, since the GFP-α-tubulin containing dimers readily polymerized into the MT lattice. The cMTs in the CLC8 strain and in the wild-type strain ADY101:pADwt were recorded and analyzed to determine whether there were any differences in the MT dynamic instability behavior.

A: Construction of yeast strains expressing GFP-α-tubulin.

To enable real-time visualization of MTs in living yeast cells, pTS417-ETA2, the plasmid encoding a GFP-α-tubulin construct was transfected into the wild-type and mutant yeast strains. After transfection of the modified plasmid into the various yeast strains, cells expressing GFP-α-tubulin were easily identified by fluorescence microscopy. Figure 3.2A shows a field of yeast cells by bright field microscopy, while Figure 3.2B shows the same field of cells in the fluorescein channel of the microscope. Cytoplasmic MTs, spindles and spindle pole bodies appeared bright green. One characteristic that was common in all of the strains transformed with

61

either the modified or the original plasmid was the non-uniform GFP expression among a field of cells. The arrow in Figure 3.2A marks a cell that is not expressing, or is very weakly expressing GFP-α-tubulin. However, despite the non-uniformity of GFP expression, there were sufficient numbers of cells expressing adequate levels of GFP for recording of dynamic cMTs. The advantage of using the GFP-α-tubulin expression plasmid was the ease in obtaining numerous recordings of cMTs in a number of different yeast strains under a variety of conditions. The time limiting step, unlike the *in vitro* approach to examining MT dynamics, was not in obtaining sufficient amounts of pure protein to assemble adequate numbers of recordable MTs, but in the image processing of the recordings.

Figure 3.2: Yeast cells transfected with the pTS417-ETA2 GFP-α-tubulin expression plasmid. Figure 3.2A shows yeast cells by bright field illumination. Figure 3.2B shows the same field of yeast cells illuminated by the fluorescein channel. The arrow in Figure 3.2A indicates a cell that is not expressing, or is very weakly expressing GFP-α-tubulin.
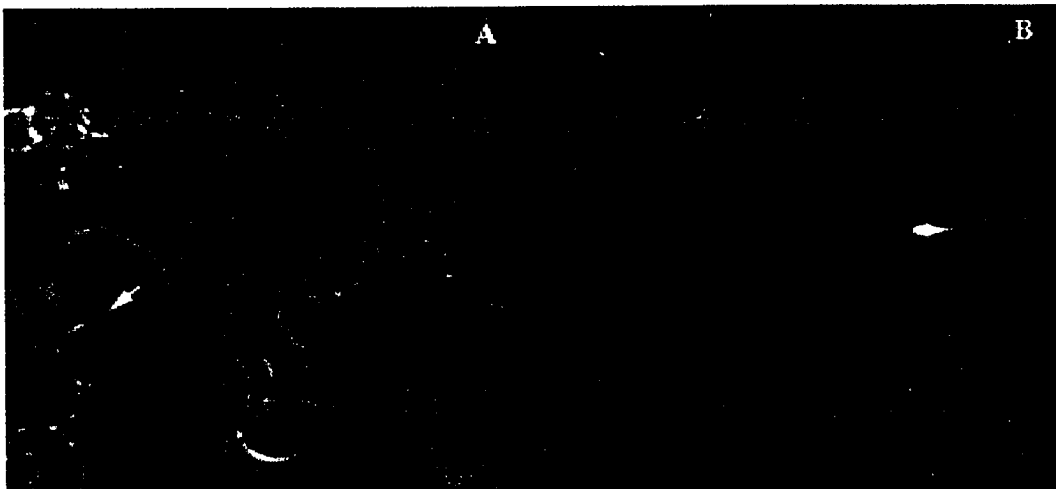
B1: Benomyl sensitivities of uninduced and induced GFP-plasmid-containing yeast strains.

In order to visualize the MTs in the various yeast strains, it was necessary to transfect all the strains with a plasmid which when expressed produced GFP-α-tubulin. Since expression of the GFP-α-tubulin plasmid, pTS417-ETA2, in the yeast strains increased the overall amount of α-tubulin in the cells (Carminati and Stearns, 1997), it was necessary to determine whether the expression conferred any growth advantage, or altered sensitivity to the antimitotic drug benomyl. All yeast strains containing the GFP-plasmid were tested under non-inducing and inducing conditions, and all transformed strains displayed sensitivities to benomyl that were similar to the original strains (Table 2.4). Sensitivity was determined as the minimal concentration of benomyl required to inhibit growth of cells, compared to the growth in the absence of drug. Whether the GFP-α-tubulin was induced or not, growth of the WT diploid strain was sensitive to 10 μg/ml benomyl and the cells ceased to grow at 20 μg/ml, while the mutant strain, CLC8, was sensitive to 2 μg/ml benomyl and ceased to grow at 10 μg/ml. The sensitivities of the GFP-plasmid-containing strains on noninducing (YPD) and inducing plates (YPD+G) after 3 days at 25 °C are shown in Figures 3.3A and B. The additional α-tubulin that the induced strains produced did not alter the sensitivity to benomyl.

63

Figure 3.3A: Benomyl sensitivities of yeast strains transfected with pTS417-ETA2, on YPD media. On each plate, columns left to right: ADY101:pADwt, CLC8, ADY101:pADwt-A6B, ADY101:pADwt-1Ia, CLC9. Dilutions: Row 1: 2 μl of overnight culture, Row 2: 2 μl of 1:10 dilution, Row 3: 2 μl of 1:100 dilution, Row 4: 2 μl of 1:1000 dilution, Row 5: 2 μl of 1:10000. Plates: Row 1, left to right: no drug, 2 μg/ml benomyl, 5 μg/ml benomyl, 10 μg/ml benomyl; Row 2, left to right: 20 μg/ml benomyl, 30 μg/ml benomyl, 40 μg/ml benomyl, 50 μg/ml benomyl; Row 3, left to right: 60 μg/ml benomyl, 70 μg/ml benomyl. See Materials and Methods for growth assessment.

64
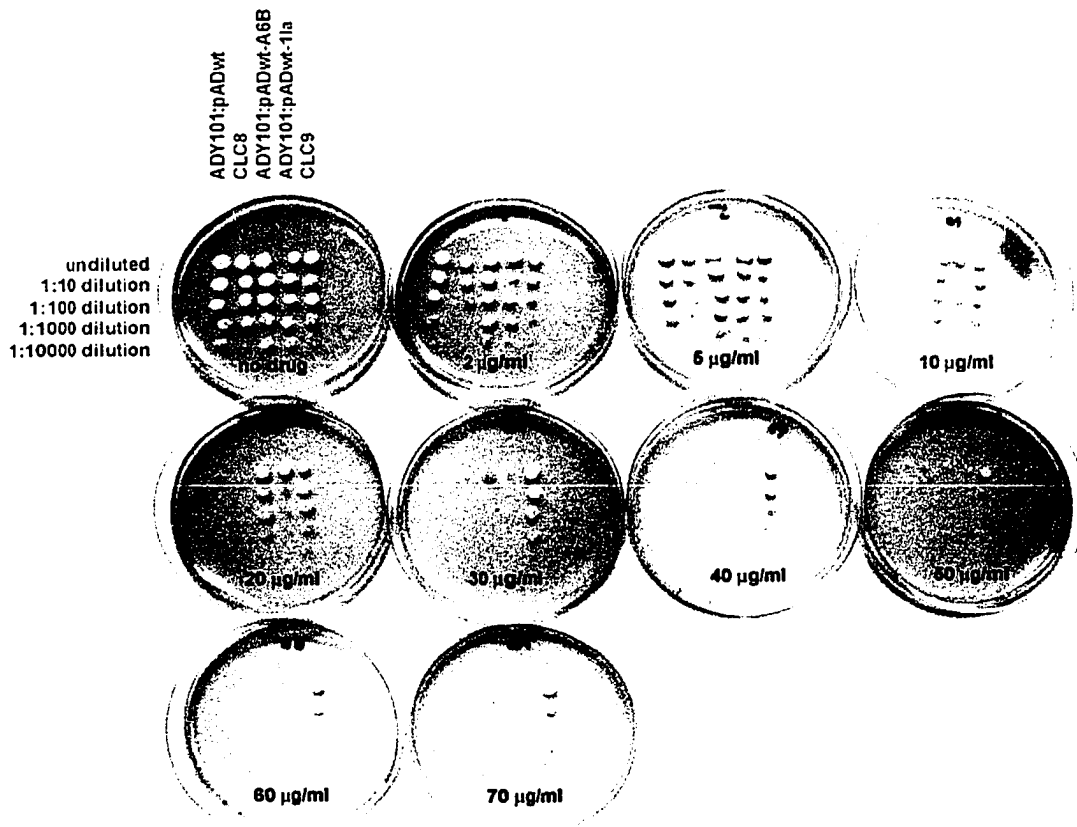
Figure 3.3B: Benomyl sensitivities of yeast strains transfected with pTS417-ETA2, on YPD+G GFP induction plates. On each plate, columns left to right: ADY101:pADwt, CLC8, ADY101:pADwt-A6B, ADY101:pADwt-IIa, CLC9. Dilutions: Row 1: 2 μl of overnight culture, Row 2: 2 μl of 1:10 dilution, Row 3: 2 μl of 1:100 dilution, Row 4: 2 μl of 1:1000 dilution, Row 5: 2 μl of 1:10000. Plates: Row 1, left to right: no drug, 2 μg/ml benomyl, 5 μg/ml benomyl, 10 μg/ml benomyl; Row 2, left to right: 20 μg/ml benomyl, 30 μg/ml benomyl, 40 μg/ml benomyl, 50 μg/ml benomyl; Row 3, left to right: 60 μg/ml benomyl, 70 μg/ml benomyl.

65
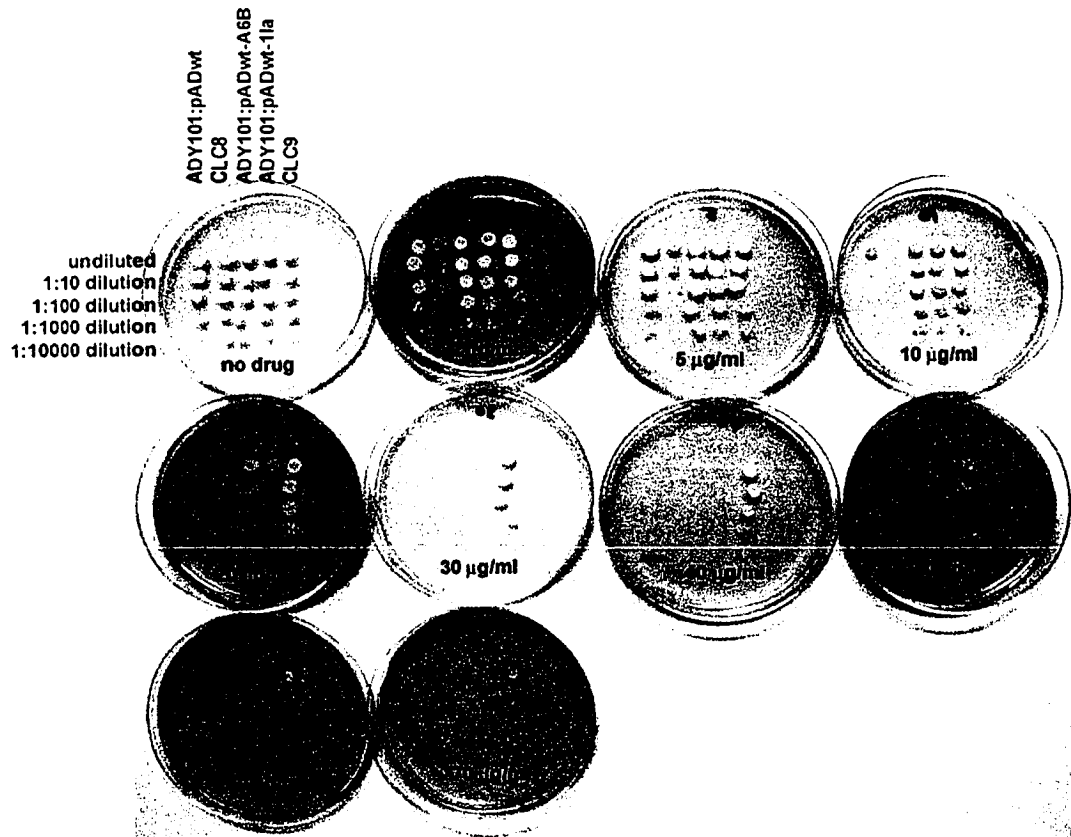
B2: Doubling times of uninduced and induced GFP-plasmid-containing yeast strains in the absence and presence of benomyl.

Another test of whether the presence of additional α-tubulin, in the form of GFP-α-tubulin, altered the transformed yeast strains was to determine the DTs of the cells. In order to determine whether induction of the GFP-α-plasmid altered the vegetative growth of the strains, the DT of all strains containing the plasmid were followed in the absence and presence of benomyl over 5 generation times. Figures 3.4A and B show the DTs of the diploid yeast strains in the absence of benomyl and in the presence of 2, 10 and 50 μg/ml benomyl, under the 2 induction conditions. The diploid WT yeast strain ADY101:pADwt doubled in the absence of benomyl in 127 min under induced conditions and in 126 min when not induced. The mutant diploid strain CLC8 doubled in 143 min when the plasmid was induced, and doubled in 146 min when not induced. DTs increased in the presence of benomyl, for both induction conditions, and the lengths of time required for doubling were not different between the two induction conditions.

Synthesis and presence of GFP-α-tubulin does not affect the DTs of the diploid yeast strains and strains containing the GFP-α-tubulin plasmid had similar DTs, whether or not the plasmid was induced. The presence of additional α-tubulin in the form of GFP-α-tubulin did not confer increased sensitivity or resistance to benomyl at any of the conditions examined.

66

Figure 3.4A: Doubling times for ADY101:pADwt cells containing the GFP-plasmid under uninduced and induced conditions, in the absence and presence of different benomyl concentrations. Solid line with squares, uninduced condition; broken line with open circles, induced condition.

67
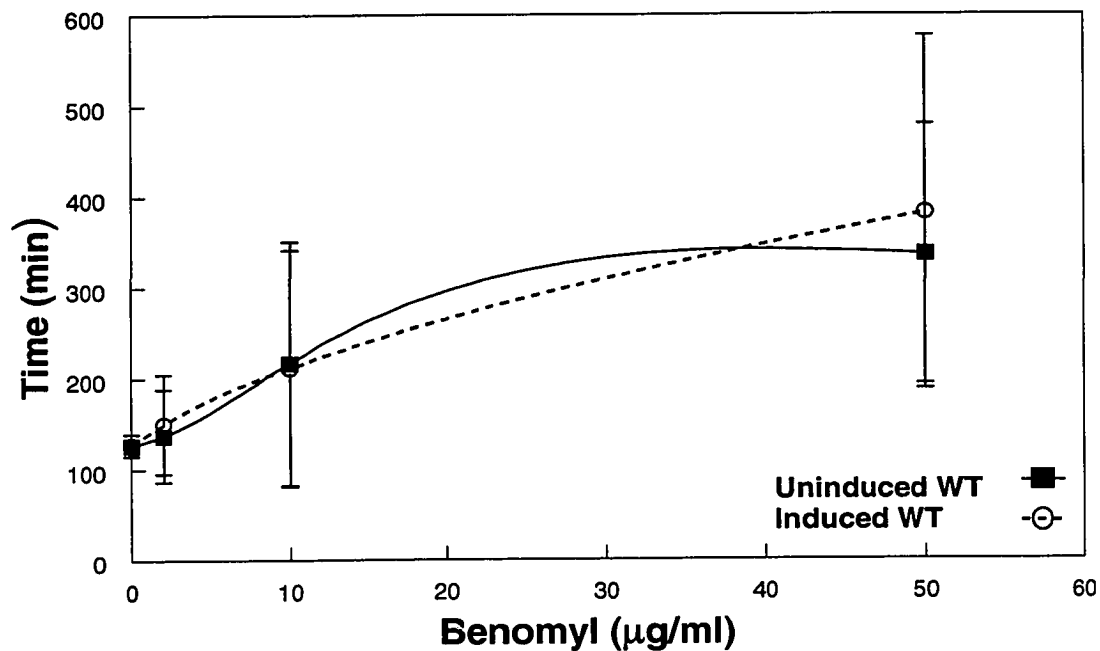
Figure 3.4B: Doubling times for CLC8 cells with the GFP-plasmid under uninduced and induced conditions, in the absence and presence of different benomyl concentrations. Solid line with squares, uninduced condition; dotted line with open circles, induced condition.
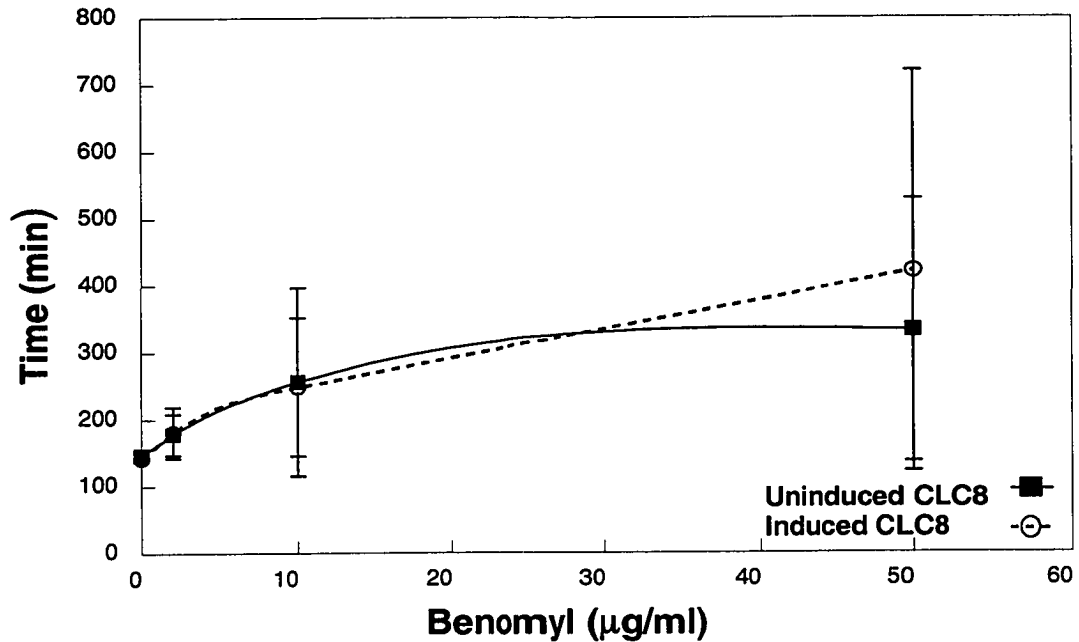
C: cMT dynamic instability measurements *in vivo* in yeast strains expressing GFP-α-tubulin.

While the gross phenotypic characteristics of the mutated yeast strains can indicate whether the function of the MTs in the strains have been altered, these characteristics are an indirect measurement of MT function. Using the inducible pTS417-ETA2

68

construct, MTs were visualized in the yeast strains after induction of GFP-α-tubulin. Images of a typical cMT in the wild-type yeast strain ADY101:pADwt are shown as a function of time in Figure 3.5. This is a montage of some fluorescent images of three cMTs in an unbudded cell, taken with the MetaMorph™ imaging system. The longest cMT, indicated with a triangle in the top left panel, was in an attenuated state until 2 min 40 sec of the recording, when it began to depolymerize. The depolymerization of the cMT, tracked with arrowheads, proceeded to the spindle pole body (which is indicated with an astrisk in the top left panel). The life history trace of this cMT is shown in Figure 3.6A as MT2 (—). The shorter cMT grows until it reaches the cell cortex. The shortest cMT is difficult to visualize and appears and disappears from the montage as it moves in and out of the Z-planes.

cMTs in the induced diploid yeast strains ADY101:pADwt and CLC8 were recorded, and the lengths of the cMTs were measured over time. Representative life history traces are shown in Figure 3.6A and B. For simplicity, five typical MT traces are shown both for the wild-type strain, ADY101:pADwt (Figure 3.6A), and for the mutant strain, CLC8 (Figure 3.6B).

69

Figure 3.5: Time lapse montage of a cMT in a wild-type yeast cell. The triangle in the top left panel indicates the cMT which was measured over time; its life history plot is shown in Figure 3.6A (WT2 ▬). The spindle pole body is marked with an asterisk in the first panel. The arrowhead indicates the tip of the plus-end of the MT as it depolymerizes to the spindle pole body. The cMT begins to shorten at 2 min 40 sec, and is completely depolymerized by 5 min 20 sec. Elapsed time is shown in the bottom right corner of each panel (min:sec).

70
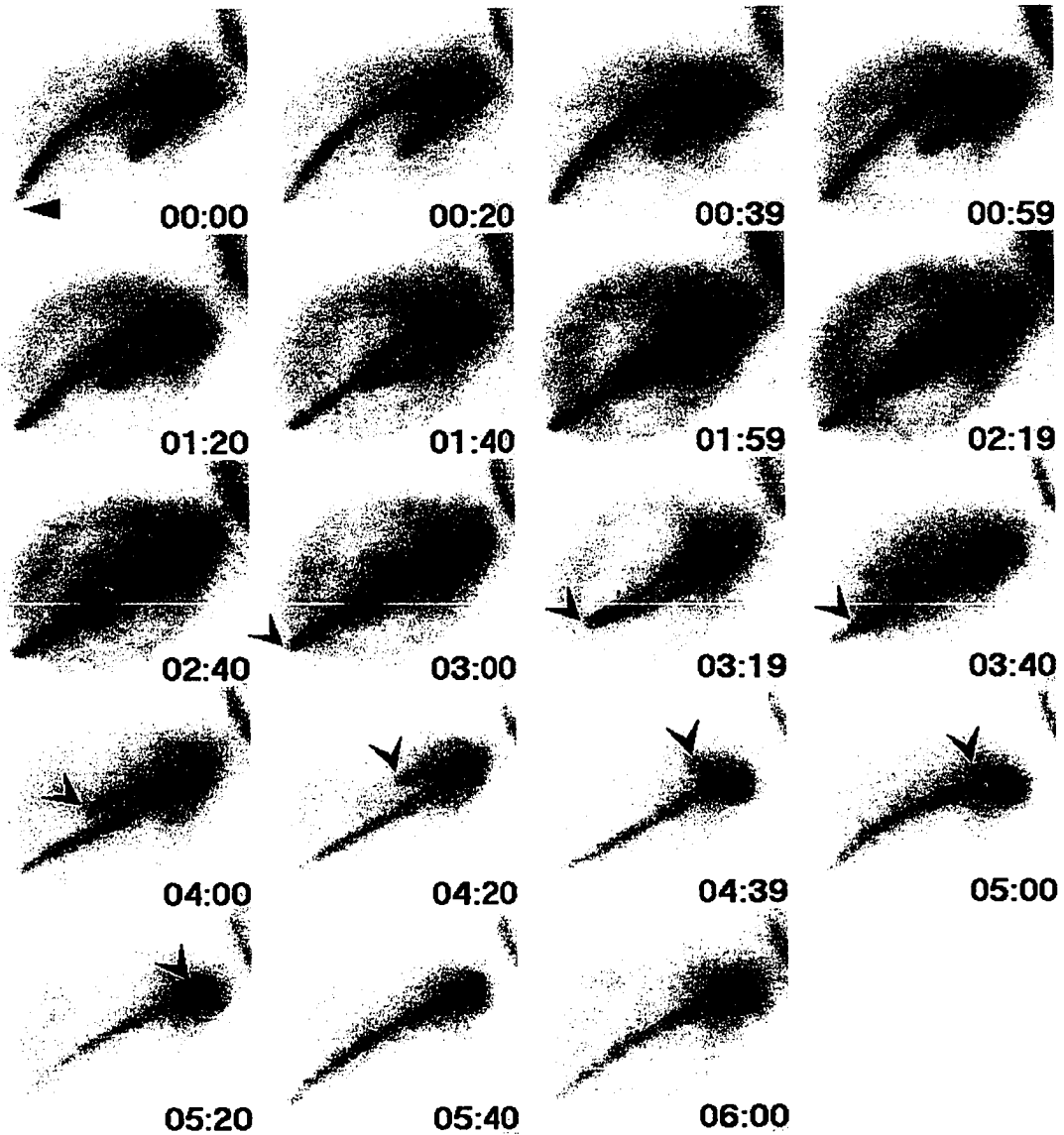
Figure 3.6: Examples of typical life history traces of individual cMTs in the diploid yeast strains. Figure 3.6A: Wild-type strain ADY101:pADwt. Figure 3.6B: Mutant strain CLC8.

71
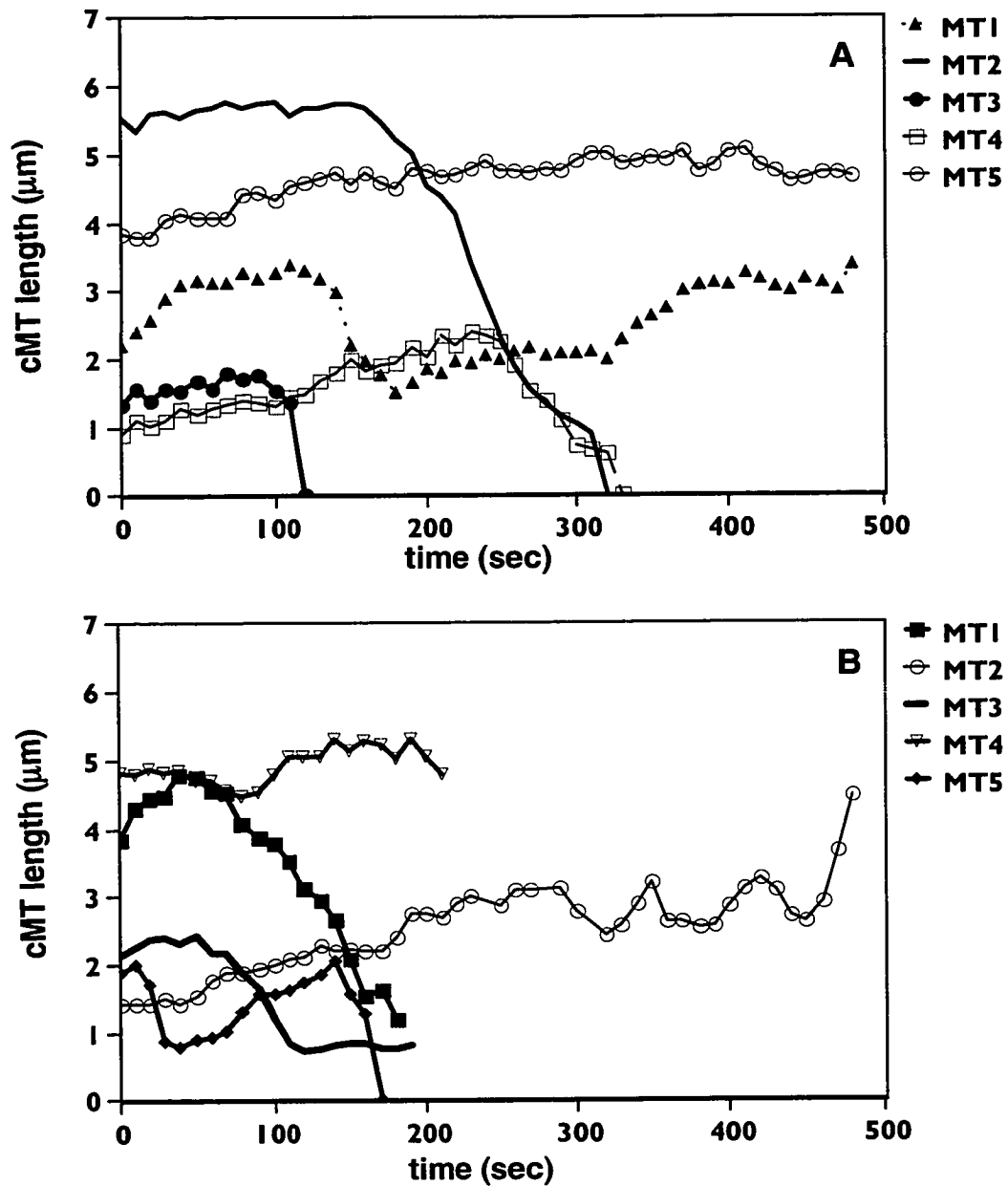
The cMTs in both strains displayed phases of growth, shortening, and spent a fraction of the time neither growing nor shortening, that is, in an attenuated state. Transitions between growth and shortening also occurred. The behaviors of MTs in the two strains were first analyzed in the absence of benomyl, to determine the dynamic parameters under control conditions. To determine how dynamics of MTs assembled from mutated β-tubulin proteins were modulated by benomyl, the cells were placed on agar pads with either low (2 μg/ml) or high (3 μg/ml or 10 μg/ml) concentrations of the drug. In this manner, the effect of modifying the putative CLC binding site of β-tubulin on the kinetic parameters of microtubule dynamics could be assessed to gain an understanding of the basic structural features of the protein that regulate microtubule behavior as well as the regions of the protein that respond to modulation by drugs such as benomyl.

C1: Dynamics of cMTs in the untreated wild-type yeast strain ADY101:pADwt.

Typical life history traces of five cMTs in the wild-type strain ADY101:pADwt are shown in Figure 3.6A. cMTs in the wild-type strain displayed growth and shortening events, as well as episodes where there was no detectable growth or shortening (attenuation). Transitions between growth or attenuation to shortening ("catastrophe") and shortening to growth or attenuation ("rescue") occurred often during the lifetime of a MT. Twenty eight cMTs from 9 WT cells were recorded and

72

analyzed in the absence of benomyl. The individual dynamic parameters measured and the values for the MTs in the wild-type strain ADY101:pADwt are shown in Tables 3.1 - 3.4.

The mean growth rate for ADY101:pADwt MTs was 1.1 ± 0.5 μm/min (Table 3.1), while the shortening rate was faster at 1.8 ± 1.5 μm/min. These rates were very close to previously published *in vivo* dynamics rates of yeast MTs (see Table 3.5). MTs spent approximately equal proportions of their total recorded lifetimes in episodes of growth, shortening and attenuation (Table 3.3). The mean durations of growth, shortening and attenuation were also very similar to each other, and ranged from 32 to 42 sec (Table 3.2). Catastrophes and rescues, occurred at similar frequencies (0.018 and 0.020 per min, respectively) (Table 3.4). Twenty six percent of all catastrophes were not rescued. The overall rate of dimer exchange (dynamicity) at the plus end of the MTs was 26.5 dimers/sec (Table 3.4).

Table 3.1: Mean growth rates and shortening rates of cMTs in the wild-type yeast strain, ADY101:pADwt, in the absence and presence of benomyl.

Rate ± SD (μm/min)	Benomyl (μg/ml)		
	0	2	10
Growth	1.1 ± 0.5 n = 75	1.0 ± 0.6 n = 43	0.7 ± 0.4† n = 36
Shortening	1.8 ± 1.5 n = 73	1.3 ± 0.9‡ n = 54	0.7 ± 0.4# n = 33

n is the number of events
† significantly slower than the untreated condition (P = 0.0002) and low drug conditions (P = 0.02)
‡ significantly slower than the untreated condition (P = 0.04)
# significantly slower than the untreated (P < 0.0001) and low drug conditions (P = 0.0001)

Table 3.2: Mean phase durations of cMTs in the wild-type yeast strain, ADY101:pADwt, in the absence and presence of benomyl.

Duration ± SD (sec)	Benomyl (μg/ml)		
	0	2	10
Growth	35.6 ± 32.7 n = 75	34.9 ± 29.1 n = 43	35.2 ± 15.3 n = 36
Shortening	32.6 ± 28.2 n = 73	35.8 ± 25.3 n = 54	34.5 ± 22.0 n = 33
Attenuation	42.7 ± 30.6 n = 68	62.4 ± 73.4† n = 43	79.2 ± 68.1‡ n = 58

n is the number of events
† significantly longer duration than the untreated condition (P = 0.05)
‡ significantly longer duration than the untreated condition (P = 0.0001)

74

Table 3.3: Fraction of total time cMTs in the diploid wild-type yeast strain ADY101:pADwt spent growing, shortening and in the attenuated state.

Benomyl (μg/ml)	Growth	Shortening	Attenuated State
0	0.34	0.30	0.36
2	0.25	0.32	0.44
10	0.18	0.16	0.66

Table 3.4: Transition frequencies and overall dynamicity of cMTs in ADY101:pADwt cells.

Benomyl (μg/ml)	Frequencies (sec^{-1}) ± SD		% unrescued catastrophes	Dynamicity (dimers/sec)
	Catastrophe	Rescue		
0	0.018 ± 0.019 n = 28	0.020 ± 0.021 n = 28	26	26.5
2	0.024 ± 0.023 n = 24	0.019 ± 0.023 n = 24	33	18.2
10	0.006 ± 0.003‡ n = 14	0.035 ± 0.012† n = 14	0	6.5

n is the number of events

‡ significantly less frequent than the untreated condition ($P = 0.03$) and low drug conditions ($P = 0.006$)

† significantly more frequent than the untreated ($P = 0.02$) and the low drug conditions ($P = 0.02$)

Table 3.5: Published *in vivo* cMT dynamic instability parameters in yeast

	Shaw et al., 1997	Carminati and Stearns, 1997	Tirnauer et al., 1999 *	Adames and Cooper, 2000	Kosco et al., 2001 *	Gupta, 2001 *
growth rate (μm/min) ± SEM	0.5	0.491 ± 0.036	1.883	4.6 + 0.81	0.831	1.422
shortening rate (μm/min) ± SEM	0.5	1.350 ± 0.159	2.775	4.8 ± 0.4	1.44	2.211
catastrophe frequency (s^{-1})		0.006	0.007	0.026	0.008	0.007
rescue frequency (s^{-1})		0.002	0.005	0.019	0.008	0.004
dynamicity (dimers/sec)			34.9		21.3	36.8
cell cycle differences?	no statistical difference between interphase and mitotic cells	yes – unbudded cells had faster shortening rates than small budded cells	yes – more dynamic in G1 than preanaphase or anaphase	no – rates and frequencies similar during G1, S and G2/M	no significant differences in rates, slightly higher frequencies of transitions in preanaphase cells	yes – faster dynamics in G1, decreases as cell cycle progresses
ploidy?		diploid	haploid	haploid	haploid	haploid
imaging?	2D	2D	3D	2D	3D	3D

* Because MT dynamics were measured separately for different stages of the cell cycle, the values for these studies are weighted averages.

76

C2: Dynamics of ADY101:pADwt cMTs in the presence of benomyl.

Since the mutations in β-tubulin were made in the putative CLC binding site, we wanted to examine the behavior of MTs in the mutant yeast strains in the presence of an antimitotic drug that binds at or near the CLC binding site. However, before we could assess the effects of benomyl on the dynamic instability properties of MTs in the mutated strains, we needed to determine the dynamic instability characteristics of MTs in the wild-type yeast strains in the presence of benomyl. Typical life history traces for cMTs in ADY101:pADwt cells in the presence of 2 μg/ml and 10 μg/ml benomyl are shown in Figures 3.7A and 3.8A, respectively. With increasing benomyl concentrations, the peaks and valleys in each individual life history trace decreased in amplitude. At 10 μg/ml benomyl, the life history traces for cMTs in the wild-type strain were approximately flat; there were very few obvious growth and shortening events and even fewer phase transitions. For the ADY101:pADwt strain, 23 MTs were analyzed in the presence of 2 μg/ml benomyl, and 14 MTs were analyzed at 10 μg/ml benomyl.

At 2 μg/ml benomyl, the cell DT for ADY101:pADwt increased slightly (1.14-fold), while in 10 μg/ml benomyl, the cell DT increased 1.7-fold over untreated controls. Since no cMTs were observed in the presence of 50 μg/ml benomyl, which is 5 times higher than the concentration this strain is sensitive to, no dynamic parameters could be determined. Background fluorescence increased within the cells at this high

77

benomyl concentration, therefore, it is assumed that all of the cMTs had depolymerized, although occasionally spindles still persisted. Since the spindle is encased by the nuclear envelope, it is likely that the spindle MTs are in a very different environment than the cMTs. The persistence of spindles at high benomyl concentrations suggests that there may be a large difference in the drug concentration inside and outside the nucleus, although it is not possible to measure the benomyl concentration within the nucleus or within the cell cytoplasm outside of the nucleus. The difference in proteins binding to spindle MTs versus cMTs may also contribute to spindle MT persistence in the presence of high drug concentrations.

The dynamics of the cMTs in the wild type strain ADY101:pADwt at 2 μg/ml and 10 μg/ml benomyl were determined and compared to the dynamics of the wild-type strain's cMTs in the absence of benomyl. The growth rate of MTs in the wild-type strain was not altered at 2 μg/ml benomyl, however, 10 μg/ml benomyl decreased the rate by almost 40 % (1.1 μm/min versus 0.7 μm/min) (Table 3.1). This decreased rate was significantly slower than the growth rates at the low drug and no drug conditions. In contrast, the shortening rate was more sensitive to benomyl than the growing rate: 2 μg/ml benomyl significantly decreased the shortening rate compared to the control. At this low benomyl concentration, the shortening rate was decreased by nearly 28 % over the shortening rate in the absence of drug. A higher drug concentration (10 μg/ml) had a more dramatic effect, reducing the shortening rate by

78

60 % (Table 3.1). The growing and shortening rates became equal in the presence of 10 μg/ml benomyl (0.7 μm/min).

Suppression of the rates of growth and shortening presumably impairs the ability of the cMTs to probe cellular space and likely increases the time required to find the bud and make stable attachments to the bud cortex. Since nuclear migration results from shortening of the cMTs to pull the nucleus from the mother cell into the bud neck (Shaw et al., 1997), this part of the cell cycle would also require more time. The increase in time required for the cell to complete these functions would contribute to the increase in DT for the wild-type yeast strain in the presence of benomyl.

The mean phase durations of growth and shortening were not affected by benomyl. However, the mean duration of the attenuated state increased significantly (Table 3.2). In the absence of benomyl, the mean attenuation duration was only slightly higher than the durations of growth or shortening (Table 3.2). However, in the presence of 2 μg/ml benomyl, the mean attenuation duration increased by almost 50 %, whereas 10 μg/ml benomyl increased it by over 80 %. The proportion of time the cMTs spent growing was more sensitive to benomyl than the proportion of time spent shortening, and decreased with increasing drug concentration. Only at the high benomyl concentration (10 μg/ml) did the proportion of time spent shortening decrease. The behavior of the cMTs shifts from approximately equal proportions of total lifetime spent in growth, shortening and attenuation, to a decrease in the former

79

two states in favor of the attenuated state (Tables 3.2 and 3.3). The life history traces of the cMTs in the presence of benomyl reveal that the cMTs are less dynamic, but the decrease in the rates of growth and shortening, as well as the increase in the percentage of the total lifetime the cMTs spend in the attenuated state confirms this observation. While 50 μg/ml benomyl caused, what appears by the increase in background fluorescence, the complete depolymerization of cMTs, 10 μg/ml benomyl reduced and virtually eliminated dynamic instability at the plus ends of cMTs.

In addition to analyzing growth and shortening rates, and phase durations, another way to assess the dynamic nature of MTs is to examine the transition frequencies and the rate of dimer exchange. These parameters also indicated that benomyl caused a decrease in the dynamic nature of the cMTs of the wild-type strain. The catastrophe frequency increased slightly in the presence of 2 μg/ml benomyl, however, the higher (10 μg/ml) benomyl concentration significantly decreased the catastrophe frequency to 33 % of that in the absence of drug. The rescue frequency increased significantly only at 10 μg/ml of benomyl. The number of unrescued catastrophes increased slightly at the low drug concentration, but at the highest drug concentration, all catastrophes were rescued (Table 3.4). Therefore, as the mean attenuation duration increased and the magnitudes of the mean growing and mean shortening rates decreased, there is an increased probability that a shortening event will get rescued. Dynamicity steadily decreased with increasing drug concentration, from 26.5

80

dimers/sec in the absence of benomyl, to 18.2 dimers/sec at 2 μg/ml benomyl and

even lower to 6.5 dimer/sec at 10 μg/ml benomyl (Table 3.4).

81

Figure 3.7: Examples of typical life history traces of cMTs in the diploid yeast strains ADY101:pADwt and CLC8 in the presence of 2 μg/ml benomyl. Figure 3.7A: Wild-type strain ADY101:pADwt. Figure 3.7B: Mutant strain CLC8.

82
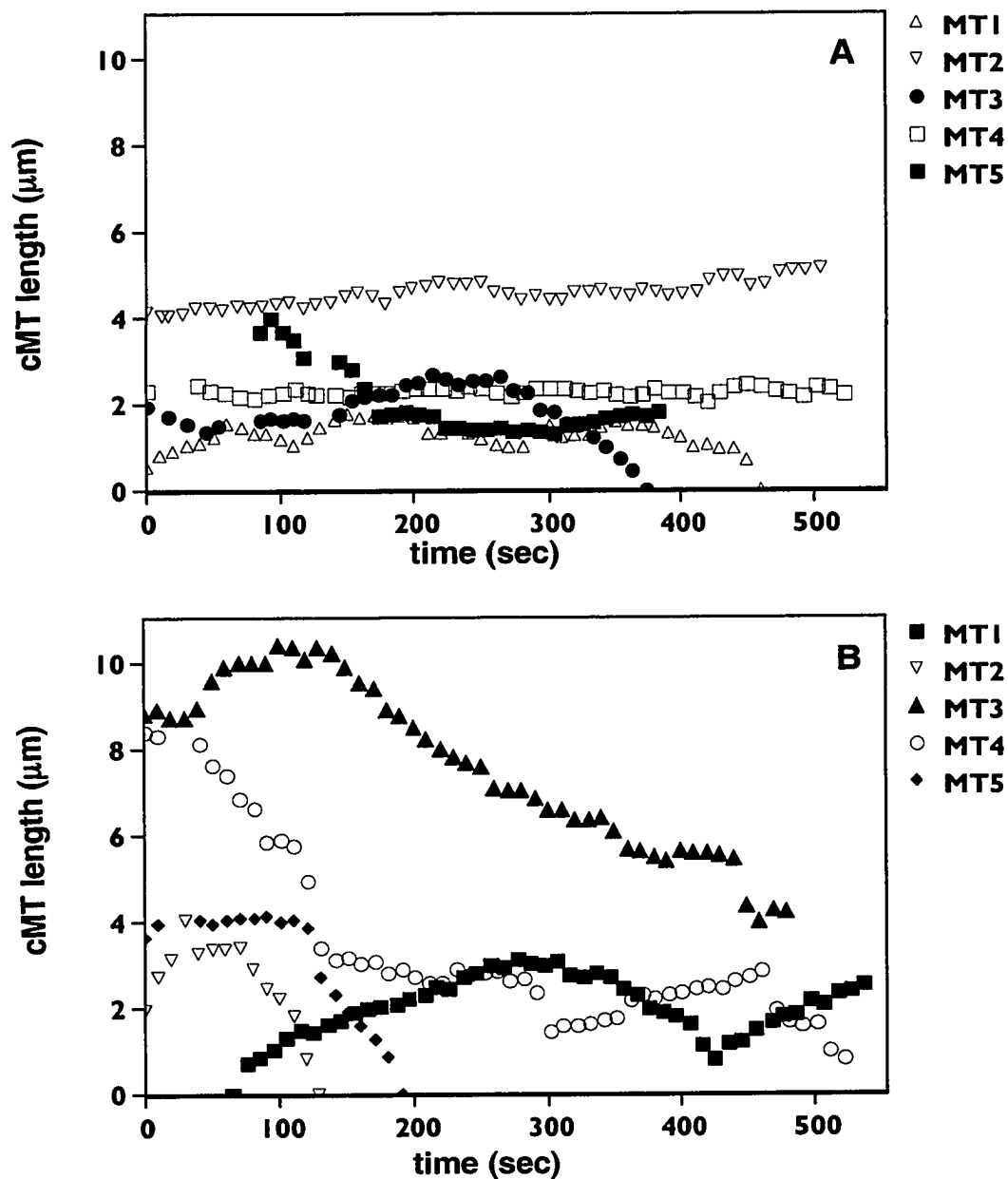
Figure 3.8: Examples of typical life history traces of cMTs in the diploid yeast strains ADY101:pADwt and CLC8 in the presence of high concentrations of benomyl. Figure 3.8A: Wild-type strain ADY101:pADwt. The high benomyl concentration used for this was 10 μg/ml. Figure 3.8B: Mutant strain CLC8. The high benomyl concentration used for this strain was 3 μg/ml.
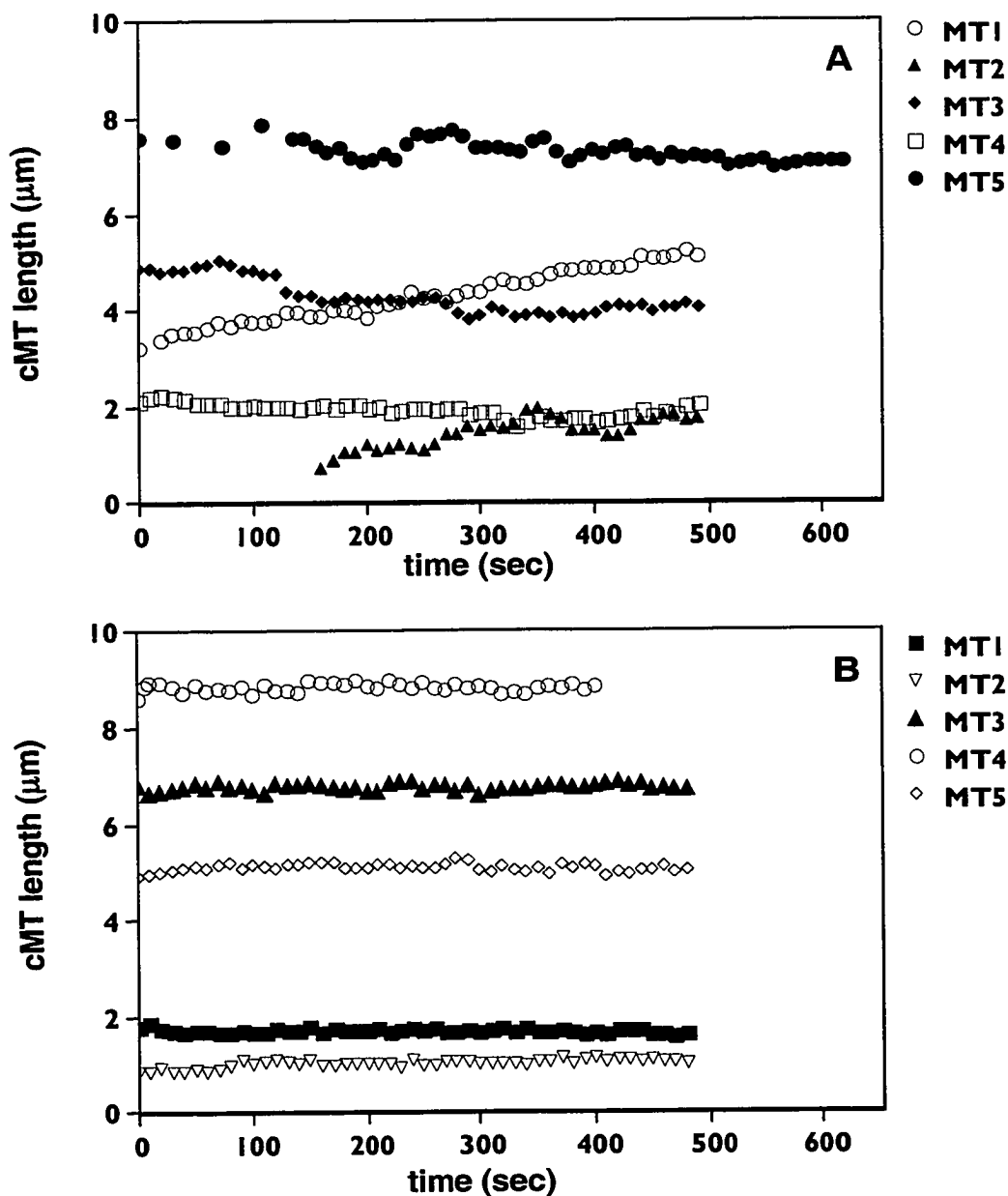
C3: Dynamics of cMTs in the mutant yeast strain CLC8 in the absence of benomyl.

Mutations were made in the putative colchicine binding site in the yeast strain CLC8. The mutations in the yeast β-tubulin gene resulted in changing the amino acid sequence between residues 310 and 324 so that it exactly resembled mammalian β-tubulin (see Table 2.1). At the cellular level, CLC8 had several interesting phenotypes that indicated altered MT function: increased DT, inability to undergo meiosis, haploid inviability, and benomyl supersensitivity (see Chapter 2). Here, we examine the dynamic properties of those MTs which are composed of the mutated and pseudo wild-type β-tubulins. Typical life history plots for individual cMTs in the mutant yeast strain, CLC8, are shown in Figure 3.5B. Like the cMTs in the WT strain, these MTs also exhibited episodes of growth, shortening and attenuation. Catastrophes and rescues also occurred. The individual dynamic instability parameters and the values that characterize the MT dynamics for this strain are shown in Tables 3.6 to 3.9. Forty eight cMTs in 21 cells were analyzed in the absence of drug.

Examination of the kinetic parameters for the MTs of the CLC8 strain reveals that the dynamic properties of the mutant strain's MTs are more dynamic than those of the WT strain. The mean shortening rate of MTs in CLC8 cells (2.7 μm/min) was almost two and a half times faster than the mean growth rate (1.1 μm/min) (Table 3.6).

84

Although cMTs spent equal proportions of total lifetime growing and shortening (Table 3.8), the mean growth duration was longer than the mean shortening duration (32.3 sec versus 25.2 sec). The mean duration cMTs spent in an attenuated state was similar to that spent shortening, but, the overall fraction of time MTs spent attenuated (24 %) was less than the fraction of time spent either growing (38 %) or shortening (38 %) (see Tables 3.7 and 3.8). The cMTs of CLC8 cells spend more time growing and shortening than in the attenuated state.

The mutant cMTs underwent a higher frequency of catastrophes (0.028 per sec) than rescues (0.020 per sec) and 42 % of all catastrophes were not rescued. Dynamicity at the plus-ends of the cMTs was 40.4 dimers per sec. Based upon these kinetic parameters, the cMTs of CLC8 are highly dynamic relative to those in WT cells.

C4: Dynamics of CLC8 cMTs in the presence of benomyl.

In the presence of benomyl, examination of the dynamic properties of CLC8 cMTs revealed that these are very sensitive to the drug. For the CLC8 strain, which is supersensitive to benomyl, the high drug concentration used for the examination of the *in vivo* dynamic properties of the cMTs was 3 μg/ml, not 10 μg/ml, since cMTs were not observed at 5 μg/ml or above. Twenty four cMTs from 8 cells were analyzed in the presence of 2 μg/ml drug, while 16 cMTs from 12 cells were examined in 3 μg/ml benomyl. Examples of typical life history plots for cMTs in the

85

mutant yeast strain CLC8, in the presence of 2 µg/ml and 3 µg/ml benomyl, are shown in Figures 3.7B and 3.8B. The kinetic parameters of the cMTs are summarized in Tables 3.6 to 3.9.

In the mutant strain CLC8, the mean growth rate and mean durations of growth and shortening increased significantly in the presence of the low drug concentration (2 µg/ml), an interesting phenomenon (Table 3.6 and 3.7). The low concentration of benomyl appeared to enable more tubulin subunits to assemble on the end of the MT before a catastrophe occurred. However, both the growth and shortening rates decreased significantly at the higher (3 µg/ml) benomyl concentration.

The proportions of the total MT lifetime that CLC8 MTs spent growing and shortening did not change in the presence of 2 µg/ml benomyl, however, in 3 µg/ml drug, the MTs were predominantly in an attenuated state (Table 3.8, Figure 3.8B). The number of growing and shortening events declined with increasing drug concentration. At 3 µg/ml benomyl, there were very few growing and shortening events (n = 9 and n = 8, respectively). cMTs in CLC8 cells had significantly longer mean durations and spent a higher fraction of total lifetime in the attenuated phase with increasing drug concentration (Table 3.7 and 3.8). As the benomyl concentration increased from 0 to 3 µg/ml, the mean duration in the attenuated state increased from 26.3 sec to 40.0 sec to 233.0 sec, and the percentage of total MT lifetime in the attenuated state increased from 24 % to 29% and then jumped to 94 %.

86

The catastrophe frequency was more sensitive to the effects of benomyl than the

rescue frequency, and was significantly reduced (Table 3.9) over the drug

concentration range; the rescue frequency did not change. At the highest benomyl

concentration (3 μg/ml), every catastrophe was rescued. Dynamicity remained high

(40.4 dimers/sec) and did not change at the low drug concentration, but was

practically eliminated at the high concentration (1.2 dimers/sec). The dynamics of

cMTs in the mutated yeast strain CLC8 are potently suppressed by very low

concentrations of benomyl.

Table 3.6: Mean growth rates and shortening rates of cMTs in the mutant yeast strain, CLC8, in the absence and presence of benomyl.

Rate ± SD	Benomyl (μg/ml)		
(μm/min)	0	2	3
Growth	1.1 ± 0.5	1.4 ± 0.9†	0.8 ± 0.6‡
	n = 75	n = 48	n = 9
Shortening	2.7 ± 2.1	2.3 ± 1.4	0.6 ± 0.2#
	n = 90	n = 56	n = 8

n is the number of events
† significantly faster than the untreated condition (P = 0.01)
‡ significantly slower than the low drug condition (P = 0.06)
# significantly slower than the untreated (P = 0.005) and low drug conditions (P = 0.0008)

87

Table 3.7: Mean phase durations of cMTs in the mutant yeast strain, CLC8, in the absence and presence of benomyl.

Duration ± SD (sec)	Benomyl (μg/ml)		
	0	2	3
Growth	32.3 ± 20.0 n = 71	45.6 ± 43.7† n = 48	25.1 ± 12.8 n = 9
Shortening	25.2 ± 18.7 n = 90	43.5 ± 37.3‡ n = 56	25.0 ± 5.4 n = 8
Attenuation	26.3 ± 17.0 n = 54	40.0 ± 33.2# n = 47	233 ± 176 # n = 29

n is the number of events
† significantly longer duration than the untreated condition (P = 0.03)
‡ significantly longer duration than the untreated condition (P = 0.0001)
# significantly longer duration in the presence of drug (P = 0.009 and P < 0.0001)

Table 3.8: Fraction of total lifetime cMTs in the mutant yeast strain CLC8 spend growing, shortening and in the attenuated state.

Benomyl (μg/ml)	Growth	Shortening	Attenuation
0	0.38	0.38	0.24
2	0.34	0.37	0.29
3	0.03	0.03	0.94

88

Table 3.9: Transition frequencies, and overall dynamicity of cMTs in the mutant yeast strain CLC8.

Benomyl (μg/ml)	Frequencies (sec⁻¹) ± SD		% unrescued catastrophes	Dynamicity (dimers/sec)
	Catastrophes	Rescues		
0	0.028 ± 0.029 n = 48	0.020 ± 0.025 n = 48	42	40.4
2	0.019 ± 0.020 n = 24	0.017 ± 0.016 n = 24	32	40.4
3	0.001 ± 0.002† n = 16	0.016 ± 0.023 n = 16	0	1.2

n is the number of events
† significantly fewer than the untreated (P = 0.0005) and low drug conditions (P = 0.0008)

C5: A comparison of the dynamic properties of the MTs in the diploid yeast strains ADY101:pADwt and CLC8.

Examination of the kinetic values characterizing the dynamic instability behavior of the MTs in the two diploid yeast strains revealed that the MTs of the CLC8 strain were more dynamic than the MTs of the WT strain; perhaps the mutations in the putative CLC binding site on β-tubulin uncovered an important region of β-tubulin that regulates dynamics. The parameters and values that characterize the dynamic behavior of MTs of the WT and CLC8 yeast strains are compared in Tables 3.10 to 3.13.

Although the mean growth rates and growth durations of the cMTs in the mutant and wild-type strains were similar, the mean shortening rate of MTs in the CLC8 strain, was significantly faster than MTs in the wild-type strain (2.7 versus 1.8 μm/min, Table 3.10). In addition, the mean shortening and mean attenuation durations of MTs in the CLC8 strain were significantly shorter than MTs in the wild-type strain. For example, while wild-type MTs spent an average of 43 sec in the attenuated state, MTs in the CLC8 strain spent only 26 sec in the attenuated state (see Table 3.11). Similarly, MTs in the CLC8 strain spent a smaller fraction of their total lifetime attenuated compared with WT MTs (Table 3.12). Interestingly, the decreased fraction of time that mutant MTs spent attenuated was compensated by an increase in the proportion of time spent growing and shortening (Table 3.12). These parameter differences reflect an overall increased dynamic state of MTs in the mutant versus WT cells, which is also revealed by the higher dynamicity of the MTs in the mutant strain (40.4 dimers/sec; Table 3.13) which is 50 % greater than the MTs in the wild-type strain (26.5 dimers/second; Table 3.13). Other indications of MT instability in the CLC8 strain are the significantly higher catastrophe frequency (0.028 sec^{-1} versus 0.018 sec^{-1}), and the higher fraction of catastrophes that are not rescued. Forty two percent of the shortening events were not rescued in the mutant strain, whereas only 26 % of catastrophes remained unrescued in the wild-type strain (Table 3.13).

The higher dynamicity value, higher catastrophe frequency, higher percentage of unrescued catastrophes, more rapid shortening rate, and the shorter average lifetime

90

of a mutant MT (124.6 sec) all combined indicate that cMTs in the mutant strain are

highly dynamic, and thus, unstable relative to the MTs in the wild-type strain. The

average lifetime of a cMT in a wild-type cell was 283.9 sec, over twice the average

duration of a cMT lifetime in a CLC8 cell.

Table 3.10: Mean cMT Growth Rates and Shortening Rates: ADY101:pADwt versus CLC8 cells.

	No Benomyl	2 µg/ml Benomyl	high Benomyl[#]
Growth Rate (µm/min)			
ADY 101:pADwt	1.1 ± 0.5 n = 75	1.0 ± 0.6 n = 44	0.7 ± 0.4 n = 36
CLC8	1.1 ± 0.5 n = 71	1.4 ± 0.9† n = 48	0.8 ± 0.6 n = 9
Shortening Rate (µm/min)			
ADY 101:pADwt	1.8 ± 1.5 n = 73	1.3 ± 0.9 n = 54	0.7 ± 0.4 n = 33
CLC8	2.7 ± 2.1‡ n = 90	2.4 ± 1.4‡ n = 56	0.6 ± 0.2 n = 8

\# High benomyl concentration for ADY101:pADwt cells is 10 µg/ml, and 3 µg/ml for CLC8 cells.
n is the number of events
† significantly faster than the wild-type strain (P = 0.004)
‡ significantly faster than the wild-type strain (P = 0.003, in untreated; P < 0.0001, at 2 µg/ml)
± = SD

91

Table 3.11: Mean Phase Durations for cMT Growth, Shortening and Attenuation: ADY101:pADwt versus CLC8 cells.

	No Benomyl	2 µg/ml Benomyl	high Benomyl[#]
Growth Duration (sec)			
ADY 101:pADwt	35.6 ± 32.7 n = 75	34.9 ± 29.1 n = 43	35.2 ± 15.3 n = 36
CLC8	32.3 ± 20.0 n =71	45.6 ± 43.7 n = 48	25.1 ± 12.8† n = 9
Shortening Duration (sec)			
ADY 101:pADwt	32.6 ± 28.2 n = 73	35.8 ± 25.3 n = 54	34.5 ± 22.0 n = 33
CLC8	25.2 ± 18.7‡ n = 90	43.5 ± 37.3 n = 56	25.0 ± 5.4 n = 8
Attenuation Duration (sec)			
ADY 101:pADwt	42.7 ± 30.6 n = 68	62.4 ± 73.4 n = 43	79.2 ± 68.1 n = 58
CLC8	26.3 ± 17.0£ n = 54	40.0 ± 33.2^ n = 47	233 ± 176 ¥ n = 29

\# High benomyl concentration for ADY101:pADwt cells is 10 µg/ml, and 3 µg/ml for CLC8 cells.

n is the number of events

† significantly shorter duration than the wild-type strain ($P = 0.07$)

‡ significantly shorter duration than the wild-type strain ($P = 0.05$)

£ significantly shorter duration than the wild-type strain ($P = 0.0006$)

^ significantly shorter duration than the wild-type strain ($P = 0.06$)

¥ significantly longer duration than the wild-type strain ($P < 0.0001$)

± = SD

92

Table 3.12: Fraction of total cMT lifetime spent growing, shortening or in the attenuated phase: ADY101:pADwt versus CLC8 cells.

	Fraction of total recorded cMT lifetime in		
	Growth Phase	Shortening Phase	Attenuation Phase
ADY101:pADwt untreated	0.34	0.30	0.36
CLC8 untreated	0.38	0.38	0.24
ADY101:pADwt 2 µg/ml benomyl	0.25	0.32	0.44
CLC8 2 µg/ml benomyl	0.34	0.37	0.29
ADY101:pADwt 10 µg/ml benomyl	0.18	0.16	0.66
CLC8 3 µg/ml benomyl	0.03	0.03	0.94

93

Table 3.13: Transition Frequencies and Dynamicity: cMTs in ADY101:pADwt versus CLC8 cells.

	No Benomyl	2 µg/ml Benomyl	high Benomyl[#]
Catastrophe Frequency (sec^{-1})			
ADY 101:pADwt	0.018 ± 0.019 n = 28	0.024 ± 0.023 n = 24	0.006 ± 0.003 n = 14
CLC8	0.028 ± 0.029† n = 48	0.019 ± 0.020 n = 24	0.001 ± 0.002‡ n = 16
Rescue Frequency (sec^{-1})			
ADY 101:pADwt	0.020 ± 0.021 n = 28	0.019 ± 0.023 n = 24	0.035 ± 0.012 n = 14
CLC8	0.020 ± 0.025 n = 48	0.017 ± 0.016 n = 24	0.016 ± 0.023£ n = 16
% Unrescued Catastrophes			
ADY 101:pADwt	26	33	0
CLC8	42	32	0
Dynamicity (dimers/sec)			
ADY101:pADwt	26.5	18.2	6.5
CLC8	40.4	40.4	1.2

High benomyl concentration for ADY101:pADwt cells is 10 µg/ml, and 3 µg/ml for CLC8 cells.
n is the number of events
† significantly more frequent than the wild-type strain (P = 0.09)
‡ significantly less frequent than the wild-type strain (P = 0.0001)
£ significantly less frequent than the wild-type strain (P = 0.009)
± = SD

94

C6: Dynamic properties of the cMTs in the diploid strains ADY101:pADwt and CLC8, in the presence of benomyl.

The CLC8 strain was mutated in the putative CLC binding site in β-tubulin; the amino acid sequence in the altered protein between residues 310 and 324 exactly resembled the amino acid sequence for mammalin tubulin. Here, the dynamic instability properties of cMTs in the wild-type and CLC8 cells were examined, in the presence of 2 different concentrations of benomyl, to determine how the drug altered MT dynamic instability in the two yeast strains.

A comparison of MT dynamics in the presence of 2 µg/ml benomyl

The MTs of the wild-type strain behaved differently from the MTs of the mutant strain in the presence of 2 µg/ml benomyl. At this, the lowest benomyl concentration examined, the growth and shortening rates for CLC8's MTs were significantly faster than the MTs of the WT strain (Table 3.10). The growth rate for the cMTs in the mutant strain was 40 % faster than in the wild-type strain, while the shortening rate was 85 % faster. The growth and shortening durations for the mutant cMTs were slightly longer than for the WT, but they were not significantly different. The attenuation duration of CLC8 MTs, however, was significantly shorter than that of the WT MTs (62.4 sec for WT compared to 40.0 sec for CLC8, Table 3.11). At 2 µg/ml benomyl, while the fraction of the total lifetime the MTs in WT cells spent in each

95

dynamic phase shifted from approximately equal to favoring attenuation, MTs in

CLC8 cells still spent a greater fraction of their total lifetime in growth and

shortening than in the attenuated state at that drug concentration (Table 3.12).

At the lowest benomyl concentration, the transition frequencies as well as the

percentage of unrescued catastrophes were approximately equal for both yeast strains

(Table 3.13). The differences in the MT dynamics of the two strains at 2 μg/ml

benomyl was due to the differences in the rates and phase durations rather than the

transition frequencies. Although the dynamicity of the MTs of the wild-type strain

decreased from 26.5 to 18.2 dimers/sec in the presence of 2 μg/ml benomyl (Table

3.13, Figure 3.9), the dynamicity of CLC8 MTs did not change (40.4 dimers/sec;

Table 3.13, Figure 3.9). Furthermore, the dynamicity of CLC8 MTs remained higher

than the wild-type MTs at this concentration of benomyl as in the no drug condition.

While some of the kinetic parameters changed at 2 μg/ml benomyl in the CLC8

strain, the overall dynamicity did not change relative to the dynamicity in the absence

of drug. At the lowest benomyl concentration, subtle differences in the dynamics of

the MTs in the wild-type and mutant strains could be uncovered through modulation

of specific kinetic parameters.

96

A comparison of MT dynamics at the highest concentration of benomyl

At the highest benomyl concentration examined (10 μg/ml benomyl for ADY101 :pADwt and 3 μg/ml for CLC8), dynamics were potently suppressed in both strains. However, while the dynamics were greatly reduced in both strains, differences in some of the kinetic parameters were evident. The rates of MT growing and shortening were not statistically different in the two strains, but the growth duration was significantly longer for the WT than the mutant, whereas the attenuation duration for the mutant was almost 3-fold longer than the WT. The catastrophe and rescue frequencies of the mutant strain's MTs in the highest drug concentration were significantly lower than for the WT MTs. However, all catastrophes were rescued in both strains, and the dynamicities decreased dramatically (6.5 dimers/sec for WT, 1.2 dimers/sec for CLC8, Table 3.13, Figure 3.9). The MTs of the wild-type strain, although suppressed at 10 μg/ml benomyl, were more dynamic than the MTs of the CLC8 strain.

97

Figure 3.9: Dynamicity values for cMTs in the diploid yeast strains ADY101:pADwt and CLC8 in the absence and presence of different concentrations of benomyl. Wild-type, solid line with open circles; CLC8 mutant strain, dotted line with filled squares.
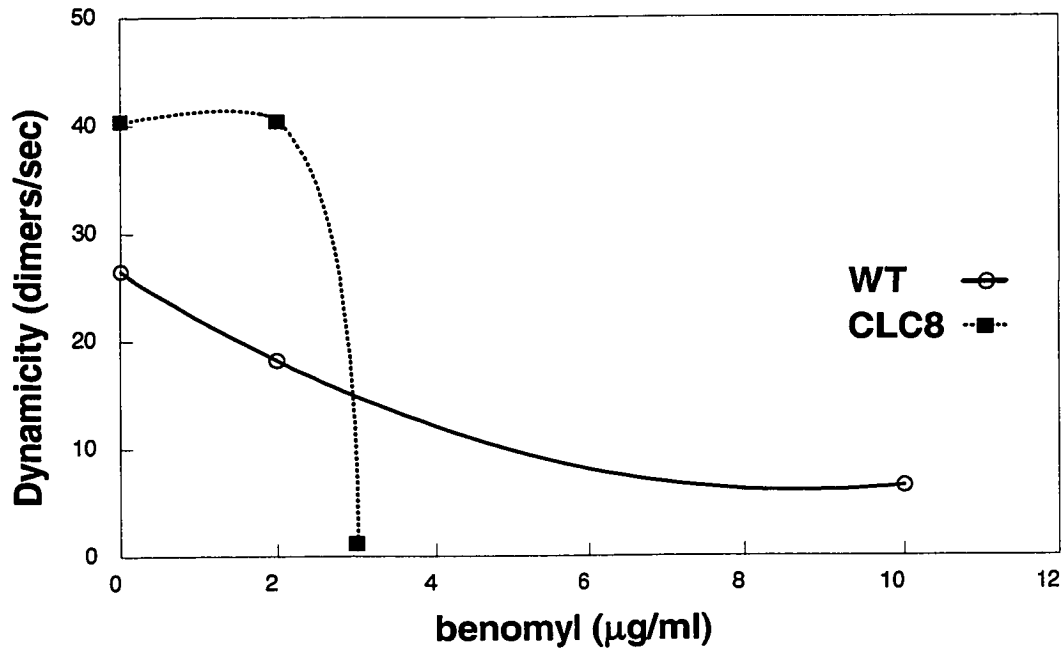
Discussion

In past studies in yeast, the effects of mutations in tubulin have been assessed by

analysis of gross phenotypic characteristics, such as in the DT, nuclear migration,

temperature sensitivity, and sensitivity to antimitotic drugs such as benomyl

(Huffaker et al., 1988; Reijo et al., 1994; Li et al., 1996; Richards et al., 2000, Gupta

et al., 2001; refer also to Chapter 2). These gross phenotypic characteristics provide a

98

rough assessment of microtubule function, and can be indicators of compromised MT function when the cells fail to grow and divide. Subtle perturbations in the dynamic behavior of MTs can also affect the function of the MTs *in vivo*, and result in gross phenotypic changes at the cellular level. We examined the dynamic instability parameters of the cMTs in the wild-type and yeast strains mutated in the putative CLC binding site of β-tubulin to determine how mutations affected MT function, by directly assessing MT function.

Using a plasmid construct with an inducible GFP linked to α-tubulin to analyze the dynamic instability properties of the cMTs has permitted us to directly assess changes in MT function as a result of alterations in the sequence and structure of β-tubulin. Determining the dynamic parameters of MTs in the mutant and WT strains *in vivo*, using this system, has revealed that differences in specific dynamic instability parameters are linked to gross phenotypic properties of the cells such as the DT and the drug sensitivity. Because the DTs and drug sensitivities of the induced GFP-α-tubulin-producing WT and mutant strains are not appreciably different from their respective uninduced strains, the presence of the GFP tag on α-tubulin subunits incorporated into the MT lattice does not appear to affect the function of the MTs. Other studies have also reached the same conclusion (Carminati and Stearns, 1997; Tirnauer et al., 1999; Maddox et al. 1999; Gupta, 2001). However, the most rigorous test of whether or not the GFP tag affects MTs dynamics would be to purify GFP-

99

tubulin and native tubulin from yeast cells, and compare the dynamics of the purified tubulins *in vitro*.

Most of the dynamic instability characteristics of MTs that normally occur *in vivo* in other systems are similar to those observed using GFP-α-tubulin in yeast (Carminati and Stearns, 1997; Tirnauer et al., 1999; Adames and Cooper, 2000; Kosco et al., 2001; Gupta, 2001). Although the actual rates and durations that characterize the dynamic instability behavior of yeast MTs are quantitatively different, they are qualitatively the same as found in higher eukaryotes.

Yeast tubulins share a high degree of homology to tubulin in higher eukaryotes, but are there are fewer genes encoding α and β-tubulin in *Saccharomyces cerevisiae*, making yeast a much simpler system than higher eukaryotes. The advantages of tubulin homogeneity, due to the lack of multiple isotypes, and the genetic and molecular tools available in yeast that allow for the dissection and modification of the tubulin molecule (which are impossible in other systems), makes yeast a superior system with which to probe how the structure of tubulin can affect the function of MTs directly at the MT level, as well as indirectly at the cellular level.

100

Analysis of cMT Dynamics in WT and CLC8 strains

This study showed that dynamics of cMTs in the diploid WT strain are comparable to the dynamics of yeast cMTs reported in other studies (see Table 3.5). There is a range of rates for growth and shortening; some of the range can be attributed to strain differences, ploidy, whether the phases of the cell cycle were taken into consideration, as well as the conditions under which the MT dynamics were measured, such as temperature. In terms of methodology, there are two common methods for measuring MT lengths. One is to compress the 3D image and measure the MT from the 2D image resulting from the compression, which is the methodology used in this study, as well as by Carminati and Stearns, (1997) and Shaw et al., (1997). Others, like Tirnauer et al., (1999), Kosco et al., (2001) and Gupta (2001) calculated the lengths of the MTs by also taking into account the number of Z-planes in which the MT is visible. Because the MT lengths in this study were measured from a 2D image instead of 3D (the Z-stack was compressed into a 2D image), the rates of growth and shortening are conservative. However, the mean rates for MTs in the wild-type strain, as determined in this study are somewhat faster than those reported by Shaw et al., (1997), Carminati and Stearns (1997) and Kosco et al., (2001), yet slower than those reported by Tirnauer et al., (1999) and Gupta (2001) (see Table 3.5).

In this study, the growth rates of MTs in the wild-type and mutant strains were the same (1.1 µm/min), but the shortening rate of the mutant strain CLC8 was 50 % faster than that of the WT cells (2.7 µm/min versus 1.8 µm/min). Since the rate of shortening is independent of tubulin concentration (Walker et al., 1988), the faster shortening rate of CLC8 MTs indicates that these MTs are not as stable as the MTs in the wild-type strain. MTs of the mutant strain had significantly shorter mean durations of shortening and attenuation than those of the wild-type strain. A larger percentage of the total mutant MT lifetime was spent growing and shortening (76 %) than the MTs of the wild-type strain (64 %); MTs in wild-type cells spent over one third of their lifetime in an attenuated state while MTs in CLC8 cells spent one quarter of their lifetime in an attenuated state. The significantly higher frequency of catastrophes (0.028 s^{-1} versus 0.018 s^{-1}), higher percentage of unrescued catastrophes, and overall higher dynamicity of the mutant strain's MTs also indicated that MTs in CLC8 were more dynamic than MTs in the WT strain. As characterized by all of these kinetic parameters, the mutations made in the amino acid sequence between 310 and 324, which alters that region to exactly resemble mammalian β-tubulin, renders the MTs of CLC8 highly dynamic, and unstable relative to the MTs of the wild-type strain.

102

Analysis of cMT Dynamics in WT and CLC8 strains, in the presence of 2 μg/ml benomyl

In the presence of benomyl, cells of the WT strain were sensitive at a concentration of 10 μg/ml, however, with respect to MT dynamics, the effects of the drug could be detected at a concentration as low as 2 μg/ml benomyl. At 2 μg/ml benomyl, the MT growth rates and mean phase durations for growth and shortening were the same as untreated cells, but the shortening rate decreased by 28 % and the mean attenuation duration increased by 46 % (see Tables 3.1 and 3.2, Figure 3.5A). The WT MTs were in an attenuated state for a larger fraction of their total lifetime than either growing or shortening states at this drug concentration. Because the catastrophe frequency increased while the rescue frequency did not change, the percentage of unrescued catastrophes increased. The overall dimer exchange rate decreased 31 % from 26.5 to 18.2 dimers per sec, but the transition frequency increased. Thus, the dynamics of MTs in the wild-type strain were dampened by 2 μg/ml benomyl.

Both the growth and shortening rates of the MTs in the mutant CLC8 strain were affected by 2 μg/ml benomyl. Surprisingly, the growth rate of CLC8 MTs increased significantly (1.4 μm/min versus 1.0 μm/min), while the shortening rate decreased (2.3 μm/min versus 2.7 μm/min). Unlike MTs in the WT strain, 2 μg/ml benomyl caused all mean phase durations of CLC8 MTs to increase significantly. For example, the mean shortening duration increased from 25.2 sec in untreated cells to

103

43.5 sec at 2 μg/ml. However, the proportion of the total lifetime that mutant MTs

spent in each of the 3 phases at 2 μg/ml benomyl was not very different from MTs in

untreated cells, except that there was a slight shift (4 %) in the fraction of time MTs

spent growing to the attenuated state. The catastrophe frequency decreased by 32 %

(0.028 s^{-1} to 0.019 s^{-1}) and the percentage of unrescued catastrophes decreased by 10

% (42 % to 32 %). While 2 μg/ml benomyl decreased the transition frequency of

MTs in the CLC8 strain, because there was no net change in rates of dimer loss or

addition and no major change in the overall proportion of total lifetime in the 3

phases, the dynamicity also remained unchanged from MTs in untreated cells. Thus,

cMTs in CLC8 cells remained dynamic at 2 μg/ml benomyl.

Analysis of cMT Dynamics in WT and CLC8 strains, in the presence of a high

concentration of benomyl (10 or 3 μg/ml)

The effects of 10 μg/ml benomyl, on MT dynamic instability in the wild-type strain

were much more striking than at 2 μg/ml benomyl, as expected (see Figures 3.8A and

B). Benomyl at 10 μg/ml significantly suppressed both the MT growth and

shortening rates, and significantly increased the mean attenuation duration. The

percentage of the total lifetime wild-type MTs spent growing, shortening and in the

attenuated state also shifted dramatically in favor of attenuation; at 10 μg/ml, MTs in

the wild-type strain spent 66 % of their total lifetime in an attenuated state. The

catastrophe frequency decreased significantly, from 0.018 per sec in untreated cells to

104

0.006 per sec at 10 μg/ml benomyl, and the rescue frequency increased from 0.020

per sec in untreated cells to 0.035 per sec at 10 μg/ml benomyl, such that every

catastrophe was rescued. Thus, the dynamic instability behavior of cMTs in the wild-

type strain were severely suppressed at 10 μg/ml.

The highest benomyl concentration (3 μg/ml) at which the MTs of the CLC8 strain

were tested, caused significant decreases in the rates of growth and shortening; the

rate of growth decreased from 1.1 μm/min in untreated cells to 0.8 μm/min at 3 μg/ml

while the rate of shortening decreased from 2.7 μm/min in untreated cells to 0.6

μm/min at 3 μg/ml benomyl. The mean attenuation duration significantly increased

to nearly 9-fold that of MTs in untreated CLC8 cells. The proportion of total lifetime

spent in phase was dramatically shifted in favor of attenuation. The frequency of

rescues was not affected by this benomyl concentration, however the frequency of

catastrophes significantly decreased from 0.028 per sec in untreated cells to 0.001 per

sec at 3 μg/ml. Thus, cMTs of the mutated strain CLC8 became extremely attenuated

at 3 μg/ml benomyl.

In the WT yeast strain, with increasing benomyl concentration, the proportion of total

lifetime cMTs spent growing decreased while the proportion of time cMTs spent in

an attenuated state increased. In either the wild-type or mutant yeast strain, the

proportion of time cMTs spent shortening was not affected at the lowest benomyl

concentration (2 μg/ml), but at the highest drug concentration it decreased to roughly

105

half that for wild-type, and less than one tenth for the mutant strain, relative to their untreated controls. MTs in the CLC8 strain spent proportionally less time attenuated in the absence of benomyl and at the lowest benomyl concentrations compared with WT MTs, but at the high drug concentration, dynamics were potently suppressed in both strains.

The dynamicity of MTs in the WT strain decreased 30 % by 2 μg/ml benomyl, however, dynamicity of MTs in the mutant strain was unaffected by this drug concentration. At the highest concentration of benomyl tested, the dynamicity was decreased to such an extent that the dynamics of the MTs in both diploid strains were completely attenuated. As can be seen in Figure 3.8, both strains had severely attenuated MTs; the dynamic instability behavior of the mutant strain's MTs were effectively eliminated, as there were very few growth or shortening events observed (Table 3.11). It is important to note that a three-fold higher benomyl concentration was required to dampen the MT dynamics in WT cells to the same extent as required to dampen the mutant strain's MT dynamics. While the dynamicity of MTs in the WT strain decreased gradually from control values over the range of benomyl concentrations examined, MTs of the mutant strain shifted dramatically from a highly dynamic state to a completely attenuated state between 2 μg/ml and 3 μg/ml benomyl (see Figure 3.9).

Although a low concentration of benomyl suppressed the dynamics of MTs in the WT strain, in CLC8 cells, the same benomyl concentration appeared to enable additional dimers to add to the growing ends of MTs. Perhaps the drug-bound dimers at the plus end of the microtubule stabilized the lattice enough to facilitate the addition of more dimers. This could explain the increases in the growth rate and mean duration of growth while not affecting the shortening rate. The catastrophe frequency also decreased in the presence of 2 μg/ml benomyl. These observations suggest that benomyl is stabilizing the GTP cap at the plus ends of the MTs. Therefore, by allowing more time for the cap to persist, the MT plus end has a greater probability of adding subunits and undergoing growth events that persists for longer durations of time. Determining the size and chemical nature of the stabilizing cap in the MTs from CLC8 versus WT cells might reveal important mechanistic insight into how the colchicine binding site regulates the hydrolysis of GTP and, therefore, regulates MT dynamics.

Based on the longer DT for the strain, and also the dynamic instability parameters displayed, it appears that the MTs in CLC8 cells are more unstable than those of the WT cells. It follows that excessively rapid MT dynamics may be responsible for increased time required for this strain to double; the cell may require more attempts in the form of multiple growing and shortening events, and perhaps, multiple cMTs to locate the incipient bud site and form stable attachments to the cortical patch in order for spindle alignment and movement of the spindle into the bud neck (Carminati and

Stearns, 1997; Shaw et al., 1997; Adames and Cooper, 2000). In terms of the cell cycle, there is a very slight increase in the percentage of cells in the unbudded stage (8 %, Table 2.3) in the CLC8 strain. However, because this is such a small shift in the proportion of cells in the unbudded stage, it is unlikely that this is the sole stage that is affected by unstable MTs. Although it is not possible to directly assess the stability of the MTs within the nucleus by the method used, it is likely that the spindle MTs are also affected by the mutation in β-tubulin. Thus, increased dynamics of the nuclear MTs may also contribute to an increase in the time required for the mutant strain to double.

A particularly striking aspect of the instability of the MTs in CLC8 cells is that there are 2 copies of the β-tubulin gene expressed, one that is mutated, and the other that is a truncated WT gene (i.e. pseudo-WT). In spite of the fact that up to 50 % of the β-tubulin in the cells is pseudo-WT, the strain is supersensitive to benomyl and exhibits highly dynamic MTs. Perhaps the mutation in the β-tubulin of CLC8 cells is affecting the ability of endogenous regulators to bind to β-tubulin, or the sequence changes are causing weaker than normal lateral interactions between adjacent protofilaments. The evidence that the strain is supersensitive to benomyl, and that highly dynamic cMTs become severely attenuated over a small benomyl concentration range (2 μg/ml to 3 μg/ml) suggests that the effect of the mutated β-tubulin subunits is dominant over the WT subunits.

108

Another phenotypic characteristic of the CLC8 strain is that the cells fail to sporulate; the strain is likely to be haploid inviable. Prior to meiosis, there are few spindle or cytoplasmic MTs. In meiosis, there are apparently no cMTs (Moens and Rapport (1971). In meiosis I, the spindle is formed within the nucleus, and when the spindle reaches its maximal separation, the spindle plaques duplicate. Within the single nuclear mass, the two spindles of meiosis II form at the ends of the spindle of meiosis I (Moens and Rapport, 1971). In the CLC8 strain, the MTs in the spindles required to segregate the chromosomes may be too unstable for the meiotic process to occur successfully. Alternatively, there may be chromosomal abnormalities, such as aneuploidy, which is preventing sporulation. Since functional tubulin is critical for mitosis and meiosis to occur correctly, and since the CLC8 mutant strain is a tubulin mutant, aneuploidy is very plausible.

At benomyl concentrations at which no cMTs were visible, mitotic spindle MTs were still present (for WT cells, 50 µg/ml, while for CLC8 cells, 5 µg/ml). This phenomenon has also been reported by Carminati and Stearns (1997). Perhaps the relatively large number of microtubules in the spindle, the presence of microtubule associated proteins along spindle microtubules, or the fact that the spindle is compartmentalized within the nucleus, renders spindle microtubules more resistant than cMTs to the depolymerizing effects of benomyl.

109

Low concentrations of antimitotic drugs have been shown to suppress MT dynamics in mammalian cells and *in vitro* systems using tubulin purified from mammalian brain tissue (Derry et al., 1995; Panda et al., 1995; Vasquez et al., 1997). In the case of the antimitotic drug benomyl and yeast tubulin, the same phenomenon exists. In the wild-type diploid strain, ADY101:pADwt, benomyl attenuated MT dynamics in a concentration dependent manner, at concentrations below those necessary for complete depolymerization of cMTs. In the mutant diploid strain CLC8, whose MTs exhibit considerably less stability than those in the WT strain, low concentrations of benomyl stabilize the plus-ends of the MT, while a slightly higher concentration completely suppress the growing and shortening dynamics of the cMTs. At benomyl concentrations lower than that required to attenuate the wild-type MTs, the cMTs of CLC8 cells are completely depolymerized. Thus, the mutations in β-tubulin, which convert the amino acid sequence between 310 and 324 in CLC8 cells to exactly resemble that of higher eukaryotes, are responsible for the instability in the MTs, which is reflected in inability of the strain to undergo meiosis, the increase in the time necessary for vegetative cell growth to occur, and the super-sensitivity of the strain to the MT destabilizing drug benomyl.

110

Chapter IV: *In vivo* Dynamics of Cytoplasmic Microtubules in the Haploid

Wild-type Yeast Strains ADY101:pADwt-A6B, ADY101:pADwt-1Ia,

and the Highly Benomyl-Resistant Yeast Strain CLC9

111

Chapter IV: *In vivo* **Dynamics of Cytoplasmic Microtubules in the Haploid Wild-type Yeast Strains ADY101:pADwt-A6B, ADY101:pADwt-1Ia, and the Highly Benomyl-Resistant Yeast Strain CLC9**

Introduction

In Chapter 3, the dynamic instability properties of the cMTs of the diploid wild-type strain ADY101:pADwt and the mutant diploid strain CLC8 were examined. In the mutant CLC8 strain, the β-tubulin gene was altered so that the expressed protein exactly resembled mammalian tubulin in the protein sequence between amino acids 310 and 324. The CLC8 strain expressed both a pseudo wild-type (truncated β-tubulin) and the mutated β-tubulin. Even though half the β-tubulin in the CLC8 strain was pseudo wild-type, the mutated β-tubulin (CLC8) rendered the cMTs more dynamic than those of the wild-type strain, ADY101:pADwt.

In this chapter, the dynamic instability properties of the cMTs in another mutant strain, CLC9, are examined. The sole β-tubulin gene in the strain CLC9 was mutated so that the expressed β-tubulin protein was altered at only one amino acid, resulting in the conversion of the arginine at position 318 to a tryptophan. CLC9 appears, from the phenotypic characterization in Chapter 2, to be mutated as postulated in a key amino acid involved in the binding of the antimitotic drug benomyl. All other phenotypes for this strain, except for its resistance to benomyl, resemble those of the

112

wild-type strain; MTs composed of the mutated β-tubulin appear to function identically to the MTs in the wild-type strains, at least at the gross phenotypic level. Whether the cMT dynamics in this strain also resemble cMT dynamics in the wild-type strain, in the absence and presence of drug will be determined.

Materials and Methods

Please refer to Chapter 3 for details.

Results

A: Creation of haploid WT yeast strains ADY101:pADwt-A6B and ADY101:pADwt-1Ia.

ADY101:pADwt-A6B is a haploid *S. cerevisiae* strain created by sporulating the diploid wild-type strain ADY101:pADwt and isolating the 4 spores. β-tubulin in this strain is the full length WT copy linked to the URA gene. ADY101:pADwt-1Ia is also a haploid strain created by sporulation of the diploid WT strain. In this haploid strain, which is ura-, the β-tubulin gene is the truncated tub2-590 copy. Among the haploid strains transformed with the pTS417ETA2 plasmid, the 1Ia isolate fluoresced brighter than the A6B isolates; cMTs were easier to visualize in the 1Ia isolate since the GFP appeared to fluoresce more intensely.

113

B: Phenotypic characterization of GFP-α-tubulin-expressing strains.

B1: Benomyl sensitivities of uninduced and induced GFP-plasmid containing haploid strains.

To determine whether induction and expression of GFP-β-tubulin from plasmid pTS417-ETA2 altered the sensitivity of the strain to benomyl, samples of the yeast cultures (both diluted and undiluted) were 'spotted' in 2 µl volumes onto a series of induction (YPD+G) and non-induction plates (YPD) containing a range of benomyl concentrations. As shown in Figures 3.3A and B, both the full length and truncated haploid strains were sensitive to benomyl at 20 µg/ml, and failed to grow at 30 µg/ml. The original strains, which did not contain the plasmid, were also sensitive to benomyl at 20 µg/ml and failed to grow at 30 µg/ml (see Figure 2.3B). Neither the presence of the plasmid, nor induction of the plasmid affected the sensitivity of either haploid wild-type strain to benomyl.

When compared to the haploid wild-type strains, the mutant strain, CLC9, was resistant to benomyl, and was able to grow at a benomyl concentration of 70 µg/ml (see Figure 2.3B). The CLC9 strain transformed with the GFP-induction plasmid pTS417-ETA2 was also resistant to 70 µg/ml benomyl, under both inducing and non-inducing conditions (see Figure 3.3A and B). The increase in the amount of α-

114

tubulin, when the transformed strain was placed under the induction conditions, did not alter benomyl resistance of the mutant strain.

B2: Doubling times of uninduced and induced GFP-plasmid containing yeast strains.

The vegetative DT of the strains containing the GFP-induction plasmid was determined under inducing and non-inducing conditions to assess whether the increase in the amount of tubulin in the form of GFP-α-tubulin, conferred any growth advantage. Strains containing the GFP-α-tubulin plasmid had similar DTs, whether the GFP-TUB3 on the plasmid was induced or not. The WT haploid strain doubled in 136 ± 22 min when the plasmid was not induced, and 135 ± 14 min when induced. The mutant CLC9 strain doubled in 119 ± 4 min when the plasmid was not induced, and 129 ± 20 min when induced. Figures 4.1A and B show the DTs of the strains, in the absence of benomyl, and in the presence of 2, 10 and 50 µg/ml benomyl under the two induction conditions. For the haploid wild-type strain, DT increased such that starting at benomyl concentrations between 10 and 50 µg/ml, it took over 200 min to complete one cell cycle, compared to roughly 130 min in the absence of drug. The wild-type strains were affected by 20 µg/ml benomyl on the plate and failed to grow in the presence of 30 µg/ml drug (Figure 3.3A and B). For the mutant strain, CLC9, even in the presence of 50 µg/ml benomyl, the DT remained below 200 min. Based on the spot test (Figure 3.3A and B) and these DT experiments, the CLC9 strain was

115

able to grow in extremely high concentrations of benomyl whether the GFP-α-tubulin

production was induced or not. Induction of the plasmid, and subsequent increase of

α-tubulin in the cell, did not change the growth or drug resistance of the wild-type

and mutant yeast strains.

Figure 4.1A: Doubling times for ADY101:pADwt (haploid) cells containing the GFP-plasmid in the presence and absence of benomyl, under uninduced and induced conditions. Uninduced condition, solid line with squares; induced condition, dotted line with open circles.
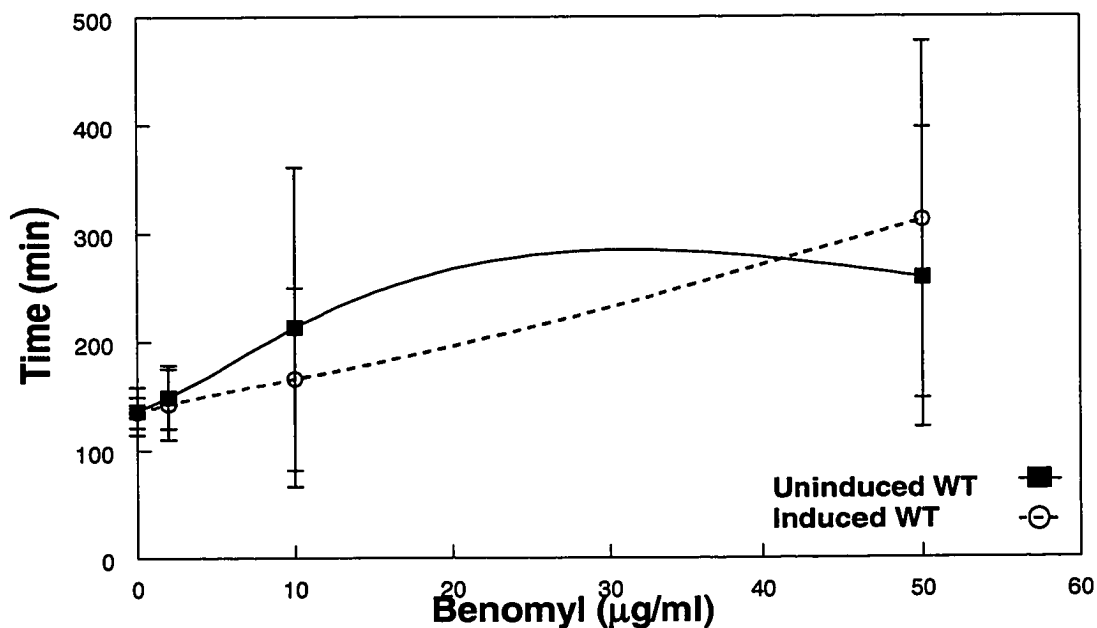
Figure 4.1B: Doubling time for CLC9 cells containing the GFP-plasmid in the presence and absence of benomyl, under uninduced and induced conditions. Uninduced condition, solid line with squares; induced condition, dotted line with open circles.
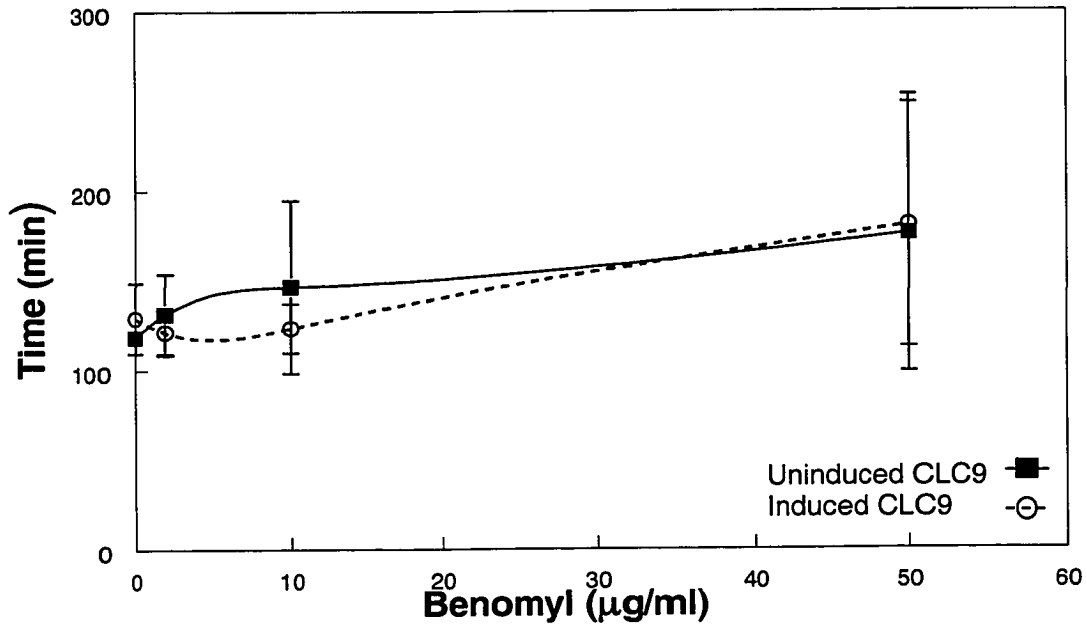
C: *In vivo* Microtubule Dynamics in the Haploid Strains.

C1: Dynamics of cMTs composed of either full length WT β-tubulin (TUB2) or truncated WT β-tubulin (tub2-590).

Since the MTs of both haploid wild-type strains were examined as controls to compare the dynamics of the MTs of the mutant haploid strain, it was necessary to

117

determine whether the MTs of the two wild-type strains behaved in a similar manner.

For the dynamic parameters listed in Table 4.1, only the mean attenuation duration

and the rescue frequency were statistically different between cMTs composed of the

full length and truncated wild-type β-tubulin strains. The attenuation duration for

cMTs in the truncated (ADY101:pADwt-1Ia) strain was 50 % longer than in the full

length (ADY101:pADwt-A6B) strain. The rescue frequency of cMTs in the full

length (ADY101:pADwt-A6B) strain was almost 4.5 times greater than in the

truncated (ADY101:pADwt-1Ia) strain. Twelve full length WT β-tubulin

(ADY101:pADwt-A6B) cMTs from 6 cells, and 15 truncated WT β-tubulin

(ADY101:pADwt-1Ia) cMTs from 9 cells were analyzed.

The differences between the two haploid wild-type strains could be a result of

examining a different composition of cells in different stages of the cell cycle. The

ratio of cMTs in cells sorted by stage of the cell cycle for ADY101:pADwt-1Ia

(truncated) was 9 unbudded, 0 small budded, and 6 big budded while the ratio for

ADY101:pADwt-A6B (full length) was 4 unbudded, 8 small budded, and 0 big

budded. Carminati and Stearns (1997), and Gupta (2001) reported that there are

differences in MT dynamics in cells at different stages of the cell cycle. Specifically,

Carminati and Stearns (1997) found faster rates of shortening in interphase

(unbudded) cells, while Gupta (2001) reported faster rates of growth and shorteing in

unbudded cells. Tirnauer et al., (1999) also found that there was greater dynamic

118

instability in unbudded cells, and reported that it was due to increased shortening rates as well as increased frequencies of catastrophes and rescues.

There were some differences in the proportion of time that cMTs spent in each dynamic phase, but the dynamicities of cMTs from the two strains were very similar, as shown in Table 4.2. The dynamic behavior of cMTs in each of these strains were similar in most respects. Based on these results, and the fact that the two strains have identical drug sensitivities, it was reasoned that both the full length β-tubulin and truncated β-tubulin expressing strains could be used in the analysis of cMT dynamics. For examination of the dynamic behaviors of the cMTs in the presence of benomyl, ADY101:pADwt-1Ia was the preferred strain because the GFP-tubulin in that strain appeared to fluoresce brighter than in the ADY101:pADwt-A6B strain, making the cMTs easier to visualize and track.

119

Table 4.1: **Comparison of dynamic parameters in the haploid wild-type strains ADY101:pADwt-A6B (full length WT) and ADY101:pADwt-1Ia (truncated WT)**

Mean of Dynamic Parameter ± SD	ADY101:pADwt-A6B (full length WT) n = 12 cMTs	ADY101:pADwt-1Ia (truncated WT) n = 15 cMTs
Growth rate (μm/min)	1.1 ± 0.6	1.3 ± 0.6
Shortening rate (μm/min)	2.3 ± 1.5	2.1 ± 1.3
Growth Duration (sec)	32.2 ± 22.3	32.9 ± 26.5
Shortening Duration (sec)	27.1 ± 19.0	36.8 ± 23.2
Attenuation Duration (sec)	27.6 ± 18.6	42.4 ± 25.3†
Catastrophe frequency (sec^{-1})	0.013 ± 0.013	0.014 ± 0.013
Rescue frequency (sec^{-1})	0.031 ± 0.030‡	0.007 ± 0.011
Dynamicity (dimers/sec)	28.4	30.3

† significantly longer duration (P = 0.02)
‡ significantly more frequent rescues (P = 0.007)

Table 4.2: **Proportion of time spent in phase in the haploid wild-type strains ADY101:pADwt-A6B (full length WT) and ADY101:pADwt-1Ia (truncated WT)**

	Growth Phase	Shortening Phase	Attenuation Phase
ADY101:pADwt-A6B	0.49	0.21	0.30
ADY101:pADwt-1Ia	0.35	0.31	0.34

120

C2: Dynamic instability behaviors of haploid WT cMTs.

The dynamic instability behaviors of MTs in the haploid WT strains were examined to establish the control parameters with which the MTs in the mutant strain could be compared. Typical life history traces of the WT cMTs are shown in Figure 4.2A. Like the cMTs in typical diploid WT cells (life history traces shown in Figure 3.5A), the cMTs of the haploid WT cells (with either full length or truncated β-tubulin) exhibited episodes of growth, shortening and attenuation, and showed transitions between growth or attenuation and shortening, and between shortening and attenuation or growth. The individual dynamic parameters and values for the cMTs in the haploid WT cells are shown in Tables 4.3 – 4.6. Twenty seven cMTs from 15 haploid WT cells were analyzed.

The mean MT growth rate in the haploid WT strains was 1.2 μm/min, the same as the growth rate in the diploid WT strain. The mean shortening rate (2.2 μm/min) was slightly faster in the haploid WT strains than in the diploid WT strain (1.8 μm/min), but this difference was not statistically significant. The MTs in the haploid WT strains, like in the diploid WT strain, exhibited faster shortening rates than the growth rates. The cMTs in the haploid WT strains spent approximately equal durations of time growing, shortening and in the attenuated state; for example, the mean duration for growth was 32.5 sec. cMTs in the diploid WT strain spent slightly longer periods of time in each attenuation phase (42.6 sec) than the haploid strains (33.8 sec), P =

121

0.09. The MTs in the haploid WT strains spent proportionally more of the total MT lifetime growing than in the diploid WT strain (42 % for the haploid compared to 34 % for the diploid), but the proportion of total lifetime spent in an attenuated state was similar in the WT strains (32 % for the haploid strain compared to 36 % for the diploid).

Catastrophes occurred slightly more frequently than rescues in the haploid WT strains (0.013 per sec for catastrophes and 0.018 per sec for rescues), but occurred slightly less frequently than in the diploid WT strain (0.018 per sec catastrophe frequency in the diploid wild-type strain). The frequency of rescues in the haploid and diploid WT strains was similar. More catastrophes were unrescued in the haploid WT strains (47 %) than in the diploid WT strain (26 %). However overall, dynamicity in the WT strains was similar (30.7 dimers per sec in the haploid strains, and 25.9 dimers per sec in the diploid strain).

122

Figure 4.2: Examples of typical MT life history traces in the haploid yeast strains: WT and CLC9. Figure 4.2A: MTs in the wild-type strains. Figure 4.2B: MTs in the mutant strain CLC9.

123
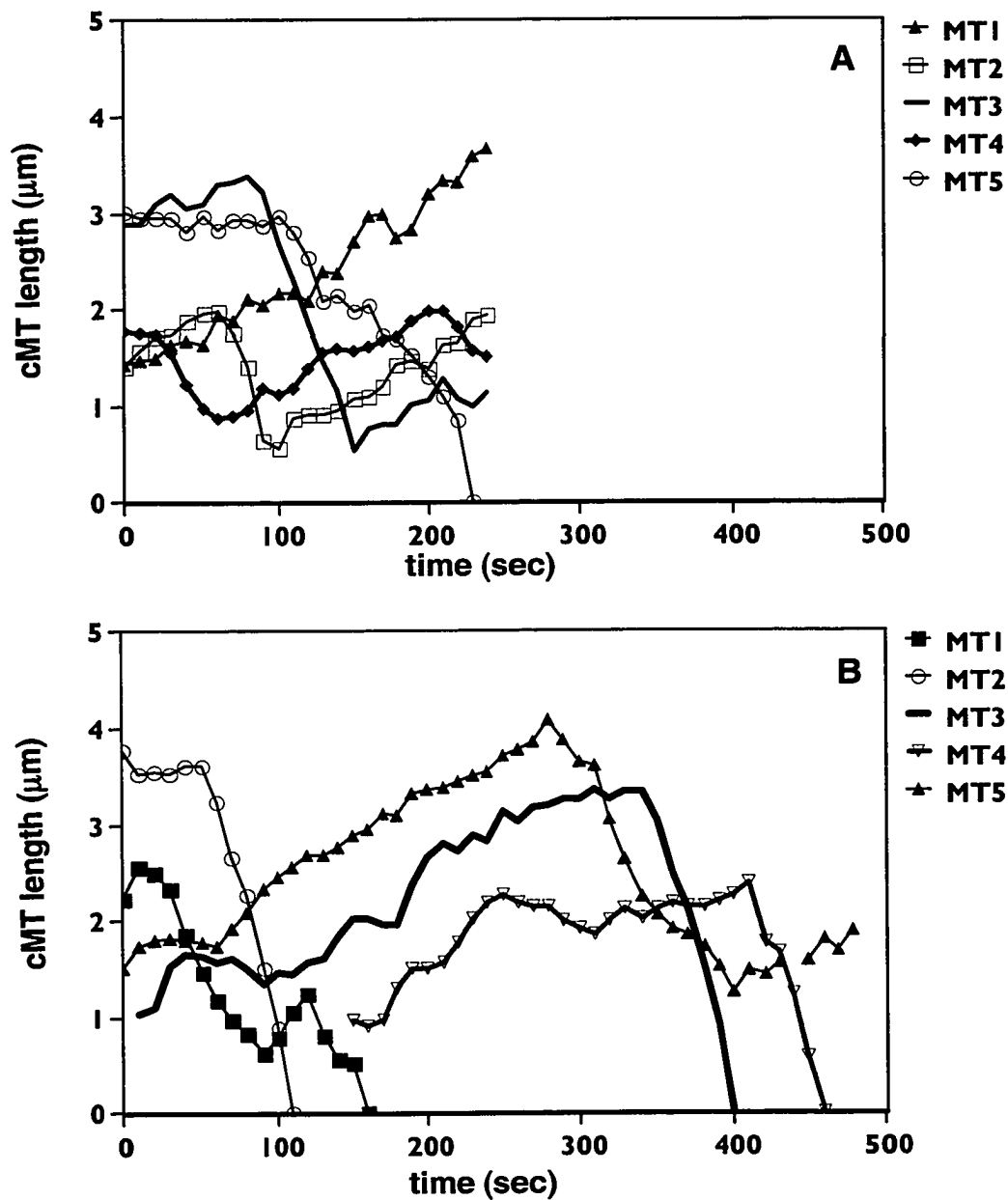
Table 4.3: Mean growth and shortening rates of MTs in the haploid wild-type yeast strains in the absence and presence of benomyl.

Rate ± SD	Benomyl (μg/ml)		
(μm/min)	0	2	10
Growth	1.2 ± 0.6 n = 69	1.1 ± 0.5 n = 46	0.6 ± 0.3† n = 9
Shortening	2.2 ± 1.4 n = 43	2.1 ± 1.1 n = 46	0.7 ± 0.3‡ n = 21

n is the number of events
† significantly slower than the untreated ($P = 0.007$) and low drug conditions ($P = 0.02$)
‡ significantly slower than the untreated ($P < 0.0001$) and the low drug conditions ($P < 0.0001$)

Table 4.4: Mean phase durations of MTs in the haploid wild-type yeast strains in the absence and presence of benomyl.

Duration ± SD	Benomyl (μg/ml)		
(sec)	0	2	10
Growth	32.5 ± 23.9 n = 60	49.1 ± 40.5† n = 46	35.3 ± 19.5 n = 9
Shortening	32.1 ± 21.6 n = 43	48.9 ± 35.9‡ n = 46	30.4 ± 14.7# n = 21
Attenuation	33.8 ± 22.7 n = 50	39.4 ± 37.3£ n = 35	99.7 ± 75.6£ n = 45

n is the number of events
† significantly longer duration than in the untreated condition ($P = 0.007$)
‡ significantly longer duration than in the untreated condition ($P = 0.009$)
# significantly shorter duration than the low drug condition ($P = 0.03$)
£ significantly longer duration in the presence of drug ($P < 0.0001$)

124

Table 4.5: Proportion of total lifetime MTs in the haploid WT yeast strain spend in growing, shortening and attenuated states.

Benomyl (µg/ml)	Growth	Shortening	Attenuation
0	0.42	0.26	0.32
2	0.38	0.38	0.23
10	0.06	0.12	0.82

4.6: Transition frequencies and overall dynamicity of cMTs in the Haploid WT yeast strains.

Benomyl (µg/ml)	Frequencies (sec^{-1})		% unrescued catastrophes	Dynamicity (dimers/sec)
	Catastrophe	Rescue		
0	0.013 ± 0.012 n = 27	0.018 ± 0.024 n = 27	47	30.7
2	0.020 ± 0.021 n = 25	0.008 ± 0.010‡ n = 25	56	34.5
10	0.005 ± 0.005† n = 21	0.022 ± 0.020# n = 21	5	3.2

n is the number of events
‡ less frequent than in untreated cells (P = 0.06)
† less frequent than the untreated (P = 0.007) and the low drug (P = 0.002) conditions
# more frequent than the low drug condition (P = 0.004)

125

C3: Dynamic instability characteristics of MTs in the haploid WT in the presence of benomyl.

The β-tubulin mutation in the haploid strain CLC9 rendered the cells super-resistant to benomyl. To determine how MTs composed of the mutant β-tubulin behaved in the presence of benomyl, it was necessary to determine how MTs composed of wild-type tubulin behaved in the presence of benomyl, to serve as an experimental control. Typical life history traces of cMTs of the haploid WT strains in the presence of benomyl are shown in Figures 4.3A and 4.4A. Cells in the presence of 2 μg/ml benomyl (Figure 4.3A) had cMTs that went through episodes of growth, shortening and attenuation, and transitions between the various phases were evident; the cMTs at this drug concentration appeared to be quite dynamic. However, as the life history traces in Figure 4.4A revealed, haploid WT cells in the presence of 10 μg/ml benomyl showed markedly reduced dynamics: periods of growth and shortening were few and the extent that the cMTs grew and shortened was reduced. These cMTs are very attenuated, compared to cMTs in the absence of benomyl. Twenty five cMTs in 9 haploid WT cells were analyzed at 2 μg/ml benomyl, and 21 cMTs in 17 haploid WT cells were analyzed at 10 μg/ml benomyl.

126

Figure 4.3: Examples of typical MT life history traces in haploid WT and CLC9 strains, in the presence of 2 µg/ml benomyl. Figure 4.3A: MTs in the wild-type strain. Figure 4.3B: MTs in the mutant strain CLC9.

127
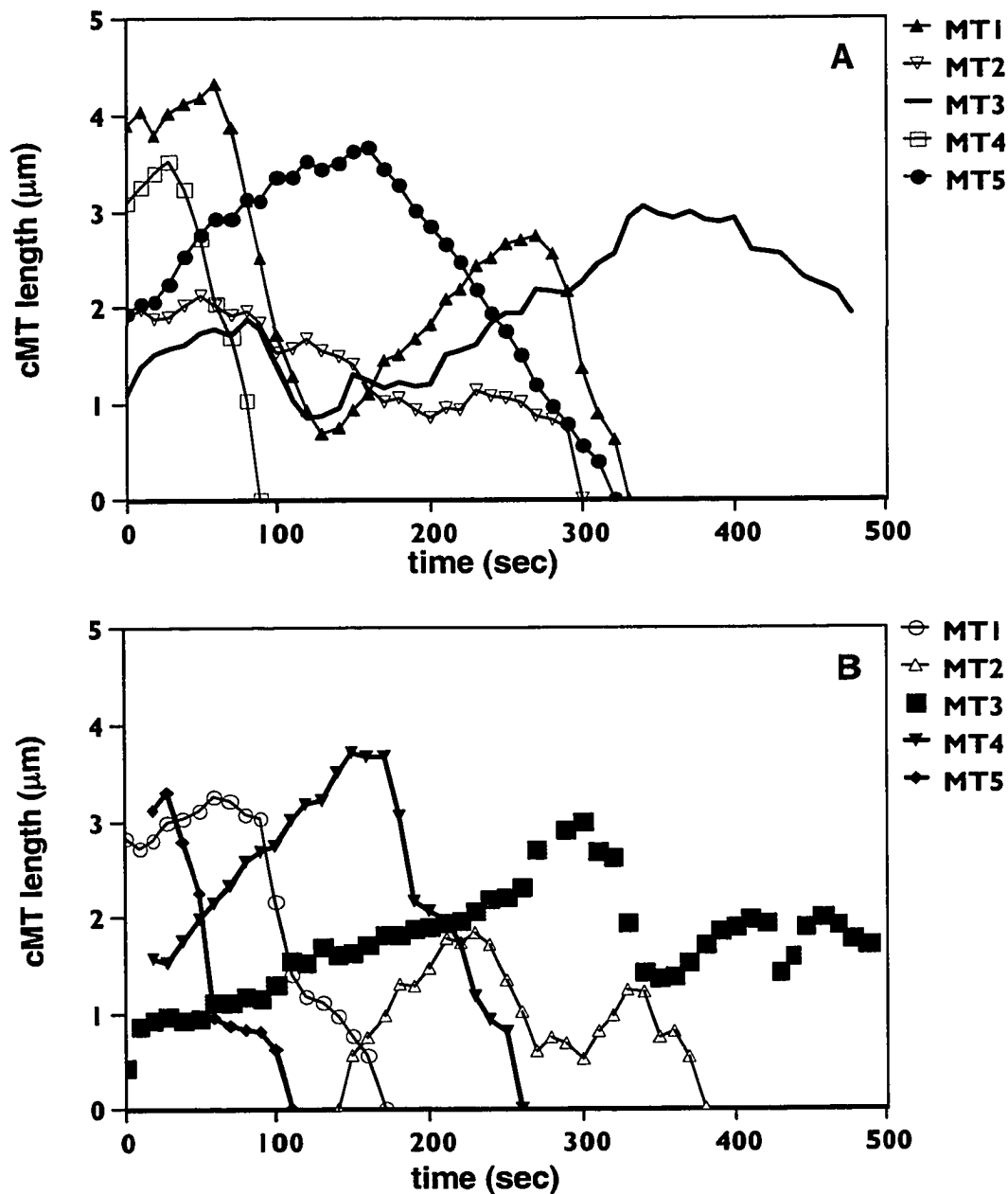
Figure 4.4: Examples of typical MT life history traces in haploid WT and CLC9 strains, in the presence of 10 μg/ml benomyl. Figure 4.4A: MTs in the wild-type strain. Figure 4.4B: MTs in the mutant strain CLC9 at 10 μg/ml benomyl.

128
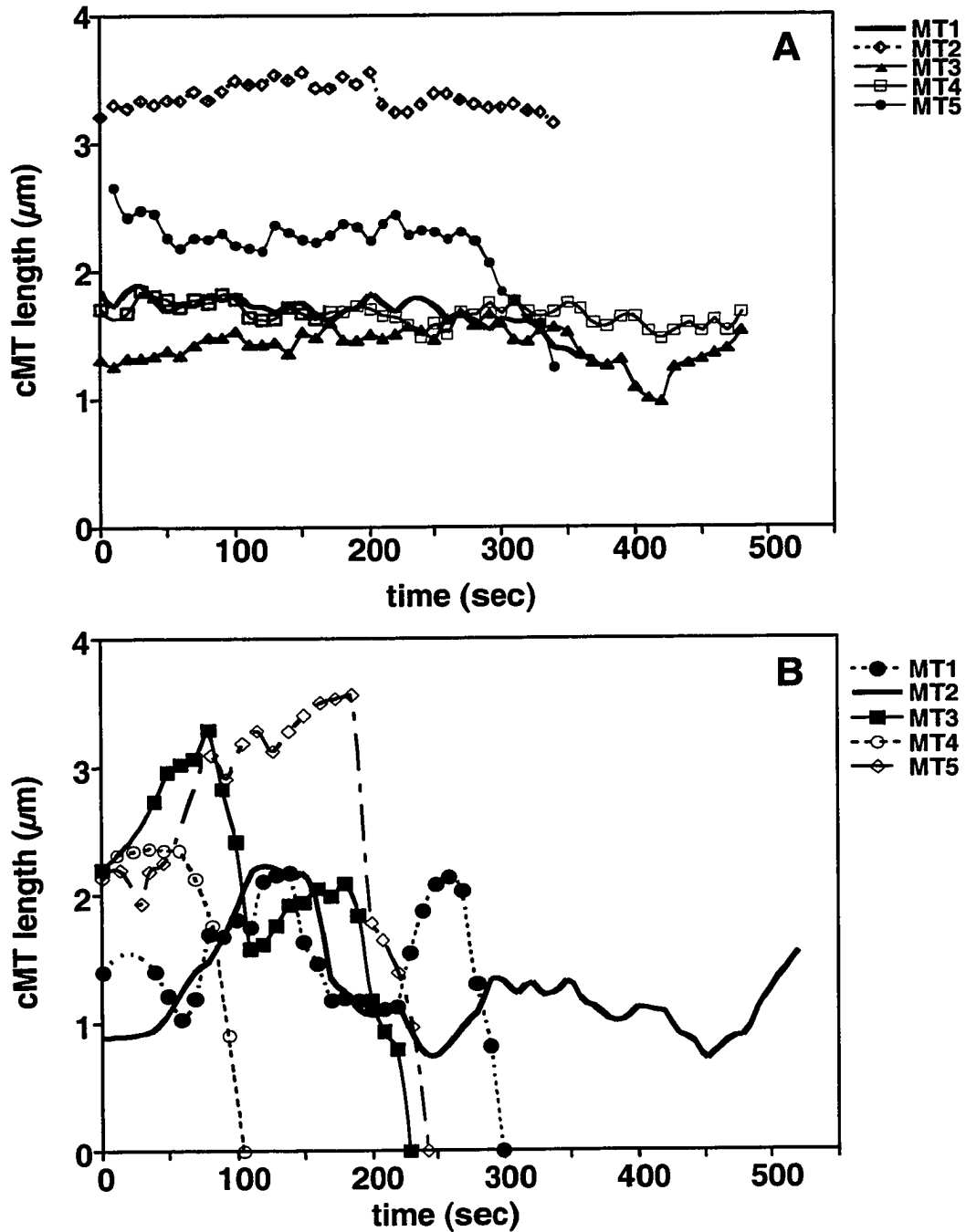
The growth and shortening rates of cMTs in the haploid WT cells in the presence of 2 μg/ml were the same as in the untreated cells (Table 4.3). Ten μg/ml benomyl reduced the growth and shortening rates significantly; the mean growth rate was one half and the shortening rate was one third of the rates in the absence of benomyl. The mean phase durations, of all phases, of haploid WT cMTs was increased significantly by 2 μg/ml benomyl (Table 4.4). Curiously, at 10 μg/ml benomyl, the mean shortening phase duration (30.4 sec) was significantly shorter than at 2 μg/ml benomyl (48.9 sec), but was similar to the duration in the absence of drug (32.1 sec). The mean growth duration at the highest drug concentration was also similar to the mean growth duration in the absence of benomyl. The MTs at the highest drug concentration (10 μg/ml) were attenuated for a significant duration of time (99.7 sec); this was significantly longer than the duration spent in the attenuated state in both the low drug (39.4 sec) and the no drug (33.8 sec) conditions. The WT MTs at 2 μg/ml benomyl spent equal proportions of total lifetime growing and shortening (38 %), but less time attenuated (23 %) (Table 4.5). At 10 μg/ml benomyl, however, the MTs were attenuated for over 80 % of their lifetime.

Catastrophes occurred more frequently than rescues in the presence of 2 μg/ml benomyl (0.020 per sec for catastrophes compared to 0.008 per sec for rescues), and were more frequent than in the absence of benomyl (0.013 catastrophes per sec) (Table 4.6). Rescues occurred significantly less frequently in the presence of 2 μg/ml benomyl than in the absence of drug (0.018 per sec). This may be due in part to the

129

strain used in the analysis at this drug concentration; ADY101:pADwt-IIa, in the

absence of drug, had a lower frequency of rescue than ADY101:pADwt-A6B. The

percent of catastrophes that were not rescued was higher in this low drug condition

than in the absence of drug (56 % versus 47 %). In the presence of 10 μg/ml

benomyl, the catastrophe frequency was significantly reduced (0.005 per sec), and the

frequency of rescue increased significantly (0.022 per sec). As a result of this shift,

95 % of all catastrophes were rescued at the high benomyl concentration. The

dynamicity of haploid WT cMTs at 10 μg/ml benomyl (3.2 dimers/sec) decreased to

roughly one tenth of the dynamicity in the absence or presence of 2 μg/ml benomyl.

While cMTs in the haploid WT strain remained dynamic in the presence of 2 μg/ml

benomyl (34.5 dimers/sec), a high benomyl concentration (10 μg/ml) severely

attenuated MT dynamics.

C4: Dynamic characteristics of MTs in the mutant CLC9 strain.

Since CLC9 is a haploid strain, all of the β-tubulin produced in these cells is the

mutated form. The β-tubulin in this strain has been altered, so that the amino acid at

position 318 is tryptophan instead of arginine. Typical life history traces of MTs in

the mutant CLC9 strain, are shown in Figure 4.2B. As in the haploid WT strains, the

mutant strain's MTs also displayed episodes of growth, shortening and attenuation.

Transitions from growth to shortening or attenuation, and from shortening to either

130

growth or attenuation also occurred. The life history traces of these MTs assembled

from mutated β-tubulin are indistinguishable from those of the haploid WT strains.

The parameters examined and the values that characterize the dynamics of the MTs in

the CLC9 strain are shown in Tables 4.7 to 4.10. The mean shortening rate was twice

as fast as the mean growth rate. The mean phase duration and proportion of total

lifetime in phase were the greatest for growth, followed by shortening and the

attenuated state; the MTs spent a mean of 37.7 sec per growth event, 30.6 sec per

shortening event, and 26.3 sec per attenuation event. Only 20 % of the total MT

lifetime was spent in the attenuated state. The catastrophe frequency was slightly

higher than the rescue frequency, but this difference was not statistically significant.

Forty percent of all catastrophes were not rescued. The dynamicity was relatively

high, at 36.2 dimers per sec.

Table 4.7: Mean growth rates and shortening rates of MTs in the mutant yeast strain, CLC9, in the absence and presence of benomyl.

Rate ± SD (μm/min)	Benomyl (μg/ml)		
	0	2	10
Growth	1.0 ± 0.6 n = 64	1.3 ± 0.6† n = 28	1.1 ± 0.7 n = 69
Shortening	2.2 ± 1.4 n = 67	2.0 ± 1.2 n = 37	1.9 ± 1.2 n = 68

n is the number of events
† significantly faster than in untreated cells (P = 0.05)

131

Table 4.8: Mean phase durations for MTs in the mutant yeast strain, CLC9, in the absence and presence of benomyl.

Duration ± SD (sec)	Benomyl (μg/ml)		
	0	2	10
Growth	37.7 ± 27.0 n = 64	38.4 ± 39.5 n = 28	46.9 ± 46.6 n = 69
Shortening	30.6 ± 18.7 n = 67	32.4 ± 25.0 n = 37	33.0 ± 20.6 n = 69
Attenuation	26.3 ± 16.9 n = 43	23.8 ± 16.6 n = 31	28.7 ± 16.1 n = 38

n is the number of events

Table 4.9: Proportion of total lifetime that MTs in the mutant strain, CLC9, spent in each phase.

Benomyl (μg/ml)	Growth	Shortening	Attenuation
0	0.43	0.37	0.20
2	0.36	0.40	0.25
10	0.49	0.34	0.17

132

Table 4.10: Transition frequencies and overall dynamicity of MTs in the mutant strain, CLC9.

Benomyl (μg/ml)	Frequencies (sec^{-1})		% unrescued catastrophes	Dynamicity (dimers/sec)
	Catastrophe	Rescue		
0	0.028 ± 0.025 n = 32	0.019 ± 0.023 n = 32	40	36.2
2	0.025 ± 0.016 n = 18	0.014 ± 0.016 n = 18	49	36.7
10	0.021 ± 0.016 n = 29	0.015 ± 0.015 n = 29	40	36.0

n is the number of events

C5: Dynamic characteristics of MTs in the CLC9 strain, in the presence of benomyl.

The mutant haploid strain, CLC9, is super-resistant to benomyl. This yeast strain is capable of growing even in the presence of 70 μg/ml benomyl (see Figures 2.3B, 3.3A and 3.3B). As can be seen in Figures 4.2B, 4.3B and 4.4B, the life history plots of the MTs in this strain display episodes of growth, and shortening, up to and including in the presence of 10 μg/ml benomyl. Catastrophes and rescues also occurred at all drug conditions. When the dynamic parameters were calculated, the only parameter to significantly change was a small but significant increase in growth rate at 2 μg/ml drug. All other parameters were not affected with either low or high concentrations of benomyl. In the three other strains examined, the duration and

133

proportion of total lifetime that MTs were in an attenuated state increased with drug

concentration. However, for CLC9, these parameters were not affected. The percent

of catastrophes that remained unrescued and the dynamicity also remained high even

in the presence of 10 μg/ml drug. MTs in the mutant strain CLC9, when exposed to

benomyl, behaved like untreated WT MTs.

C6: Dynamic properties of cMTs in the haploid yeast strains ADY101:pADwt-A6B, ADY101:pADwt-1Ia and CLC9, in the absence and presence of benomyl.

The dynamics of the MTs in the haploid WT strains were affected by increasing

concentrations of benomyl. In comparison, the dynamics of the MTs in the CLC9

strain were unaffected by drug. (See Tables 4.11 – 4.14).

In the absence of benomyl, the MT growth and shortening rates of the WT and mutant

strains were the same. For both strains, the shortening rate was approximately twice

as fast as the growth rate. The mean phase durations of the MTs for the two strains

were very similar, with the exception of the mean attenuation duration; the mean

duration that WT MTs were attenuated was slightly longer than the mutant MTs (33.8

and 26.3 sec, respectively). In the absence of drug, the MTs of both strains spent the

same proportion of time growing (42 % of the MT lifetime). MTs in the mutant

strain spent proportionally more time shortening and less time attenuated than the

MTs in the WT strain. The mutant strain MTs underwent catastrophes twice as

134

frequently than the WT MTs, a significant difference. The rescue frequencies in the

WT and mutant strains were similar, but the percentage of unrescued catastrophes

was slightly higher in the WT strain than then mutant strain. MT dynamicity in the

mutant strain (35.3 dimers/sec) was higher than that in the WT strain (29.9

dimers/sec).

Table 4.11: Mean MT Growth and Shortening Rates in the Haploid WT and mutant strain, CLC9

	Benomyl (μg/ml)		
	0	2	10
Growth Rate (μm/min)			
Haploid WT	1.2 ± 0.6 n = 69	1.1 ± 0.5 n = 46	0.6 ± 0.3 n = 9
CLC9	1.0 ± 0.6 n = 64	1.3 ± 0.6 n = 28	1.1 ± 0.7† n = 69
Shortening Rate (μm/min)			
Haploid WT	2.2 ± 1.4 n = 43	2.1 ± 1.1 n = 46	0.7 ± 0.3 n = 21
CLC9	2.2 ± 1.3 n = 67	2.0 ± 1.2 n = 37	1.9 ± 1.2‡ n = 69

n is the number of events
† significantly faster than the wild-type strain (P = 0.05)
‡ significantly faster than the wild-type strain (P < 0.0001)
± = SD

At 2 μg/ml benomyl, as in the absence of drug, the MT growth and shortening rates

of the two strains were similar. The mean growth duration of the MTs in the WT

135

strain (49.1 sec) was longer than those of the mutant strain (38.4 sec), but this difference was not statistically significant. The mean shortening and mean attenuation durations of the WT MTs were significantly longer than those of the MTs in the CLC9 strain. The overall proportions of total lifetime that MTs of the two strains spent in the 3 phases, however, were within 2 percent of each other in all phases, at 2 µg/ml benomyl; cMTs in the wild-type strain spent 38 % of their total lifetime in the growth phase, while cMTs in the mutant strain spent 36 % of their total lifetime growing. The frequencies of catastrophe and rescue for MTs in the haploid WT strain were lower than in the mutant strain, but the differences were not statistically significant. The rescue frequency of the MTs in the mutant strain was almost twice that of the MTs in the WT strain (0.014 per sec versus 0.008 per sec). The percentage of unrescued catastrophes for both strains increased 9 % from the untreated condition. The percentage of unrescued catastrophes for the WT strain increased from 47 % in the untreated cells to 56 %, while that for MTs of CLC9 cells increased from 40 % in the untreated cells to 49 %. The dynamicity of the WT strain's MTs increased slightly at 2 µg/ml benomyl as compared to the untreated condition, and the dimer exchange rate became very similar to that of the mutant MTs (34.5 dimers per sec for the WT and 36.7 dimers per sec for the CLC9 strain).

At 10 µg/ml benomyl, the MT life history traces revealed that the WT MTs were very attenuated while the mutant MTs remained dynamic (Figure 4.4A and B). The growth rate for MTs in the WT at 10 µg/ml benomyl was reduced to 50 % of the MT

136

growth rate in the mutant strain, and the shortening rate was reduced to 63 % of the rate in the CLC9 strain. The mean growth durations of the MTs in the WT and mutant cells were not significantly different from each other, but the duration of growth of the MTs in the WT cells (35.3 sec) was somewhat shorter than in the mutant cells (46.9 sec). The mean shortening durations for the two strains at 10 $\mu g/ml$ benomyl were similar to each other; the shortening duration for MTs in the WT strain was 35.3 sec while the shortening duration for MTs in the mutant cells was 33.0 sec. The mean attenuation duration of the MTs in the WT strain was almost 3.5 fold longer than the attenuation duration of the mutant MTs, and was statistically significant. MTs in the WT strain remained in an attenuated state for more than 80 % of their recorded lifetime at 10 $\mu g/ml$ benomyl, while MTs in the CLC9 strain were in an attenuated state for four-fold less time.

With respect to transition frequencies, at 10 $\mu g/ml$ benomyl, the catastrophe frequency in the wild-type strain was greatly reduced in comparison to the catastrophe frequency of MTs in CLC9 cells. The MTs in the WT cells transitioned to shortening significantly less frequently than MTs in the mutant strain (0.005 per sec versus 0.021 per sec). The rescue frequencies of MTs in the two strains, however, were not significantly different from each other at 10 $\mu g/ml$ benomyl. Because of the reduced frequency of catastrophe in the WT strain, the percentage of unrescued catastrophes of the MTs in this strain was greatly reduced, and was eight-fold less than for MTs in CLC9 cells. Not surprising was the decrease in the dynamicity of the

137

MTs in the WT strain. The dynamicity was more than 10-fold lower than the dynamicity in the mutant cells (3.2 dimers per sec compared to 36.0 dimers per sec). The change in dynamicity for the haploid strains are shown over the range of benomyl concentrations used in Figure 4.5.

Table 4.12: Mean Phase Durations for MT Growth, Shortening and Attenuation in the Haploid WT and mutant strain, CLC9

	Benomyl (μg/ml)		
	0	**2**	**10**
Growth Duration (sec)			
Haploid WT	32.5 ± 23.9 n = 69	49.1 ± 40.5 n = 46	35.3 ± 19.5 n = 9
CLC9	37.7 ± 27.0 n = 64	38.4 ± 39.5 n = 28	46.9 ± 46.6 n = 69
Shortening Duration (sec)			
Haploid WT	32.1 ± 21.6 n = 43	48.9 ± 35.9 n = 46	35.3 ± 19.5 n = 9
CLC9	30.6 ± 18.7 n = 67	32.4 ± 25.0† n = 37	33.0 ± 20.6 n = 69
Attenuation Duration (sec)			
Haploid WT	33.8 ± 22.7 n = 50	39.4 ± 37.3 n = 35	99.7 ± 75.6 n = 45
CLC9	26.3 ± 16.9‡ n = 43	23.8 ± 16.6# n = 31	28.7 ± 16.1£ n = 38

n is the number of events
† significantly shorter duration than the wild-type (P = 0.02)
‡ significantly shorter duration than the wild-type (P = 0.08)
# significantly shorter duration than the wild-type (P = 0.04)
£ significantly shorter duration than the wild-type (P < 0.0001)

139

Table 4.13: Proportion of total lifetime that MTs in the Haploid WT and mutant strain, CLC9, spent growing, shortening, or in an attenuated phase.

	Growth Phase	Shortening Phase	Attenuated Phase
Haploid WT untreated	0.42	0.26	0.32
CLC9 untreated	0.43	0.37	0.20
Haploid WT 2 µg/ml benomyl	0.38	0.38	0.23
CLC9 2 µg/ml benomyl	0.36	0.40	0.25
Haploid WT 10 µg/ml benomyl	0.06	0.12	0.82
CLC9 10 µg/ml benomyl	0.49	0.34	0.17

140

Table 4.14: Transition Frequencies and Dynamicity of MTs in the Haploid WT and mutant strain, CLC9

	Benomyl (μg/ml)		
	0	**2**	**10**
Catastrophe Frequency (sec^{-1})			
Haploid WT	0.013 ± 0.012 n = 27	0.020 ± 0.021 n = 25	0.005 ± 0.005 n = 21
CLC9	0.028 ± 0.025‡ n = 32	0.025 ± 0.016 n = 18	0.021 ± 0.016† n = 29
Rescue Frequency (sec^{-1})			
Haploid WT	0.018 ± 0.024 n = 27	0.008 ± 0.010 n = 25	0.022 ± 0.020 n = 21
CLC9	0.019 ± 0.023 n = 32	0.014 ± 0.016 n = 18	0.015 ± 0.015 n = 29
% Unrescued Catastrophes			
Haploid WT	47	56	5
CLC9	40	49	40
Dynamicity (dimers/sec)			
Haploid WT	30.7	34.5	3.2
CLC9	36.2	36.7	36.0

n is the number of events
‡ significantly more frequent catastrophes than the wild-type (P = 0.006)
† significantly more frequent catastrophes than the wild-type (P < 0.0001)

141

Figure 4.5: Dynamicity of the MTs in the haploid yeast strains ADY101:pADwt wild-type (ADY101:pADwt-A6B and ADY101:pADwt-1Ia) and CLC9 at a range of benomyl concentrations. Wild-type, solid line and open circles, CLC9 mutant strain, dotted line and filled squares.
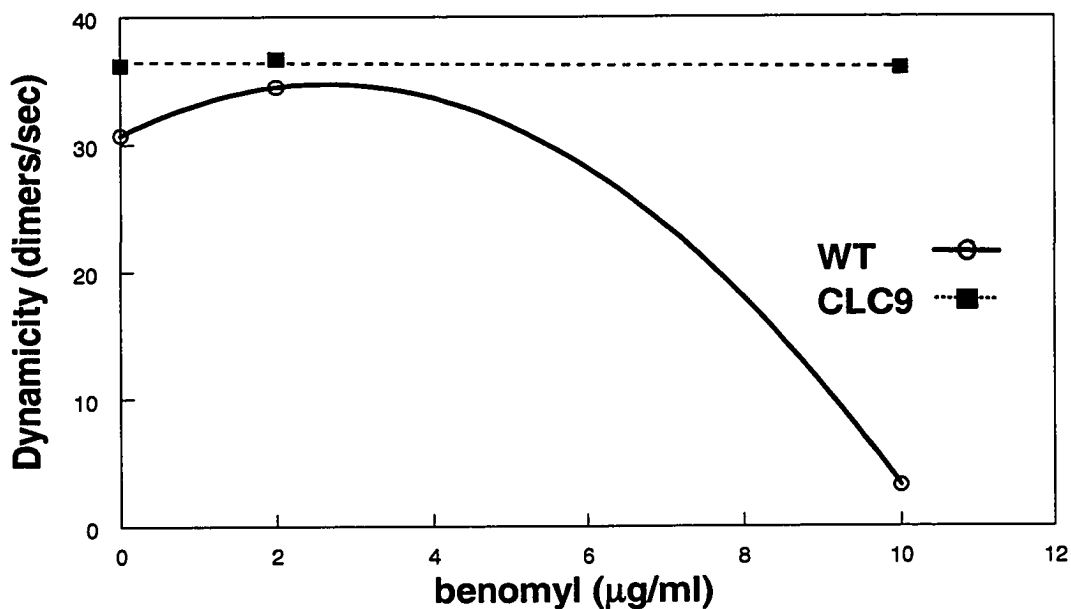
Discussion

The yeast *Saccharomyces cerevisiae* is a very good model system in which to study

how alterations in the structure of tubulin affect the function of the MTs. By using an

inducible GFP-α-tubulin construct to permit the visualization of the cMTs *in vivo*, the

dynamics of MTs in yeast strains with mutated and wild-type β-tubulin could be

examined and characterized. In this chapter, the dynamic properties of cMTs in the

142

haploid yeast strains ADY101:pADwt-A6B, ADY101:pADwt-1Ia, and CLC9 were examined. In these strains, the β-tubulin composition was either completely wild-type or completely mutant.

The difference between the wild-type haploid strains and CLC9, (outside of the presence or absence of the C-terminal 12 amino acids), was a mutation which changed amino acid 318 from an arginine to a tryptophan. The effects of this single amino acid change on the dynamic properties of the MTs in CLC9 are striking, particularly in the presence of the antimitotic drug benomyl.

The behavior of the MTs in the haploid wild-type strains was similar to that of the MTs in the diploid WT and CLC8 strains. The WT strains and the mutant strain, CLC8, were all sensitive to benomyl and the dynamics of their MTs were severely diminished by 10 μg/ml benomyl (3 μg/ml for the CLC8 strain). Benomyl effectively diminished the rates of growth and shortening, and extended the duration that the MTs remained in an attenuated state. MTs were in an attenutated state for the majority of their lifetime. While 10 μg/ml benomyl was the concentration necessary to effectively eliminate MT dynamics for the wild-type strains (ADY101:pADwt, ADY101:pADwt-A6B, and ADY101:pADwt-1Ia), only 3 μg/ml benomyl was required to do the same to MTs in the mutant strain CLC8. The MTs of the mutant haploid strain CLC9, however, behaved very differently and were not affected even in

143

the presence of 10 μg/ml benomyl. MTs in the CLC9 strain remained very dynamic at 10 μg/ml benomyl.

The β-tubulin of CLC9 cells is different from the full length haploid strains by only one amino acid (R318W), and the dynamics of the MTs are unaffected by benomyl. CLC9 MTs appear insensitive to the drug under all conditions examined; the MT dynamics in CLC9 cells at 10 μg/ml behaved like MTs in untreated cells. According to Richards et al., (2000), the pocket in which amino acid 318 is positioned, is either the benomyl binding site or changes conformationally with benomyl binding. Given that a one amino acid change alters the sensitivity to benomyl so drastically, it is possible that R318 plays an important role in the binding of benomyl, or that the alteration of an arginine to a tryptophan changes the conformation of the β-tubulin subunit such that the benomyl binding site, which may be in another part of the molecule, is altered.

144

References

Adames, N.R., and Cooper, J.A. (2000). Microtubule interactions with the cell cortex causing nuclear movements in *Saccharomyces cerevisiae*. J. Cell Biol. 149: 863-874.

Bai, R., Pei, X-F., Boye, O., Getahun, Z., Grover, S., Bekisz, J., Nguyen, N.Y., Brossi, A., and Hamel, E. (1996). Identification of cysteine 354 of β-tubulin as part of the binding site for the A-ring of colchicine. J. Biol. Chem. 271:12639-12645.

Banerjee, A., and Luduena, R.F. (1992). Kinetics of cochicine binding to purified β-tubulin isotypes from bovine brain. J. Biol. Chem. 267: 13335-13339.

Barnes, G., Louie, K.A., and Botstein, D. (1992). Yeast proteins associated with microtubules in vitro and in vivo. Mol. Biol. Cell 3:29-47.

Becker, D.M., and Guarente, L. (1991). High-efficiency transformation of yeast by electroporation. Methods in Enzymology 194: 182-187.

Belmont, L.D., Hyman, A.A., Sawin, K.E., and Mitchison, T.J. (1990). Real-time visualization of cell cycle-dependent changes in microtubule dynamics in cytoplasmic extracts. Cell 62:579-589.

Blohkin, A.V., Yoo, H.D., Geralds, R.S., Nagle, D.G., Gerwick, W.H., and Hamel, E. (1995). Characterization of the interaction of the marine cyanobacterial natural product curacin A with the colchicine site of tubulin and initial sturcture-activity studies with analogues. Mol. Pharm. 48: 523-531.

Bond, J.F., Fridovich-Keil, J.L., Pillus, L., Mulligan, R.C., and Solomon, F. (1986). A chicken-yeast chimeric β-tubulin protein is incorporated into mouse microtubules in vivo. Cell 44: 461-468.

Borisy, G.G., and Taylor, E.W. (1967a). The mechanism of action of colchicine. Binding of colchicine-^{3}H to cellular protein. J.Cell Biol. 34: 525-533.

Borisy, G.G., and Taylor, E.W. (1967b). The mechanism of action of colchicine. Colchicine binding to sea urchin eggs and the mitotic apparatus. J. Cell Biol. 34: 535-548.

Botstein, D., Amberg, D., Mulholland, J., Huffaker, T., Adams, A., Drubin, D., and Stearns, T. (1997). The Yeast Cytoskeleton. *In* The Molecular and Cellular Biology of the Yeast *Saccharomyces*: Cell Cycle and Cell Biology. J.R. Pringle, J.R. Broach and E.W. Jones, editors. Cold Spring Harbor Laboratory, Cold Spring Harbor, NY. 1997, pp 1-90.

145

Botstein, D., Chervitz, S.A., and Cherry, J.M. (1997). Yeast as a model system. Science 277: 1259-1260.

Burns, R.G. (1992). Analysis of the colchicine-binding site of β-tubulin. FEBS Letters 297(3): 205-208.

Byers, B. (1981). Cytology of the yeast life cycle. *In* The molecular biology of the yeast Saccharomyces: Life cycle and inheritance (ed. J.N. Strathern et al.), pp.59-96. Cold Spring Harbor Laboratory Press, Cold Spring Harbor, New York.

Byers, B., and Goetsch, L. (1974). Duplication of spindle plaques and integration of the yeast cell cycle. Cold Spring Harbor Symp. Quant. Biol. 38: 123-131.

Byers, B., and Goetsch, L. (1975). Behavior of spindles and spindle plaques in the cell cycle and conjugation of *Saccharomyces cerevisiae. J Bacteriol.* **124**, 511-523.

Carminati, J.L., and Stearns, T. (1997). Microtubules orient the mitotic spindle in yeast through dynein-dependent interactions with the cell cortex. J. Cell Biol. 138(3): 629-641.

Cassimeris, L., Pryer, N.K., and Salmon, E.D. (1988). Real-time observations of microtubule dynamic instability in living cells. J. Cell Biol. 107: 2223-2231.

Davis, A., Sage, C.R., Wilson, L., and Farrell, K.W. (1993). Purification and biochemical characterization of tubulin from the budding yeast *Saccharomyces cerevisiae.* Biochemistry 32:8823-8835.

Davis, A., Sage, C.R., Dougherty, C.A., and Farrell, K.W. (1994). Microtubule dynamics modulated by guanosine triphosphate hydrolysis activity of β-tubulin. Science 264: 839-842.

Davidse, L.C., and Flach, W. (1977). Differential binding of methyl benzimidazol – 2-yl carbamate to fungal tubulin as a mechanism of resistance to this antimitotic agent in mutant strains of *Aspergillis nidulans.* J. Cell Biol. 72: 174-193.

Derry, W.B., Wilson, L., and Jordan, M.A. (1995). Substoichiometric binding of taxol suppresses microtubule dynamics. Biochemistry 34: 2203-2211.

Derry, W.B., Wilson, L., Khan, I.A., Luduena, R.F., and Jordan, M.A. (1997). Taxol differentially modulates the dynamics of microtubules assembled from unfractionated and purified β-tubulin isotypes. Biochem. 36: 3554-3562.

Desai, A., and Mitchison, T.J. (1997). Microtubule polymerization dynamics. Ann. Rev. Cell Dev. Biol. 13: 83-117.

Downing, K.H. (2000). Structural basis for the interaction of tubulin with proteins andn drugs that affect microtubule dynamics. Annu. Rev. Cell Dev. Biol. 16: 89-111.

Downing, K.H., and Nogales, E. (1998). New insights into microtubule structure and function from the atomic model of tubulin. Eur. Biophys. J. 27: 431-436.

Downing, K.H., and Nogales, E. (1999). Crystallographic structure of tubulin: Implications for dynamics and drug binding. Cell Structure and Function 24: 269-275.

Doxsey, S. (2001). Re-evaluating centrosome function. Nature Reviews Mol.Cell Biol. 2: 688-698.

Dustin, P. (1984). Microtubules. Springer-Verlag, New York. pp.452

Dutcher, S.K., and Trabuco, E.C. (1998). The UNI3 gene is required for assembly of basal bodies of *Chlamydomonas* and encodes delta tubulin, a new member of the tubulin superfamily. Molecular Biology of the Cell 9:1293-1308.

Farrell, K.W., Jordan, M.A., Miller, H.P., and Wilson, L. (1987). Phase dynamics at microtubule ends: the coexistence of microtubule length changes and treadmilling. J. Cell Biol. 104:1035-1046.

Fridovich-Keil, J.L., Bond, J.F., and Solomon, F. (1987). Domains of β-tubulin essential for conserved functions in vivo. Mol. Cell. Biol. 7: 3792-3798.

Friedman, P.A., and Platzer, E.G. (1978). Interaction of anthelmintic benzimidazoles and benzimidazole derivatives with bovine brain tubulin. Biochim. Biophys. Acta 544: 605-614.

Gonçalves, A., Braguer, D., Kamath, K., Martello, L., Briand, C., Horwitz, S., Wilson, L., and Jordan, M.A. (2001). Resistance to Taxol in lung cancer cells associated with increased microtubule dynamics. PNAS 98: 11737-11741.

Gupta, Mohan. (2001). Mutational analysis of cysteine residues in *Saccharomyces cerevisiae* beta-tubulin: Importance of Cys354 in microtubule dynamics. Ph.D dissertation. University of Kansas, Lawrence.

Gupta, M., Bode, C.J., Thrower, D.A., Pearson, C.G., Suprenant, K.A., Bloom, K.S., and Himes, R.H. (2002). β-tubulin C354 mutations that severely decrease

microtubule dynamics do not prevent nuclear migration in yeast. Mol. Biol. Cell. *In press.*

Hamel, E. (1996). Antimitotic natural products and their interactions with tubulin. Med. Res. Rev. 16: 207-231.

Hastie, S.B. (1991). Interactions of colchicine with tubulin. Pharmac. Ther. 51: 377-401.

Huffaker, T.C., Thomas, J.H., and Botstein, D. (1988). Diverse effects of β-tubulin mutations on microtubule formation and function. J. Cell Biol. 106: 1997-2010.

Jordan, M.A., and Wilson, L. (1998). Microtubules and actin filaments: dynamic targets for cancer chemotherapy. Curr. Opin. Cell Biol. 10: 123-130.

Khan, I.A., and Luduena, R.F. (1994). Vinblastine induced inhibition of the assembly of isotypically pure tubulins from bovine brain. Mol. Cell. Biol. 5:284a.

Katz, W.S., and Solomon, F. (1988). Diversity among β-tubulins: A carboxy-terminal domain of yeast β-tubulin is not essential in vivo. Mol. Cell. Biol. 8: 2730-2736.

Kilmartin, J.V. (1981). Purification of yeast tubulin by self-assembly in vitro. Biochem. 20: 3629-3633.

Kosco, K.A., Pearson, C.G., Maddox, P.S., Wang, P.J., Adams, I.R., Salmon, E.D., Bloom, K., and Huffaker, T.C. (2001). Control of microtubule dynamics by Stu2p is essential for spindle orientation and metaphase chromosome alignment in yeast. Mol. Biol. Cell 12: 2870-2880.

Lacey, E. (1988). The role of the cytoskeletal protein, tubulin, in the mode of actrion and mechanism of drug resistance to benzimidazoles. Int. J. Parasitol. 18: 885-936.

Li, J; Katiyar, S.K.; Edlind, T.D. (1996). Site-directed mutagenesis of Saccharomyces cerevisiae beta-tubulin – interaction between residue 167 and benzimidazole compounds. FEBS Letters, 385: 7-10.

Luduena, R.F. (1979). Biochemistry of Tubulin. *In* Microtubules. K. Roberts and J.S. Hyams, editors. Academic Press, London, 1979. 65-116.

Luduena, R.F. (1998). Multiple forms of tubulin: Different gene products and covalent modifications. Int. Rev. Cytol. 178: 207-275.

148

Maddox, P., Chin, E., Mallavarapu, A., Yeh, E., Salmon, E.D., and Bloom, K. (1999). Microtubule dynamics from mating through the first zygotic division in the budding yeast *Saccharomyces cerevisiae*. J. Cell Biol. 144(5): 977-987.

Maddox, P., Bloom, K., and Salmon, E.D. (2000). The polarity and dynamics of microtubule assembly in the budding yeast *Saccharomyces cerevisiae*. Nature Cell Biology 2: 36-41.

Margolis, R.L., and Wilson, L. (1978). Opposite end assembly and disassembly of microtubules at steady state in vitro. Cell 13:1-8.

Matsuzaki, F; Matsumoto, S; and Yahara, I. (1988). Truncation of the carboxyl-terminal domain of yeast .beta.-tubulin causes temperature-sensitive growth and hypersensitivity to antimitotic drugs. Journal of Cell Biology, 107: 1427-1436

McNally, F.J. (1996). Modulation of microtubule dynamics during the cell cycle. Curr. Opin. Cell Biol. 8: 23-29.

Mitchison, T.J., and Kirschner, M. (1984). Dynamic instability of microtubule growth. Nature 312:237-242.

Moens, P.B., and Rapport, E. (1971). Spindles, spindle plaques, and meiosis in the yeast *Saccharomyces cerevisiae* (Hansen). J. Cell Biol. 50: 344-361.

Neff, N.F., Thomas, J.H., Grisafi, P., and Botstein, D. (1983). Isolation of the β-tubulin gene from yeast and demonstration of its essential function in vivo. Cell 33: 211-219.

Nogales, E., Wolfe, S.G., and Downing, K.H. (1998). Structure of αβ tubulin dimer by electron crystallography. Nature 391: 199-203.

Nogales, E., Whittaker, M., Milligan, R.A., and Downing, K.H. (1999). High-resolution model of the microtubule. Cell 96: 79-88.

Palmer, R.E., Sullivan, D.S., Huffaker, AT., and Koshland, D. (1992). Role of astral microtubules and actin in spindle orientation and migration in the budding yeast, Saccharomyces cerevisiae. J. Cell Biol. 119:583-593.

Panda, D., Daijo, J.E., Jordan, M.A., and Wilson, L. (1995). Kinetic stabilization of microtubule dynamics at steady state *in vitro* by substoichiometric concentrations of tubulin-colchicine complex. Biochemistry 34: 9921-9929.

149

Panda, D., Miller, H.P., Banerjee, A., Luduena, R.F., and Wilson, L. (1994). Microtubule dynamics in vitro are regulated by the tubulin isotype composition. Proc. Natl. Acad. Sci. USA 91:11358-11362.

Panda, D.; Miller, H.P.; Wilson, L. (1999). Rapid treadmilling of brain microtubules free of microtubule-associated proteins in vitro and its suppression by tau. PNAS 96 (22): 12459-12464.

Pillus, L., and Solomon, F. (1986). Components of microtubular structures in *Saccharomyces cerevisiae*. PNAS 83: 2468-2472.

Pringle, J.R., and Hartwell, L.H. (1981). The *Saccharomyces cerevisiae* cell cycle. *In* The Molecular Biology of the Yeast *Saccharomyces*: Life cycle and inheritance. J.N. Strathern, E.W. Jones, and J.R. Broach, editors. Cold Spring Harbor Laboratory, Cold Spring Harbor, NY. 97-142.

Pringle JR, Adams AE, Drubin DG, Haarer BK. (1991). Immunofluorescence methods for yeast. Methods Enzymol. 194: 565-602.

Reijo, R.A., Cooper, E.M., Beagle, G.J., and Huffaker, T.C. (1994). Systematic mutational analysis of the yeast β-tubulin gene. Mol. Biol. Cell 5:29-43.

Richards, K.L., Anders, K.R., Nogales, E., Schwartz, K., Downing, K.H., and Botstein, D. (2000). Structure-function relationships in yeast tubulins. Mol. Biol. Cell 11:1887-1903.

Rothstein, R. (1983). One-step gene disruption in yeast. Methods in Enzymology 101:202-211.

Rothstein, R. (1991). Targeting, disruption, replacement, and allele rescue: Integrative DNA transformation in yeast. Methods in Enzymology 194:281-301.

Sage, C.R. (1994). Analysis of putative regulatory domains of β-tubulin: Site-directed mutagenesis of budding yeast β-tubulin. Ph.D dissertation. University of California, Santa Barbara.

Sage, C.R., Davis, A.S., Dougherty, C.A., Sullivan, K., and Farrell, K.W. (1995a). β-tubulin mutation suppresses microtubule dynamics in vitro and slows mitosis in vivo. Cell Motil. Cyto. 30: 285-300.

Sage, C.R., Dougherty, C.A., Davis, A.S., Burns, R.G., Wilson, L., and Farrell, K.W. (1995b). Site-directed mutagenesis of putative GTP-binding sites of yeast β-tubulin:

150

Evidence that α-, β-, and γ-tubulins are atypical GTPases. Biochemistry 34: 7409-7419.

Sambrook, J., Fritsch, E.F., and Maniatis, T. (1989). Molecular Cloning: A Laboratory Manual. Second Edition. Cold Spring Harbor Laboratory Press, NY.

Saxton, W.M., Stemple, D.L., Leslie, R.J., Salmon, E.D., Zavortink, M., and McIntosh, J.R. (1984). Tubulin dynamics in cultured mammalian cells. J. Cell Biol. 99:2175-2186.

Schatz, P.J., Pillus, L., Grisafi, P., Solomon, F., and Botstein, D. (1986a). Two functional α-tubulin genes of the yeast Saccharomyces cerevisiae encode divergent proteins. Mol. Cell. Biol. 6: 3711-3721.

Schatz, P.J., Solomon, F., and Botstein, D. (1986b). Genetically essential and nonessential α-tubulin genes specify interchangeable proteins. Mol. Cell. Biol. 6: 3722-3733.

Shaw, S.L., Yeh, E., Maddox, P., Salmon, E.D., and Bloom, K. (1997). Astral microtubules dynamics in yeast: A microtubule-based searching mechanism for spindle orientation and nuclear migration into the bud. J. Cell Biol. 139(4): 985-994.

Shaw, S.L., Maddox, P., Skibbens, R.V., Yeh, E., Salmon, E.D., and Bloom, K. (1998). Nuclear and spindle dynamics in budding yeast. Mol. Biol. Cell 9: 1627-1631.

Shelden E, and Wadsworth P. (1993). Observation and quantification of individual microtubule behavior in vivo: microtubule dynamics are cell-type specific. J Cell Biol. 120(4): 935-45.

Skoufias, D., and Wilson, L. (1992). Mechanism of inhibition of microtubule polymerization by colchicine: inhibitory potencies of unliganded colchicine and tubulin-colchicine complexes. Biochemistry 31: 738-746.

Stearns, T. and Botstein, D. (1988). Unlinked noncomplementation: Isolation of new conditional-lethal mutations in each of the tubulin genes of Saccharomyces cerevisiae. Genetics 119: 249-260.

Sternlicht, H., Yaffe, M.B., Farr, G.W. (1987). A model of the nucleotide-binding site in tubulin. FEBS Letters 214:226-235.

Straight, A.F., Marshall, W.F., Sedat. J.W., and Murray, A.W. (1997). Mitosis in living budding yeast: Anaphase A but no metaphase plate. Science 277: 574-578.

151

Straight, A.F., Sedat, J.W., and Murray, A.W. (1998). Time-lapse microscopy reveals unique roles for kinesins during anaphase in budding yeast. J. Cell Biol. 143: 687-694.

Sullivan, K.F. (1988). Structure and utilization of tubulin isotypes. Ann. Rev. Cell Biol. 4:687-716
Sullivan, D.S., and Huffaker, T.C. (1992). Astral microtubules are not required for anaphase B in Saccharomyces cerevisiae. J. Cell Biol. 128:379-XXX.

Thomas, J.H., Neff, N.F., and Botstein, D. (1985). Isolation and characterization of mutations in the β-tubulin gene of Saccharomyces cerevisiae. Genetics 112: 715-734.

Tirnauer, J.S., O'Toole, E., Berrueta, L., Bierer, B.E., and Pellman, D. (1999). Yeast Bim1p promotes the G1-specific dynamics of microtubules. J. Cell Biol. 145(5): 993-1007.

Toso, R.J., Jordan, M.A., Farrell, K.W., Matsumoto, B., and Wilson, L. (1993). Kinetic stabilization of microtubule dynamic instability in vitro by vinblastine. Biochemistry 32: 1285-1293.

Uppuluri, S., Knipling, L., Sackett, D.L., and Wolff, J. (1993). Localization of the colchicine-binding site of tubulin. Proc. Natl. Acad. Sci. USA 90: 11598-11602.

Valiron, O., Caudron, N., and Job, D. (2001). Microtubule dynamics. Cell. Mol. Life Sci. 58: 2069-2084.

Vasquez, R.J., Howell, B., Yvon, A.M., Wadsworth, P., and Cassimeris, L. (1997). Nanomolar concentrations of nocadazole alter microtubule dynamic instability in vivo and in vitro. Mol. Biol. Cell. 8: 973-985.

Verna, J., Lodder, A., Lee, K., Vagts, A., and Ballester, R. (1997). A novel family of genes required for maintenance of cell wall integrity and for the stress response in Saccharomyces cerevisiae. PNAS 94 13804-13809.

Walker, R.A., O'Brien, E.T., Pryer, N.K., Soboeiro, M.F., Voter, W.A., and Erickson, H.P. (1988). Dynamic instability of individual microtubules analyzed by video light microscopy: rate constants and transition frequencies. J. Cell Biol. 107: 1437-1448.

Wilson, L., and Friedkin, M. (1967). The biochemical events of mitosis II. The in vivo and in vitro binding of colchicine in grasshopper embryos and its possible relation to inhibition of mitosis. Biochemistry 6: 3126-3135.

152

Wilson, L., and Jordan, M.A. (1995). Microtubule dynamics: taking aim at a moving target. Chemistry and Biology 2:569-573.

Wilson, L., Panda, D., and Jordan, M.A. (1999). Modulation of microtubule dynamics by drugs: a paradigm for the actions of cellular regulators. Cell Structure and Function 24: 329-335.

Winsor, B., and Schiebel, E. (1997). Review: An overview of the Saccharomyces cerevisiae microtubule and microfilament cytoskeleton. Yeast 13: 399-434.

Appendix A: Purification of tubulin from the budding yeast, *Sacchromyces cerevisiae* using the WSC deletion strains

Introduction

One of the original aims of this project was to purify tubulin from the *Saccharomyces cerevisiae* strains of interest, and to examine the dynamic instability properties of MTs assembled from the purified protein, *in vitro*. Examination of dynamic instability characteristics of MTs assembled from purified yeast protein would be informative of the properties that are intrinsic to the MT polymer. Davis et al., (1993, 1994) and Gupta (2001) have shown that the *in vitro* properties of yeast MTs are different from those *in vivo*, suggesting that other factors in the cell are important in the regulation of MT dynamics.

Tubulin from CLC mutant strains which showed interesting phenotypes with respect to MT function was to be purified using a modification of the protocol established by Barnes et al., (1992) and Davis et al., (1993). In the past, tubulin purification from yeast was labor intensive and cumbersome, with small yields, typically 5-10 mg of 'purified' protein from an 80 L culture [1-2 kg wet weight cells] (Davis et al., 1993). The extent of yeast cell breakage, and capacity of purification have always been major limiting factors in obtaining pure assembly-competent yeast tubulin. In order to improve cell breakage for tubulin purification purposes, two genes which were

154

identified as putative regulators of the protein kinase C-mitogen activated protein kinase (PKC1-MPK1) pathway were disrupted in the CLC strains; the PKC1-MPK1 pathway is involved in the maintenance of cell wall integrity (Verna et al., 1997). Encoding cell wall integrity and stress response components, WSC1 and WSC3 genes, when disrupted in combination, resulted in a cell wall defect phenotype. These defects allowed wild-type growth of yeast strains without the necessity of special expensive media or greatly altered growing conditions, yet vastly improve breakage efficiency. Strains carrying the double disruption could grow at 30 °C in YPD media with the addition of sorbitol as an osmotic stabilizer, but lysed easily when sorbitol was removed from the media (Verna et al., 1997). Another phenotype of the double disruption was sensitivity to 3 mM caffeine, a phosphodiesterase inhibitor. All plasmids (Table A1) containing the WSC genes and WSC disruption constructs were gifts from Jim Verna and Roymarie Ballester

155

Table A1: Reagents for disruption of the WSC1 and WSC3 genes in *Saccharomyces cerevisiae* strains.

plasmid	description	use
pUC-IRIS7	clone of WSC1 gene	plasmid digested with ApaI and PstI or ApaI and HindIII to drop fragment used as a probe in Southern blots
pUC-IRIS5	clone of WSC3 gene	plasmid digested with EcoRI and BglII to drop fragment used as a probe in Southern blots
pUC-IRIS7::ADE8	construct used to disrupt WSC1 in genome; 80 % of ORF removed; ADE8 is used as a selection marker	plasmid digested with PstI and SacI or HindIII and SacI to drop the fragment used for disruption of native WSC1 gene by transformation
pUC-IRIS5::TRP1	construct used to disrupt WSC3 in genome; 91 % of the ORF and 300 nucleotides 3' to the termination codon are removed; TRP1 is used as a selection marker	plasmid digested with BamHI and SacI to drop the fragment used for disruption of native WSC3 gene by transformation

Construction of WSC mutants

The selection procedure for haploids that carried both WSC disruptions and the β-tubulin mutation is outlined. Briefly, the haploid WT and β-tubulin mutant strains ADY101-6B, ADY103-5, CLC2-1D, CLC7-1'A, and CLC9 were transformed with a 2.3 kb BamHI- SacI fragment of pUC-IRIS5::TRP1, containing wsc3::TRP1. Transformants were plated onto supplemented SD media, selecting for TRP$^+$ colonies. Genomic DNA preparations from the candidate transformants were

156

subjected to PCR analysis using primers (ETW3A and ETW3C) designed to amplify

the WSC3 gene; wild-type WSC3 produced a 2 kb PCR product, while the

wsc3::TRP1 PCR product was 1.6 kb. Presence of the marker was confirmed by a

second round of PCR using primers (ETTA and ETTB) designed to amplify the TRP1

gene, using the first round PCR product as a template. Genotypes were determined

by 'spotting' the strains on various DO plates. For strains with the correct genotypes

and phenotypes, genomic DNA was isolated. Southern blot analysis using probes to

wsc1::ADE8, wsc3::TRP1, were used to confirmed the presence of the WSC

disruptions. Presence of the appropriate β-tubulin mutation was confirmed by PCR

sequencing.

Since the yeast strains previously created in the laboratory by A. Davis and C.R. Sage

were ADE$^+$, the ADE8 marker in the WSC1 deletion construct was exchanged for

LEU2. The LEU2 gene was isolated as a 3.1 kb BglII fragment from an incomplete

digest of YEp13; there was a BglII site 200 bp from one end. The parental plasmid

(IRIS7 BsaAI/ApaI) to the wsc1::ADE8 construct was used as the WSC1-containing

vector; IRIS7 BsaAI/ApaI was linearized by digestion with BglII, subjected to

alkaline phosphatase treatment and then purified from an agarose gel. The purified

LEU2-containing 3.1 kb BglII fragment was ligated into the purified vector, then

transfected into the XL1-B strain of *E. coli*. Plasmids were isolated from the

transfectants, and subjected to diagnostic single and double restriction enzyme digests

to confirm that WSC1 was indeed disrupted by LEU2 (see Figure 1). Direction of the

157

insert was determined to be forward, by sequencing of the wsc1::LEU2 plasmid using the ETW1A and ETW1B primers. The wsc1::LEU2 plasmid was digested with HindIII and SmaI to release the disrupted gene, and the 4.9 kb released fragment was used to transplace the endogenous WSC1 gene in the yeast strains used in this study.

WSC3 disrupted strains were transformed with the wsc1::LEU2 construct, and plated onto supplemented SD media, selecting for LEU+ TRP+ colonies. Candidates were identically streaked onto YPD and YPD + 0.25 M Sorbitol plates (YPD + S). YPD + S plates and one set of YPD plates were incubated at 30 °C, while the other set of YPD plates was incubated at 37 °C. Genomic DNA was isolated from those candidate colonies that grew on YPD + S and YPD plates at 30 °C, but not on YPD plates at 37 °C. Presence of the WSC1 disruption by LEU2 was confirmed by PCR analysis using primers (ETW1A and ETW1B) designed to amplify the WSC1 gene. Wild-type WSC1 produced a 1.6 kb PCR product, while the wsc1::LEU2 disruption produced a 3 kb PCR product. A second round of PCR using primers (ETLA and ETLB) designed to amplify the LEU2 gene was used on the first round PCR products to confirm the presence of the deletion.

158

Figure A1: Schematic of 4.9 kb HindIII-SacI transplacement fragment from the wsc1::LEU2 construct and restriction endonuclease digestion sites. LEU2 containing BglII fragment from YEp13 in broken line, WSC1 containing IRIS7 (BsaA1/ApaI) fragments in solid line. Fragment sizes in kilobases.

159
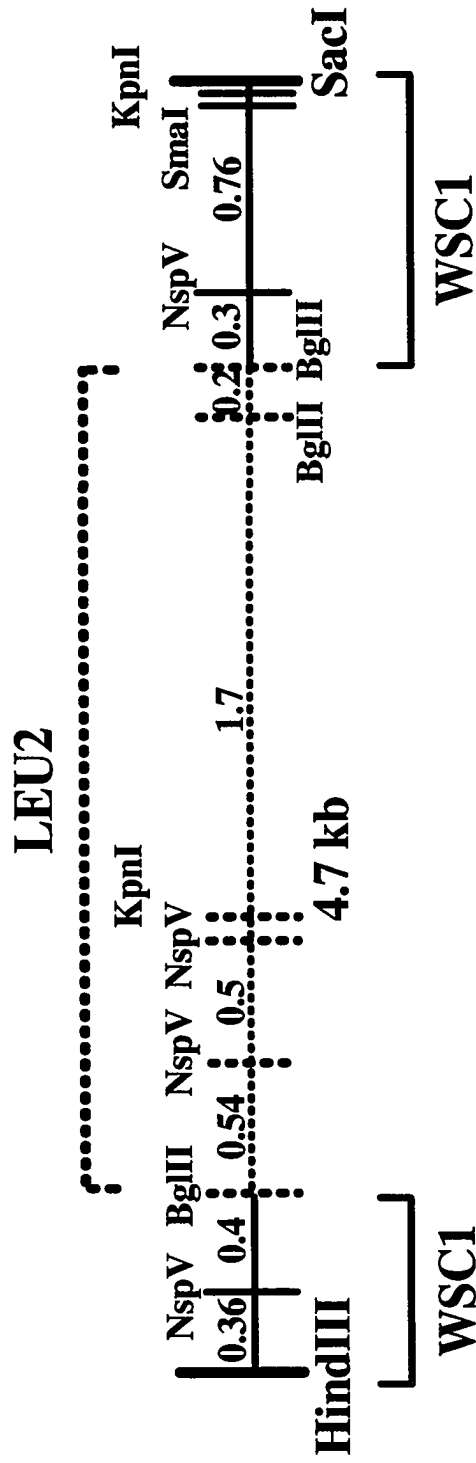
For CLC mutants that were haploid inviable, the β-tubulin mutations would have been recreated by transplacement of the mutated β-tubulin DNA sequence in the homozygous diploid strain ADY101 (tub2-590/tub2-590) in which both copies of the WSC1 and WSC3 genes were disrupted (Rothstein, 1983, 1991). TUB2 and CLC8 would have been transplaced into the modified ADY101 strain. Since both TUB2 and CLC8 were marked with the URA3 gene, candidates would have been selected by growth of transformants on ura- DO plates. Presence of the appropriate mutations in β-tubulin would have been confirmed by PCR sequencing.

Modifications to yeast tubulin purification scheme

The tubulin purification protocols of Barnes et al. (1992) and Davis et al. (1993) were modified as follows. The major modifications were in the first ion-exchange chromatography step: the clarified extract (high speed supernatant) was bound to Q-Sepharose FastFlow beads (FF) (Pharmacia) instead of DE-52 (Whatman), and then proteins were eluted from the column over an NaCl gradient instead of a one step elution using 0.6 M NaCl. Both ion-exchange chromatography steps (Q-Sepharose FF and Mono Q) were run by FPLC rather than by gravity (first column) and by FPLC (second column). The Q-Sepharose FF column was able to withstand higher flow rates for faster loading and washing, and eliminated the column pouring and settling time that was required with the DE-52 column. It is presumed that by reducing the time required for the first ion-exchange step and elution of the proteins

160

over a salt gradient would increase the yield of cleaner, assembly-competent tubulin. Davis et al. (1994) and Sage et al. (1995a, 1995b) have shown that in tubulin isolated from heterozygous diploids, the full length mutated β-tubulin appeared to be present at the same levels as full length TUB2 in the control heterozygous strain (TUB2/tub2-590), and that full length and truncated β-tubulins were in equimolar proportions.

In vitro analysis of MTs assembled from purified yeast tubulin

Purified yeast tubulin was polymerized *in vitro* using sea urchin (*Strongylocentrotus purpuratus* or *Lytechinus pictus*) axonemes as seeds, and viewed by VEDIC microscopy (Davis et al., 1993, 1994; Sage, 1994; Sage et al., 1995a,b). Purified tubulin concentrations of 0.5 mg/ml to 1 mg/ml were assembled in PEM buffer (100 mM Pipes, pH 6.8, 2 mM EGTA, 1 mM $MgSO_4$) plus 1 mM GTP at 30 °C on coverslips on the Zeiss IM-35 microscope. The original aim was to record both pre-steady state and steady state MT dynamics. MT dynamics were recorded and analyzed as in Derry et al., 1997. It was predicted that the CLC mutants would exhibit different critical concentrations for assembly; the concentrations of tubulin used would be adjusted so that MTs of similar lengths were assembled (Derry et al., 1997). MTs assembled from pure WT yeast tubulin would serve as control MTs for tubulin isolated from haploids; tubulin purified from the heterozygous diploid TUB2/tub2-590 will be used as a control for tubulin purified from strains that are haploid-lethal.

161

Concurrently, MTs in the presence of various antimicrotubule drugs, specifically, benomyl, nocodazole and colchicine, were to be recorded and analyzed. Yeast tubulin would have been polymerized in the presence of various concentrations of these antimitotic drugs, and individual MTs were to be recorded, measured and analyzed. Purified bovine brain tubulin in the presence of low concentrations of antimitotic drugs have exhibited suppressed growing and shortening behavior as well as an increase in the time spent in an attenuated state (Wilson and Jordan, 1995). Kinetic stabilization of MT dynamics is the mechanism by which these antimitotic drugs exert their effects at low concentrations. Since some of the CLC strains already show differential sensitivity to benomyl at the cellular level, it was predicted that the MT dynamics of tubulin isolated from these CLC mutants would be different from WT yeast tubulin in the presence of these drugs. Previous work by Sage (1994) showed that tubulin isolated from mutant strains were sensitive to antimitotic drugs in MT polymerization assays even when they seemed insensitive to those compounds at the cellular level.

Results

The disruption of the two WSC genes increased breakage efficiency from under 50 % in the original strains, to greater than 80 % in the double disruption strains. This increased efficiency allowed for the reduction in the culture volume from 80 L to 60 L. A smaller starting volume decreased the amount of time required for completion

162

of all the steps prior to the preparation of crude lysate. The changes made to the column chromatography purification steps allowed for greater volumes of cell lysate to be bound in a shorter amount of time. However, modification of the two column method of Davis et al. (1993) still did not permit purification of yeast tubulin to homogeneity, and the process remained long and extremely labor intensive.

Discussion

Modification of the yeast strains of interest by disruption of two of the WSC genes increased the efficiency of portions of the yeast tubulin protein purification procedure. Efficiency of cell breakage by bead beating increased 50 to 80 %, and because of the increased breakage efficiency, protein purifications could begin with a much reduced yeast culture volume of 40 to 60 L, rather than 80L. The reduced starting volume of yeast cells shortened the time required for washing of the cells, recentrifugation of cells, and cell breakage by bead beater phases of the purification procedure. Unfortunately, it was discovered that the desired phenotype, weakened cell walls that were stabilized by the addition of sorbitol in the media, was lost readily by the rapid adaptation of the cells.

In spite of the use of the Q-Sepharose FF column, and elution of proteins from the column via a salt gradient, the eluted protein spectrum showed multiple protein species. Because of the large number of non-tubulin protein species, and the fact that

163

the Mono Q column also separated proteins by the same chemistry as the Q-Sepharose column (ion exchange chromatography), it was not possible to purify the yeast tubulin to homogeneity using these two chromatography columns. To utilize a different sort of chemistry, I initiated use of ceramic hydroxyapatite as a column matrix. It was hoped that by utilizing hydroxyapatite, the protein eluted from the Q-separose FF column could be further purified via the hydroxyapatite, prior to loading onto the Mono Q column. Shortly after initiation of the use of hydroxyapatite, the laboratory obtained the MetaMorph imaging system, and the focus of my project was shifted to the *in vivo* analysis of MT dynamics.

Gupta and Himes (University of Kansas, Lawrence) were more successful with their approach to tubulin purification from *S. cerevisiae* than I was. They engineered a poly-histidine tag on the C-terminus of β-tubulin in their yeast strains, and used a Ni-affinity column to purify the tubulin. Their procedure was much shorter, partially because of the poly-His tag and use of the Ni-column, but also in part due to the additional equipment available to them. Gupta and Himes were able to start with a much smaller volume of yeast cells (34 L, 500 g wet weight), because of the high efficiency in cell breakage achieved by the methods they employed. Cell breakage was more rapid and more complete using the Microfluidizer 110-Y (Microfluidics Corp., Newton, MA), than the bead beaters used in my procedure. Ten passes on the Microfluidizer took less than an hour, and resulted in > 95 % cell breakage in the Gupta and Himes method. Since tubulin is so labile, it is critical to bind the protein

164

onto the column matrix as quickly as possible. By starting with a smaller total volume of cells, the whole procedure of Gupta and Himes from start to finish, took roughly 17 h (one long day; R. Himes, pers. comm.).

Using the poly-His tag, it was possible for Gupta and Himes to purify to homogeneity tubulin from a variety of yeast strains, even from strains that were haploid lethal. 500 g wet weight of yeast cells routinely yielded 3 - 4 mg of tubulin purified to homogeneity at 2 - 3 mg/mL (Gupta, 2001). For any large-scale purification of proteins from yeast, the tagging of the desired proteins, especially if they are present in small quantities, so that affinity column chromatography may be utilized, is an efficient method as shown by Gupta (2001). Also, efficiency in breaking open the yeast cells, is extremely important, and should not be overlooked.

165

Appendix B. Modification of the GFP-TUB3 containing plasmid, pTS417

Figure B1: The parental plasmid, pTS417, with restriction endonuclease recognition sites.
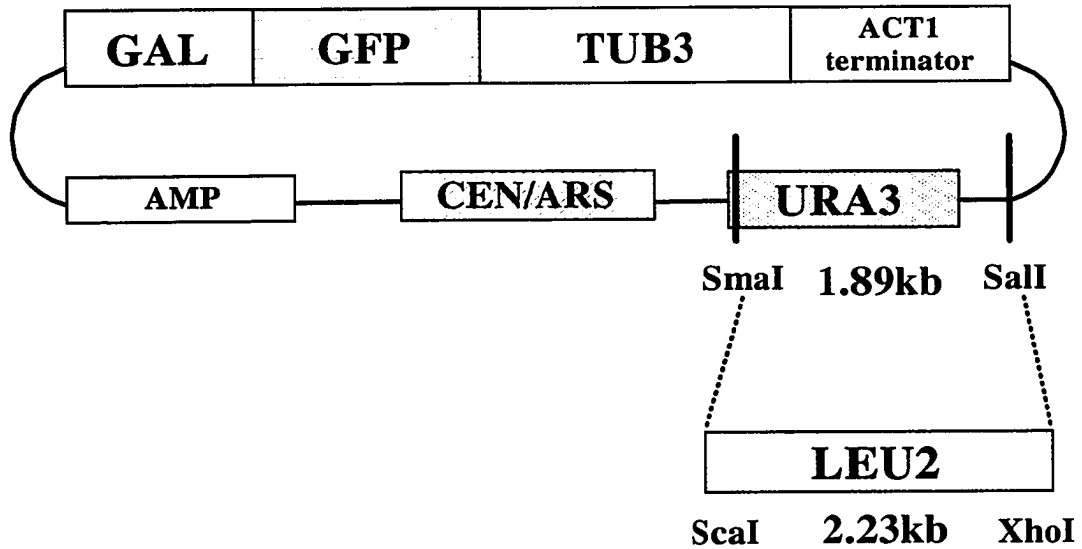
Table B1: Diagnostic restriction endonuclease digests for pTS417-LEU2 candidates.

	Number of cleavage sites in pTS417	Predicted fragment sizes in pTS417 (kb)	Number of cleavage sites in pTS417-LEU2	Predicted fragment sizes in pTS417-LEU2 (kb)
AflII	0	uncut plasmid	1	linearized plasmid >12
KpnI	2	5 7	3	2.2 3.5 6

166